A STUDY ON SYNTHESIS OF SILVER AND GOLD NANOPARTICLES BY EMPLOYING GAMMA RADIATION, THEIR CHARACTERIZATION AND APPLICATIONS

By

JAYASHREE BISWAL
Registration Number: CHEM01200804004

Bhabha Atomic Research Centre,
Mumbai 400085, India

A thesis submitted to the
Board of Studies in Chemical Sciences

In partial fulfillment of requirements
For the Degree of

DOCTOR OF PHILOSOPHY
of
HOMI BHABHA NATIONAL INSTITUTE

November, 2012

Homi Bhabha National Institute

Recommendations of the Viva Voce Board

As members of the Viva Voce Board, we certify that we have read the dissertation prepared by Ms Jayashree Biswal, entitled "A study on synthesis of silver and gold nanoparticles by employing gamma radiation, their characterization and applications" and recommend that it may be accepted as fulfilling the dissertation requirement for the Degree of Doctor of Philosophy.

Date:
Chairman- Dr. T. Mukherjee

Date:
Guide/ Convener- Prof. S. Sabharwal

Date:
External Examiner-

Date:
Member 1-

Date:
Member 2-

Date:
Member 3-

Final approval and acceptance of this dissertation is contingent upon the candidate's submission of the final copies of the dissertation to HBNI.

I hereby certify that I have read this dissertation prepared under my direction and recommend that it may be accepted as fulfilling the dissertation requirement.

Date:
Place:

STATEMENT BY AUTHOR

This dissertation has been submitted in partial fulfillment of requirements for an advanced degree at Homi Bhabha National Institute (HBNI) and is deposited in the Library to be made available to borrowers under rules of the HBNI.

Brief quotations from this dissertation are allowable without special permission, provided that accurate acknowledgement of source is made. Requests for permission for extended quotation from or reproduction of this manuscript in whole or in part may be granted by the Competent Authority of HBNI when in his or her judgment the proposed use of the material is in the interests of scholars. In all other instances, however, permission must be obtained from the author.

Jayashree Biswal

DECLARATION

I, hereby declare that the investigation presented in the thesis has been carried out by me. The work is original and has not been submitted earlier as a whole or in part for a degree / diploma at this or any other Institution / University.

Jayashree Biswal

Dedicated to my Family

ACKNOWLEDGEMENTS

I would like to take this opportunity to thank everyone who helped me to complete this PhD work.

First and foremost, I would like to express my deep sense of gratitude to my PhD guide Prof. S. Sabharwal for his invaluable guidance, encouragement and insights throughout my research career and critically going through the manuscript. I am indebted to him for believing in me and constantly encouraging me to give the best of me. I am fortunate to know him as a great scientist and above all a very kind human being, who has taught me to always look at the bright side.

I am very thankful to Homi Bhabha National Institute (HBNI), Government of India for allowing me to pursue my PhD work. I thank my PhD committee members Dr. T. Mukherjee, Dr. Manmohan Kumar and Dr. D. B. Naik for their valuable advice and input on my research. I thank Mr. S. P. Ramnani for his help and discussions in developing experimental protocol and data analysis. I also thank Mr. Nilanjal Misra for his help in carrying out some of the experimental work. I would like to thank Dr. Gursharan Singh and Dr. H. J. Pant for their timely support and encouragements for me.

I am short of words to express my gratitude to my wonderful teachers, Mr. Ajaya Kumar Nayak and late Mr. Sukadeba Mallick, who inspired me and guided me in my life.

I would like to thank my family for all the moral and emotional support they provided during the many stressful and demanding times.

I cannot finish without acknowledging the omnipresent and omnipotent, who guided me in my life's journey. Thank you Dear Lord.

CONTENTS

Synopsis of the thesis submitted to Homi Bhabha National Institute for the degree of Philosophy in Chemistry

Name of Candidate: Jayashree Biswal

Name of Guide: Prof. S. Sabharwal
Professor,
Chemical Sciences,
Homi Bhabha National Institute,
Mumbai- 400 094, India

Registration Number: CHEM01200804004

Date of Registration: 01-09-2008

Title of Thesis: A study on synthesis of silver and gold nanoparticles by employing gamma radiation, their characterization and applications

Place of Research Work: Isotope Applications Division,
Bhabha Atomic Research Centre,
Trombay, Mumbai- 400 085, India

Date of submission of synopsis: 12-03-2012

Signature of Candidate:

Signature of Guide:

SYNOPSIS

In recent years nanotechnology and nanomaterials have attracted remarkable attention in scientific community. The idea of atom-by-atom construction was first put forth, in a scientific manner, over 50 years ago by Nobel Prize winning physicist Richard Feynman (1918-1988) in a lecture delivered in December of 1959 entitled "There's plenty of room at the bottom". Many important properties of material change at nano level. In nature also there exists numerous examples of nanoscale systems, that have been highly optimized through millions of years of evolutionary development. For example the wings of a butterfly were shown to be intricately colorful because of nanoparticles that act as a photonic crystal. The experimental advancements over the past several decades have made the ability to create, manipulate, and measure atomic-scale phenomena. But there are numerous scientific challenges that must be addressed in order for this budding field to live up to the high promise and potential that nanotechnologies might offer. The main challenge lies in developing efficient synthesis methods for the systematic control of the size and shape of nanomaterials and engineering of these nanomaterials for various applications. Metal nanoparticles (nps) especially noble metal nanoparticles are being explored for their versatile applications in the area of sensing, imaging, catalysis and antimicrobial applications. These nanoparticles exhibit electronic, optical, magnetic and chemical properties that are very different from both the bulk and the constituent atoms or molecules. For example, the bright colors of metallic nanoparticle solutions, such as gold and silver are due to of the surface plasmon band, which lie in visible frequencies, unlike that for bulk metals where the absorption is in the UV region. The surface plasmon is a quantum of collective oscillation of free electrons in the metallic nanoparticles. In addition, the optical properties of nanoparticles depend significantly on their size and shape as well as on the dielectric constant of the surrounding medium [1]. Control over the size and shape of metallic nanoparticles enables tuning their optical [2-4], electronic [5], magnetic [6], and catalytic [7] properties. Chemical methods have been shown to be indispensable for synthesizing nanoparticles of various types of materials. The chemical synthesis of nanoparticles consists of three steps - seeding, particle growth, and growth termination by capping. One of the important factors that determine the quality of a synthetic procedure is the monodispersity of the nanocrystals obtained. It is desirable to have nanoparticles of nearly the same size, in order to be able to relate the size and the property under study. Hence, the narrower the size distribution, the more attractive is the synthetic procedure. The other important issues are the choice of the capping agent and control over the shape.

The extinction coefficients of noble metal nanoparticles are higher than many of the traditional dyes and these nanoparticles can be tailored to possess very good stability compared to the dye molecules. The nanoparticles are thus more suitable to be used for imaging and FRET (Fluorescence Resonance Energy Transfer) studies. For example, gold nanoparticles have extinction coefficient of the order 10^{11} L mol^{-1} cm^{-1} [8] that enables them to be used as excellent FRET-based quenchers for study of biomolecule interaction and conformational changes. The shape of gold nanoparticles can be tunable to make them absorb in near-infrared region. This region is relatively transparent for blood cells and other tissues [9], so that these gold nanoparticles can be used for diagnosis and therapeutic medical applications [10]. Particle anisotropy offers features and functions that are difficult to obtain simply by size-tuning of spherical nanoparticles. For example, a slight change in particle geometry can produce great changes in the surface plasmon peak position of a metallic nanoparticle, which can hardly be achieved in the spherical nanosystems through a similar change in diameter. In addition, the optical properties of anisotropic gold or silver nanoparticles are tunable throughout the visible and infrared regions of the spectrum, as a function of their aspect ratios. There exist several synthesis methods for generation of metal nanoparticles, such as chemical, photochemical, electrochemical, radiolytic etc., wherein metal nanoparticles are generated by reduction of metal ion precursors in solution by a reducing agent. Generation of these metal nps by high energy radiation is promising because of several advantages offered by radiolytic method. The radiolytic method is an indirect method, where reactive reducing radicals are produced *in situ* through water radiolysis. Gamma radiolysis provides a clean method for synthesis of metal nanoparticles. The gamma radiation energy is deposited throughout the solution producing primary radicals (Equation 1) in a time scale of the order of nano second (10^{-9}s) in aqueous solutions.

$$H_2O \overset{\gamma}{\rightsquigarrow} e_{aq}^{-} + H^{\cdot} + {}^{\cdot}OH + H_2 + H_2O_2 + H_3O^{+} \qquad (1)$$

These radicals are highly reactive and undergo redox reaction with suitable reactants. By adding an appropriate scavenger for oxidizing radicals a total reducing environment can be created in the system. Metal ion precursors present in a solution are converted to zerovelent metal atoms in this reducing environment, which finally give rise to metal nanoparticles in presence of a stabilizer. The radicals generated through water (solvent) radiolysis have reduction potential more negative than silver or gold ions, hence they can readily reduce these ions. Unlike chemical reduction method, the radiolytic method offers the advantage of easier control of size, shape and size distribution of nanoparticles by tuning parameters such as dose and dose rate. Generally at high dose rates the particles produce are smaller and less dispersed in size. Capping agents play very important role in stabilization of metal nanoparticles. Both natural polymer and synthetic polymers containing specific functional groups, like -OH, -NH_2, -COOH etc., can stabilize metal nanoparticles either by steric or electrostatic stabilization. The objective of present study was to utilize the high energy gamma radiation to prepare nanoparticles of noble metals with controlled shape, size and size distribution. The stabilization of nanoparticles has been explored using natural as well as synthetic polymers like guar gum, poly methacrylic acid (PMA), poly vinyl pyrrolidone (PVP) respectively. Further anisotropic nanoparticles have been synthesized by controlling experimental parameters, such as dose rate of irradiation, presence of certain adsorbing molecule like surfactant and some metal ions and presence of seed particles (either externally added or generated *in situ*). The synthesized nanoparticles have been characterized by using techniques, such as uv-visible spectroscopy, XRD, TEM and FTIR. The high surface area as well as high surface energy of metal nanoparticles make them amiable to adsorb other molecules upon their surfaces. This property of metal nanoparticles forms the basis of their use in detection and estimation of chemical and biological analytes. New methods for determination of hydrogen peroxide and dopamine have been developed in the present study. These works are presented in the thesis as described in the following manner.

Chapter 1: Introduction to metal nanoparticles and fundamental aspects of high energy radiation in synthesis of metal nanoparticles

This chapter deals with various aspects of metal nanoparticles, namely, properties, various synthesis methods and applications of noble metal nanoparticles, basic principles of aqueous radiation chemistry as applied to the synthesis of metal nanoparticles. The chapter further focuses on classification of nanomaterials, different modes of stabilization of nanoparticles, specific properties of various shape nanoparticles and theoretical aspect of optical properties of metal nanoparticles (surface plasmon resonance). The principles of energy deposition, distribution of absorbed energy in the medium, formation of various reactive species in radiolysis of water are highlighted in the chapter. Apart from this, a brief discussion about the chemical synthesis method, advantages of radiolytic method over the chemical method and principles of general characterization techniques for nanomaterials have been included in the chapter.

Chapter 2: Materials and methods

The principles and instrumentation of various experimental techniques and facilities employed in the present studies are described in this chapter. These include irradiation facility like ^{60}Co gamma irradiator, ubbelohde viscometer, UV- visible spectrophotometer, TEM instrument, FTIR spectrometer, X-ray diffractometer and thermo gravimetric instrument. Also the specifications of different reagents used are mentioned here.

Chapter 3: Synthesis of spherical silver nanoparticles in guar gum by gamma irradiation

The interaction of high-energy radiation with aqueous solution of metal ions induces ionization and excitation in the solvent, (water) leads to the formation of radical and molecular species in the solution. Reactive transient radicals produced through water radiolysis are solvated electrons (e_{aq}^-), hydrogen atom ($H^\cdot$) and hydroxyl radical ($^\cdot OH$). The first two radicals are strong reducing agents capable of reducing Ag^+ ions to lower valences and finally to metal atoms. The $^\cdot OH$ radicals are oxidizing in nature, which can oxidize the metal ions or atoms. To eliminate the oxidation process suitable $^\cdot OH$ scavenger such as isopropyl alcohol is added to the system. Thus in presence of isopropyl alcohol, only reducing radicals are produced under the irradiation condition, which leads to the reduction of metal ions into the metal atoms as shown below:

$$H_2O \overset{\gamma}{\rightsquigarrow} e_{aq}^- + H^\cdot + {}^\cdot OH + H_2 + H_2O_2 + H_3O^+ \quad (1)$$

$$CH_3CH(OH)CH_3 + {}^\cdot OH \longrightarrow CH_3{}^\cdot C(OH)CH_3 + H_2O \quad (2)$$

$$Ag^+ + e_{aq}^- \; (H^\cdot) \longrightarrow Ag^0 + (H^+) \quad (3)$$

The Ag metal atoms thus formed coalesce to form small nuclei, which grow to Ag nanoparticles. However, a capping agent is usually used in the synthesis of metal nanoparticles to both prevent the aggregation of the metal nanoparticles and impart useful chemical properties to the final nanoscale product. It is now well established that polymers are excellent host materials for nanoparticles of metals. When the nanoparticles are embedded or encapsulated in a polymer, the polymer acts as a surface-capping agent. Various synthetic polymers, such as poly(vinyl alcohol), poly(vinyl pyrrolidone), polystyrene and poly(methyl methacrylate) have been used in the synthesis of metal nanoparticles. However, very few works have been reported in which a natural polysaccharide has been used as a capping agent for the stabilization of metal nanoparticles. Natural polymers, because of their large abundance and the presence reactive functional groups may show better ability to stabilize nanoparticles. Guar gum (GG) is a naturally occurring edible carbohydrate polymer found in the seeds of guar plant. Aqueous guar gum solution is stable in the pH 4.0-10.5 range. Molecular weight of guar gum was determined from their intrinsic viscosity values and its relation to molecular weight via Mark Houwink equation $\eta = \kappa M_{\upsilon}^{\alpha}$. Where κ and α are constants, whose values are 3.8×10^{-4} and 0.732, respectively. By employing above method the viscosity average molecular weight (M_v) of guar gum was found to be 1.9×10^{6}. The silver nanoparticles were prepared by exposing aqueous solution of GG containing $AgNO_3$ and isopropyl alcohol to ^{60}Co gamma radiation. The Ag nanoparticles generated were first characterized with UV- visible absorption spectra. The un-irradiated GG solution did not show any peak in the visible region. With increasing radiation dose, the absorption in the region of 300- 600 nm started to develop, with absorption maxima at 427nm. Under the same experimental conditions, when irradiation was carried out in the absence of Ag^+, no absorption band in the region 300- 600 nm was observed. Thus, the absorption band observed at 427 nm was attributed to silver nanoparticles stabilized by GG. To obtain an optimum size and size distribution of Ag nanoparticles, a study aimed at controlling the reaction parameters was performed. This optimization process consists of the influence of the concentration of reactants like guar gum and $AgNO_3$ concentration, pH, and role of alcohol. The effect of the GG concentration on the formation of the Ag nanoparticles was studied for various GG concentrations. At low concentration, GG was not very effective in stabilizing the Ag nanoparticles, and therefore, there was less control over the particle size, as evident from the broad absorption spectrum. The effect of Ag^+ concentration on the formation of Ag nanoparticles was studied by keeping the concentration of GG fixed (0.5%) and varying the concentration of Ag^+. At high Ag^+ concentrations, more nuclei were formed and the concentration of GG, which was kept constant at 0.5%, was not sufficient to control the growth and stabilization of the Ag nanoparticles. Hence, the size distribution was not uniform, as evident from the broadening of the surface plasmon band. Thus, it appears that cluster size was governed by both GG concentration and precursor Ag^+ concentration. The Ag nanoparticles were further characterized by several physical techniques such as XRD, TEM and Thermogravimetry. In the XRD pattern, peaks at 2θ value of 38.1, 44.25 and 64.54 were observed, which confirmed the formation of metallic silver. The broad bandwidth of main peak at 2θ value of 38.1 indicates that the size of clusters is small which was confirmed from the TEM analysis. It shows spherical particles with size distribution in the range of 10-30nm. Evidence for the interaction of hydroxyl groups in the stabilization of the silver nanoparticles was obtained from the Fourier transform infrared (FTIR) spectra of the GG-containing Ag nanoparticles. The FTIR spectra of GG exhibited characteristics bands at 3426 and 2926 cm^{-1} because of the O—H stretching vibrations and C—H stretching vibrations of the polymer associated. The band at 3426 cm^{-1} was shifted to 3457 cm^{-1} in the presence of Ag and also, the band was broader in Ag/GG compared to GG. These observations clearly indicate the interaction of Ag with the —OH group of GG.

Chapter 4: **Synthesis of silver nanoparticles in methacrylic acid by radiolytic method and studying its application as sensor**

The unique optical properties of nanostructured materials make them excellent prospects for interfacing chemical or biological analytes for designing more efficient and sensitive sensors. Nanoparticles of silver and gold have absorption at certain wavelength in the visible spectrum with extremely large molar extinction coefficients than most of the organic dyes allowing higher sensitivity in optical detection of biomolecules. Spectrophotometric detection of various molecules/ species based on the optical properties of metal nanoparticles has recently been reported [11-13]. Based on the characteristic changes in the absorption spectra of metal nanoparticles with change in their size, shape or size distribution, optical sensors has been fabricated. Change in the spectral position, FWHM or intensity of absorption spectra of nanoparticles due to interaction of metal nanoparticles with biological analyte forms the basis of widely applicable colorimetric sensing [14].

The synthesis of silver nanoparticles has been carried out by irradiating $AgNO_3$ by gamma radiation in the presence of methacrylic acid (MA) and NaOH. The e_{aq}^- and $H^\bullet$ radicals generated through water radiolysis brings about the reduction of Ag^+ to Ag^0 and the $^\bullet OH$

radical takes part in polymerization of methacrylic acid. The Ag^0 thus formed subsequently coalesce to form Ag nanoparticles. The polymethacrylate (PMA) generated upon irradiation stabilizes the growing Ag nanoparicles. Polymers provide more effective capping to metal nanoparticles compared to their respective monomers because the steric stabilization is more pronounced in case of the polymers. The Ag nanoparticles solution shows absorption band at ~450nm. The average size of Ag nps known from the TEM image was found to be 6nm. The anionic carboxylate functional groups are known to stabilize smaller size metal nanoparticles due to stronger electrostatic stabilization [15]. Hence the np size obtained in this study is only 6nm. During irradiation along with formation of Ag nps, MA polymerizes to form PMA, which subsequently stabilizes the nps. This has been confirmed by monitoring the FTIR spectra of monomer (MA) and polymer stabilized Ag nanoparticles (Ag/PMA). The pristine MA shown an IR peak at 1697 cm^{-1} due to C=C double bond. This peak is absent in case of final sample after irradiation (Ag-PMA), which is an indication of polymerization of MA during irradiation. The peak at1630 cm^{-1} in both the spectra (MA and Ag/PMA) is due to >C=O stretching of carboxylate group. In case of Ag–PMA, the peak at 1630 cm^{-1} is broadened due to interaction of carboxylate group with Ag nps. IR peak at 1540 cm^{-1} in case of Ag nps/PMA is for 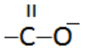 $-\overset{\|}{\mathrm{C}}-\mathrm{O}^{-}$ stretching of carboxylate group as the pH of the solution is around 12.8 and polymethacrylic acid exists in deprotonted form at this pH. The effect of MA concentration on Ag np formation has also been investigated. For lower MA concentration the spectrum is broad and for higher MA concentration a narrow spectrum has been obtained. This is because higher concentration of capping agent will more effectively confine the np size in a certain range leading to formation of narrow size distribution of nps. At high concentration the steric effect imparted by the polymer chains of the capping agent (PMA) is more pronounced. Similarly for higher Ag^+ concentration the particle size becomes larger and poly-dispersed, which causes broadening of absorption spectra.

Dopamine (DA) is an important biological compound that belongs to the group of catecholamines and it plays an important role in the function of central nervous system, hormonal, renal and cardiovascular systems [16]. Therefore, development of sensitive methods for DA quantification has been investigated in recent years [17-19]. The detection of DA in presence of excess ascorbic acid and development of a method with good selectivity, sensitivity and reproducibility remain a challenging task. In this work an attempt has been made to utilize silver nanoparticles for determination of DA in aqueous solution. The spectral behaviour of Ag nanoparticles in presence of DA was investigated. For estimation of DA, Ag nps were synthesized by different experimental set up and these nanoparticle solutions were examined to obtain uniform and gradual change in the spectral characteristic with varying DA concentration. Measured amount of as prepared Ag nps in PMA solution was added to aqueous solution containing different amount of DA. Then this solution mixture was kept for 5 hours to attain equilibrium before measuring the absorption spectra. The color change from light yellow to dark yellow with increase in DA concentration could be easily distinguished. In the present work a simple, sensitive and inexpensive spectroscopic method has been developed to estimate DA in aqueous solution in a linear range of 5.27×10^{-7} to 1.58×10^{-5} mol dm^{-3} DA. As mentioned earlier ascorbic acid (AA) is present in millimolar concentration along with DA (nanomolar to micromolar) in biological fluids. In conventional dopamine estimation method by electrochemical analysis, ascorbic acid imposes major problem, because the redox potential of ascorbic acid is close to dopamine. This affects the selectivity due to overlapping of signal of ascorbic acid with the signal of dopamine. In this study the interference of AA in estimation of DA has also been studied. It was inferred that AA concentration up to to 1.0×10^{-4} mol dm^{-3} does not interfere in the estimation of DA in the range of 5.27×10^{-7} to 1.05×10^{-5} mol dm^{-3}.

Chapter 5: Radiation induced synthesis of anisotropic gold nanoparticles and their characterization

Anisotropic nanoparticles are a class of materials whose properties are direction dependent and more than one structural parameter is required to describe them. A variety of anisotropic nanoparticles in various shapes such as nanorods, wires, tubes, prism, stars etc. have been reported in the literature [20]. Particle anisotropy possesses features that are difficult to obtain by size-tuning of spherical nanoparticles. The introduction of anisotropy in nanoparticles, besides enhancing the surface plasmon resonance band, depending upon the aspect ratio, also makes it tunable throughout the visible-NIR spectrum and thus making them useful for detection of biologically important molecules [21]. Several chemical synthesis methods based on colloid chemistry have been developed for the production of metal nanoparticles with different shapes using cetyl trimethyl ammonium bromide (CTAB) as a structure directing capping agent. Synthesis of gold nanorods in chemical method proposed by Murphy and her group consists of a seed mediated growth in presence of CTAB and a small amount of Ag^+ ions.

This chapter consists of three separate sections describing different methods to generate a variety of anisotropic shape gold nanoparticles. The role of kinetics in anisotropic metal np generation has been established. In the first synthesis method, a seed mediated approach has been developed. This is a two step seeded growth method, but instead of using ascorbic acid as a reductant, gamma radiation has been used to generate reducing radicals. Radicals generated due to absorption of gamma radiation in aqueous solution are strong reducing species. A milder reducing enviroment is suitable for formation of anisotropic shaped nanoparticles. Hence low radiation dose rate condition had been chosen to control the reaction rate for generation of Au nanorods. The mechanism of nanorod formation has been described in this section. The gold nanoseeds have certain crystallographic facets. In presence of a small amount of Ag^+ certain facets are blocked, so that the growth of nanoparticles progresses in a directional manner. CTAB assists in nanorod formation by providing a tubular template.

The above method has been further modified to develope a simple and convenient synthesis process, in which the seed solution synthesis step and external addition of seed had been eliminated. In this method a total reducing environment containing a single type of reducing species has been created by carefully choosing the nature and concentration of reactants. Isopropyl alcohol was added to the system, so that it reacts with $H^{\bullet}$ and $^{\bullet}OH$ radical to give isopropyl alcohol radical. The e_{aq}^- present in the system were converted to isopropyl alcohol radical by adding acetone. The isopropyl alcohol radical is a mild redicing agent as compared to e_{aq}^-. Hence under these reaction conditions the only reducing agent present is isopropyl alcohol radical. The milder reducing environment results in slowing the kinetics of reduction of Au^{III} or Au^{I}, thus offering favorable condition for anisotropic shape generation. It is a one-pot synthesis method, in which even at high dose rate gold nanorods generation has been achieved.

In another approach, anisotropic gold nanoplates have been synthesized by combining both radiolytic and chemical methods. Au seeds are generated in-situ by radiolysis and the Au nanoparticles are allowed to grow on these seeds by ascorbic acid reduction method. Ascorbic acid is used to reduce Au^{III} to Au^{I} in aqueous solution containing CTAB, a small amount of $AgNO_3$ and 2-propyl alcohol. This solution containing Au^{I} was irradiated for a very small duration of time, as a result a small portion of Au^I convert to Au^0 by the reducing radicals generated from water radiolysis. The Au^0 then coalesce to form seed particles. After the reaction system is removed from the irradiator Au^I ions adsorbed on these seeds, get reduced to Au^0 in presence of excess of ascorbic acid and subsequently Au nanoplates formation occurs in the presence of structure directing capping agent CTAB and Ag^+ [22].

The effect of different experimental parameters on nanoparticle formation was studied. The nanoparticles were characterized by UV-visible spectrometry and TEM. It has been demonstrated that CTAB-capped anisotropic gold nanoparticles with controllable sizes and shapes could be synthesized using radiolytic synthesis route. These shape controlled gold nanoparticles exhibit well separated plasmon absorption band with high extinction coefficient. By proper choice of radiation dose rate and precursor concentration and/or nature of reducing radical the gold nanorods can be synthesized in aqueous media. Also in radiolytic method external addition of seed has been successfully avoided.

Chapter 6: **Synthesis of gold nanoparticles in aqueous polyvinyl pyrrolidone by radiolytic method and their application for estimation of hydrogen peroxide**

Plasmonics is being investigated in recent years as a prpmising tool for analytical and biochemical estimations. Particularly, surface plasmon resonance at the surface of gold nanostructures has led to the development of widespread interest in gold nanoparticles [23]. As described in the earlier chapters the use of ionizing radiation for the synthesis of metal nanoparticles is promising as highly reactive species with high reduction potential are produced in-situ by the radiation, which is hard to achieve by other chemical methods and also it is a room temperature process. Poly (N-vinyl-2-pyrrolidone) (PVP) has been reported as a suitable capping agent in preparation of metal nanoparticles, because it has functional group namely $>C=O$ and $>N-$ and long polymer chain. The functional groups containing lone pair of electrons help in stabilization of metal nanoparticles at their surface by covalent interaction, where as the polymer chain restricts aggregation of metal nanoparticles by steric hinderance. Apart from this, PVP is a biocompatible polymer. Hence nanoparticles synthesized in PVP can have potential biological applications. In the present work gold nanoparticles (Au nps) have been synthesized in aqueous solution of polyvinyl pyrrolidone (PVP) by gamma radiolysis from $HAuCl_4.3H_2O$ precursor and in presence of small concentrations of Ag^+, 2-propanol and acetone. Different experimental parameters such as

Au^{III} concentration, PVP concentration, Ag^+ concentration and molecular weight of PVP have been optimized to get Au nps of desirable size and size distribution. Hydrogen peroxide is widely used as an oxidant, a disinfectant and a bleaching agent in various industries. It causes irritation to eye, skin and mucous membrane when present in the environment. Hydrogen peroxide is produced in stoichiometric amounts during the oxidation of biological analytes (e.g. glucose) by dissolved oxygen in the presence of corresponding oxidase. Therefore micro and trace level determination of hydrogen peroxide is considerably important in clinical chemistry, analytical biochemistry and environmental science. Existing methods for the determination of hydrogen peroxide include titrimetry, spectrophotometry, kinetic flow-injection method, fluorescence, enzymatic method, chromatographic techniques and electrochemical methods. In this work the nanoparticles synthesized by radiation method were used for estimation of H_2O_2. The H_2O_2 concentration in aqueous solution has been determined by monitoring the oxidation of o-phenylene diamine (o-PDA) by H_2O_2 in presence of enzyme, horse radish peroxidase (HRP). Au nanoparticle solution when added to the reaction system containing o-PDA, H_2O_2 and HRP the interaction of oxidation product with Au nanoparticles results in an enhanced absorption peak at 427 nm. The absorbance value of this peak at λ_{max} increased linearly with increase in H_2O_2 concentration in two ranges, i.e., 2.5×10^{-6} mol dm^{-3} to 2×10^{-4} mol dm^{-3} and 1×10^{-7} mol dm^{-3} to 3×10^{-6} mol dm^{-3} H_2O_2 in two separate set of experimental parameters. The detection limit was determined to be 1×10^{-7} mol dm^{-3} and H_2O_2 concentration could be estimated from 1×10^{-7} mol dm^{-3} to 2×10^{-4} mol dm^{-3} by choosing appropriate experimental parameters.

In summary the thesis will present an account of the use of radiation chemical technique for synthesis of noble metal nanoparticles with defined shape and size by controlling the experimental parameters. Application of the synthesized nanoparticles for estimation of low concentration of biologically relevant molecules like hydrogen peroxide and dopamine shall be presented in the thesis.

References

1. Huang, S. H., Minami, K., Sakaue, H., Shingubara, S., Takahagi, T., (2002) *J. Appl. Phys.*, 92, 7486.
2. EI-Sayed, M. A., (2001) *Acc. Chem. Res*., 34, 257.
3. Mulvaney, P., (1996) *Langmuir*, 12, 788.
4. Link, S., Mohamed, M. B., EI-Sayed, M. A., (1999) *J. Phys. Chem. B,*103, 3073.
5. McConnell, W. P., Novak, J. P., Brousseau, L. C., Fuierer, R. R., Tenent, R. C., Feldheim, D. L., (2000) *J. Phys. Chem. B,* 104, 8925.
6. Liu, C., Zhang, Z., (2001) *J. Chem. Mater*., 13, 2092.
7. Moreno-Manas, M., Pleixats, R., (2003) *Acc. Chem. Res*., 36, 638.
8. Jensen, T. R., Malinsky, M. D., Haynes, C. L., Van Duyne, R. P., (2000) *J. Phys. Chem. B* 104, 10549.
9. Link, S., Furube, A., Mohamed, M. B., Asahi, T., Masuhara, H., El-Sayed, M. A., (2002) *J. Phys. Chem. B.* 106, 945.
10. Murphy, C. J., Gole, A. M., Stone, J. W., Sisco, P. N., Alkilany, A. M., Goldsmith, E. C., (2008) *Acc. Chem. Res.* 41, 1721.
11. Stuart, D. A., Haes, A. J., Yonzon, C. R., Hicks, E.M., Van Duyne, R. P.,(2005) in "*IEE Proc.-Nanobiotechnol.*" Vol. 152, No. 1.
12. Hormozi Nezhad, M. R., Karimi, M. A., Shahheydari, F., (2010) *Transaction F: Nanotechnology*, 17, 148.
13. Wang, C., Luconi, M., Masi, A., Fernandez, L., (2010) *"Silver Nanoparticles"* (Ed. Perez, D. P.), InTech.
14. P. K., Jain, X., Huang, I. H., El-Sayed, M. A., El-Sayed, (2007) *"Plasmonics"* Vol. 2, No. 3., Springer.
15. Nishimura, S., Mott, D., Takagaki, A., Maenosono, S., Ebitani, K., (2011) *Phys. Chem. Chem. Phys.* 13, 9335.
16. Missale, C., Nash, S. R., Robinson, S. W., Jaber, M., Caron, M. G., (1998) *Physiol. Rev.* 78, 189.
17. Chen, R. S., Huang, W. H., Tong, H., Wang, Z. L., Cheng, J. K., (2003) *Anal. Chem.* 75, 6341.
18. Raj, C. R., Okajima, T., Ohsaka, T., (2003) *J. Electroanal. Chem.* 543, 127.

19. Wang, H. Y., Hui, Q. S., Xu, L. X., Jiang, J. G., Suan, Y., (2003) *Anal. Chim. Act.* 497, 93.
20. T. K., Sau, A. L., Rogach, (2010) *Adv. Mater.* 22, 1781.
21. Burda C, Chen X, Narayanan R, El-Sayed M. A., (2005) *Chem. Rev*. 105,1025.
22. Murphy, C. J., Sau, T. K., Gole, A. M., Orendorff, C. J., Gao, J., Gou, L., Hunyadi, S. E., Li, T., (2005) *J. Phys. Chem. B* 109, 13857.
23. S., Eustis, M. A., El-Sayed, (2006*) Chem. Soc. Rev.,* 35, 209.

LIST OF FIGURES

LIST OF TABLES

LIST OF ABBREVIATIONS

Abbreviations

AA	Ascorbic acid
Ag	Silver
ATR	Attenuated total reflection
Au	Gold
CTAB	Cetyl trimethyl ammonium bromide
DA	Dopamine
FTIR	Fourier transform infrared spectroscopy
GG	Guar gum
HRP	Horse radish peroxidase
MA	Methacrylic aid
np	Nanoparticles
OPDA	Orthophenylene diamine
PMA	Poly methacrylate
PVP	Polyvinyl pyrrolidone
TEM	Transmission electron microscopy
TG	Thermogravimetry
γ	Gamma

Chapter 1: Introduction to metal nanoparticles and fundamental aspects of high energy radiation in synthesis of metal nanoparticles

1.1. General introduction

In nineteenth century Michael Faraday prepared and studied gold sols which can now be seen as the foundation of modern colloid science [1]. He pointed out that colloidal metal sols were thermodynamically unstable and that the individual metal (gold) nanoparticles had to be stabilized kinetically to prevent aggregation. In 1925 Richard Zsigmondy received the Nobel Prize in chemistry for his work in the field of modern colloid chemistry by studying the properties of gold sols and inventing an ultra microscope [2]. Colloidal metal nanoparticles are of interest in both research and technology, due to their specific properties not available in isolated molecules or bulk metals. Because of these properties nanoparticles have many important applications in catalysis, sensing and imaging [3−10]. Shape and size selective synthesis of nanosized metal particles are significant both from the fundamental point of view and specific applications. Several synthesis methods have been developed for generation of metal nanoparticles, such as chemical, photochemical, electrochemical, radiolytic etc. Usually in a chemical method metal nanoparticles are generated by reduction of metal ion precursors in solution by chemical reducing agents. After discovery of radioactivity and X-ray the effect of radiation in water were well established. Gamma radiolysis provides a clean method for synthesis of metal nanoparticles. The gamma radiation energy is deposited throughout the solution producing primary radiolytic radicals. These radicals are highly reactive and can undergo redox reaction with a suitable molecule/ species. By adding an appropriate scavenger for oxidizing radicals a total reducing environment can be created in the system. Metal ion precursors present in a solution are converted to zerovelent metal atoms in this reducing environment, which finally gives rise to metal nanoparticles in presence of a stabilizer. The radicals generated through water (solvent) radiolysis have reduction potential more negative than silver or gold ions, hence they can readily reduce these ions. Unlike chemical reduction method, in radiolytic method it is easier to control the size, shape and size distribution of nanoparticles by optimising parameters such as dose and dose rate. As the dose rate increases, the particles become smaller and less dispersed in size [11]. Metal nanoparticles possess large surface energy; hence have the ability to adsorb small molecules. The recognition and capture of molecules at solid surfaces has numerous environmental and bioanalytical applications [12]. Due to ease of functionalization, greater sensitivity, size dependent optical properties and photostability metal nanoparticles are used as probe in detection and imaging of biomolecules [13−18]. The principle for non-functionalized metal nanoparticles is based on spectral changes induced by either strong interaction of nanoparticles towards the analyte molecule or aggregation of the nanoparticles in presence of the analyte [19]. In certain cases nanoparticles are functionalized to specifically bind to a target analyte.

1.2. Classification of nanomaterials

Nanoscaled materials are usually categorized as materials having structured components with at least one dimension less than 100 nm. Smaller nanoparticles containing 10^4 or less atoms are refered to as nanoclusters. These clusters are of interest because they can explain the transition from atomic properties to bulk material properties. There are different types of nanoclusters as explained below.

a). Van der Waals nanoclusters

Inert gas atoms form nanoclusters that are weakly bound by the Van der Waals force. The long-range atomic attraction is due to the induced dipole force.

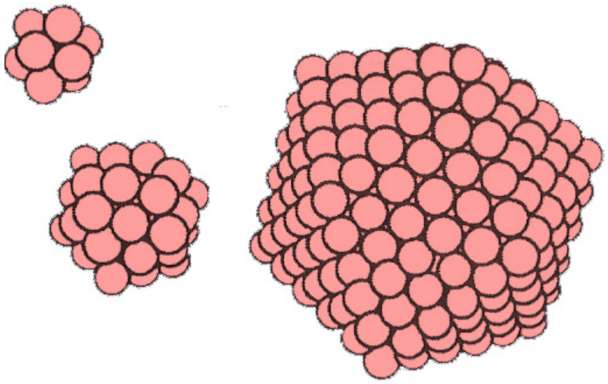

Figure 1.1: Schematic representation of icosahedral shapes of Van der Waals clusters for different numbers of atoms

The short range repulsion is due to quantum closed shell electronic interactions and the binding energy per atom is less than 0.3 eV [20].

Echt, et al. [21] have shown experimentally that rare gases form Van der Waals clusters with icosahedral shapes as shown in Figure 1.1.

b). Ionic nanocluster

Ionic clusters are formed from ions attracted by the electrostatic force. NaCl is a typical example of an ionic cluster. The electrostatic bonds in ionic clusters are around 2-4 eV per atom. This is ten times as strong as the bond of a Van der Waals nanocluster [20]. Figure 1.2. shows the crystal structure of NaCl.

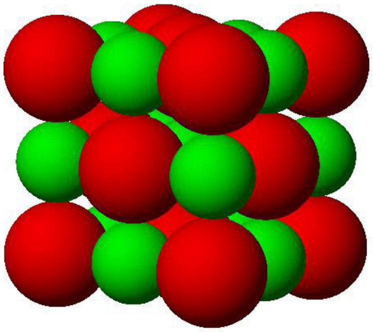

Figure 1.2: The crystal structure of NaCl

c). Metal nanoclusters

Metal nanoclusters, are more complicated in their bonding. Some metals bond primarily by the outer valence *sp* electrons. Others bond with the *d* orbitals below the valence orbitals. Because of the variation in bonds of metal clusters, the strength can vary from about 0.5 to 3 eV per atom [20]. Metal nanocluster of certain number of atoms possessing extraordinary stability originating from either atomic or electronic shell closing are known as magic clusters [22]. Most of the metal clusters show following series of magic numbers: 2, 8, 18, 20, 34, 40, 58 etc. It is important to understand the crystal structure of metal nanoparticles to explain the chemistry on their surfaces. For most of the metals the crystal structure remains intact even in nano scale. Usually the metals possess cubic lattices. Typical elements that crystallize in the face centred cubic (FCC) structure include: Cu, Ag, Au, Ni, Pd, Pt, and Al. Typical elements that crystallize in the body centred cubic (BCC) structure include: Fe, Cr, V, Nb, Ta, W and Mo [23,24].

1.3. Stabilization of metal nanoparticles

The nanoparticles having large surface energy coalesce to give thermodynamically favoured bulk particle. In the absence of any counteractive repulsive forces the van der Waals forces between two metal nanoparticles would lead towards coagulation. Hence for spatial confinement of the particles in nano range it is essential to stabilize the particles. This can be achieved by either electrostatic or steric stabilization [25,12] by using a capping agent such as polymer [26,27], surfactant [28], solid support [29] or ligand [30] having suitable functional groups. Electrostatic stabilization is realized by an electrical double layer arising from the attraction of negatively charged ions to the metal nanoparticles (Figure 1.3a) explained by DLVO theory [31].

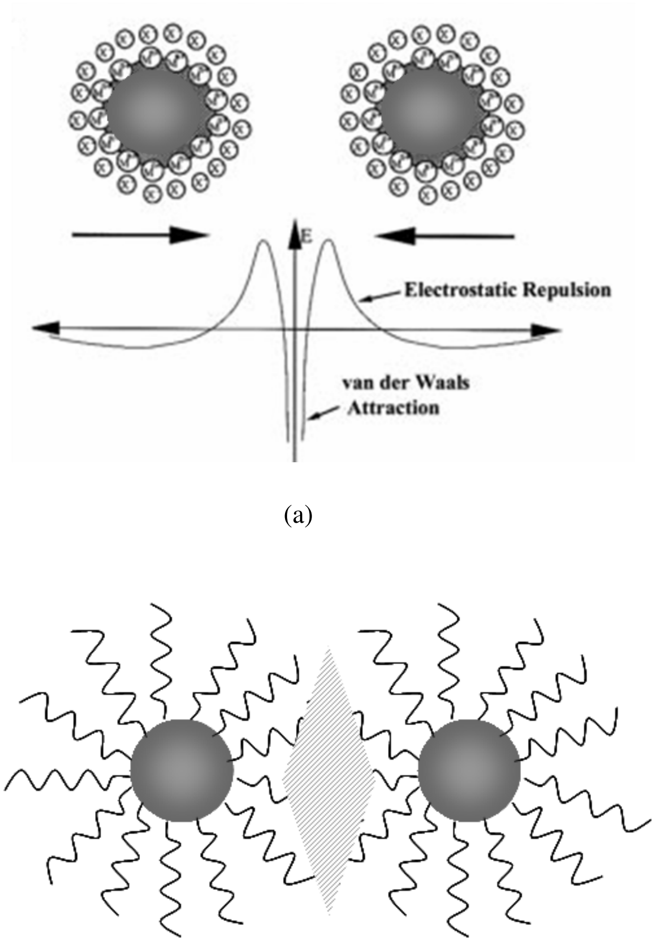

(a)

(b)

Figure 1.3: (a) Electrostatic stabilization of nanostructured metal colloids, (b) Steric stabilization of nanostructured metal colloids

The positive counter ions then form a second layer. Steric stabilization in solution is achieved by binding of polymers or surfactant molecules with long alkyl chains to the particle surface. The long chains of the organic molecules prevent the particles from coming close to each other (Figure 1.3b). The electrostatic stabilization of metal nanoparticles is rather weak and it is very sensitive to ionic strength of the dispersion medium. In addition it only works in polar liquid which can dissolve electrolytes. However, as the method is simple and economic, electrostatic stabilization is still widely used in stabilizing dispersions in aqueous media. On the other hand, steric stabilization is relatively insensitive to the presence of electrolyte and it is effective in both non-aqueous and aqueous media.

1.4. Anisotropic metal nanoparticles

Although isotropic gold nanoparticles show intense surface plasmon absorption larger than organic dye molecules, the strength of absorption is weakly dependent on its size, which limits its application in sensing. Whereas in case of anisotropic nanoparticles, especially nanorods the surface plasmon band is not only enhanced but also becomes strongly tunable as a function of aspect ratio (length/width). Nanorods possess two types of electronic oscillations in response to incident light, namely transverse and longitudinal plasmon oscillation along short axis and long axis respectively [32]. The spherical shape being thermodynamically more stable shape is easy to form, where as to generate anisotropic shaped nanoparticles parameters like, the nature of capping agent and reducing agent, concentration of metal ion precursor, capping agent and certain additives are critically controlled. Preferential adsorption of additives, namely Ag^+ on certain facets of nanocrystal induces anisotropy, whereas capping molecules (surfactants) in relatively high concentration provides tubular template for directional crystal growth.

1.5. Optical absorption properties of metal nanoparticles: Theoretical background

Unlike bulk gold metal, nanoscale gold spheres are red or violet in aqueous solution. Similarly silver metal nanoparticles are yellow in aqueous solution. The bright colors possessed by noble metal nanoparticles are due to the collective oscillations of conduction band electrons that are excited by light of appropriate frequencies. Since nanoparticles have a high surface area to volume ratio the surface plasmon resonance frequency is highly sensitive to the shape, size of nanoparticle and dielectric nature of its interface with the local environment [33–36]. These properties can be advantageously used for the purpose of the development of novel biosensors, chemical sensors, electro-optical devices, material for high-capacity data storage media and substrates for enhanced Raman spectroscopy [37-43]. The light scattering due to collective oscillation of the conduction electrons induced by the incident electric field in nanometer sized colloidal metal particles is known as localized surface plasmon resonance and these are surface electromagnetic waves that propagate in a direction parallel to the metal/dielectric (or metal/vacuum) interface [4]. Figure 1.4 shows the displacement of the conduction electron charge cloud relative to the nuclei of spherical nanoparticle. The electric field of an incoming light wave induces a polarization of the conduction electrons with respect to the much heavier ionic core of a spherical gold nanoparticle. A net charge difference is only felt at the nanoparticle boundaries (surface), which in turn acts as a restoring force. In this way a dipolar oscillation of the electrons is created with period. This is known as the surface plasmon absorption. The position of the plasmon band (extinction spectrum) is best measured on a UV-visible spectrophotometer and appears as a band with extremely high extinction coefficients (up to 10^{11} $mol^{-1}dm^{3}$ cm^{-1}) [44]. The size, shape and dielectric environment influence the optical behavior of metal nanoparticles [45–48].

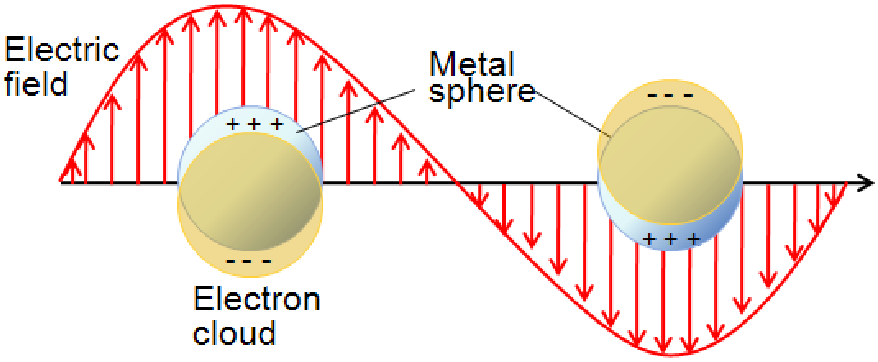

Figure 1.4: Schematic illustration of the collective oscillation of free electrons under the effect of an electromagnetic wave

In semiconductor nanomaterials the mechanism of optical absorption is different. In bulk semiconductors the charge careers are electrons and holes. The electronic excitation consists of loosely bounded electron hole pair and usually delocalised over a length much larger than the lattice constant. Such a distance is known as the Bohr radius, which is few nanometers [49]. The minimum energy required to separate the charge carriers is known as the band gap energy of the semiconductor. When the size of the semiconductor material becomes comparable to or smaller than, the Bohr radius, so that the space in which the charge carriers move decreases and this is called quantum confinement in semiconductor nanomaterials [50]. This leads to an increase in the band gap energy, the electron and hole kinetic energy, and the density of the charge carriers within and at the nanoparticle surface.

For a dilute solution of metallic small spherical particles, the resonance conditions to achieve absorption by light can be calculated using the analytical treatment of Maxwell's equations as demonstrated by Gustav Mie [45,51,52]. Gustav Mie was the first to explain the observed intense color of dispersed colloidal gold particles in 1908. Metal nanoparticles are small in respect to the wavelength of visible light and they show characteristic absorbing and scattering properties. Gustav Mie calculated the absorbance of colloidal gold particles as a function of the particle size using classical electromagnetic theory with the bulk optical properties of metallic gold. The main assumption of Mie's theory of the optical absorption by small particles is that the particle and its surrounding medium are each homogeneous and describable by their bulk optical dielectric functions. In general, solutions to Maxwell's equations for this geometry yield an expression for the absorption cross section, which is a sum over electric and magnetic multipoles (spherical vector harmonics and Legendre polynomials). When the size of a particle is much smaller than the wavelength of the exciting radiation, the absorption is dominated by the dipole term, with a cross section $\sigma(\omega)$ given by,

$$\sigma(\omega) = 9\varepsilon_m^{3/2} v_0 \frac{\omega}{c} \frac{\varepsilon_2(\omega)}{[\varepsilon_1(\omega) + 2\varepsilon_m]^2 + \varepsilon_2(\omega)^2} \tag{1.1}$$

Where, ω is the angular frequency of exciting radiation, c is the speed of exciting radiation, ε_m is the dielectric function of the surrounding medium, V_0 is the volume of absorbing particle, $\varepsilon_1(\omega)$ is the real part of the dielectric function of the metallic nanoparticle, $\varepsilon_2(\omega)$ is the Imaginary part of the dielectric function of the metallic nanoparticle.

In the resonance condition the real part of the dielectric function of the metal equals the dielectric function of the surrounding medium in which the particles are dispersed [45,53]. The resonance condition is fulfilled when,

$$\varepsilon_1(\omega) = -2\varepsilon_m \tag{1.2}$$

If $\varepsilon_2(\omega)$ is small or weakly dependent on ω.

This condition also implies that the frequency of the plasmon band depends on the dielectric constant of its local medium. The above equation has been used extensively to explain the absorption spectra of small metallic nanoparticles in a qualitative as well as quantitative manner [54,55]. However, for larger nanoparticles (greater than about 20 nm in the case of gold) where the dipole approximation is no longer valid, the plasmon resonance depends explicitly on the particle size. The larger the particles become, the more important are the higher-order modes as the light can no longer polarize the nanoparticles homogeneously. These higher-order modes peak at lower energies and therefore the plasmon band red shifts with increasing particle size [54]. At the same time, the plasmon bandwidth increases with increasing particle size. As the optical absorption spectra depend directly on the size of the nanoparticles, this is regarded as an extrinsic size effects. The mathematical equation given by Mie theory for nanoparticles, which are significantly smaller than the wavelength of the exciting light ($\lambda >> 2R$, where R is the radius of the nanoparticle) (Equation 1.1) could not predict the size dependency of the position of the surface plasmon absorption band of metallic nanoparticles. This size dependency factor was taken into account by assuming size dependent dielectric functions [56]. The spectral changes due to alloying and formation of core shell type bimetallic nanoparticles have been explained by applying Drude's theory for describing free electron behaviour in the Mie equation [57,58]. For anisotropic nanoparticles, especially nanorods the direction of the plasmon oscillation depends on the orientation of the particle axis with respect to the oscillating electric field of the incident light. In case of metal nanorods there are two axes, i.e., transverse and longitudinal axes as explained in previous section. This results in two plasmon absorptions unlike one single plasmon band for spherical nanoparticles, known as transverse plasmon resonance and the longitudinal plasmon resonance [46]. Theoretically this can be explained by modified Mie theory, known as Gans theory [59−62,52]. The optical absorption of metal nanorods depends on their aspect ratio (length/width). The linear spectral dependence of the longitudinal surface plasmon absorption can be reproduced using Gans' theory [63,64].

1.6. Basic aspects of radiation chemistry

1.6.1. Types and energy of ionizing radiation

Radiation chemistry deals with the study of chemical changes induced by absorption of high-energy electromagnetic radiation (gamma-rays, X-rays) (Figure 1.5), charged particles (electrons, protons, deuterons, α-particles) or uncharged particle (neutron), termed as "ionizing radiation", with energy in the range of 10^2 to 10^7 eV. Its origins lie in the discovery of ionizing radiations from naturally occurring isotopes in the late 19th century. The high energy radiation can cause ionization and excitation of varied types of molecules and atoms in many possible ways resulting in the formation of a variety of reactive species [65,66].

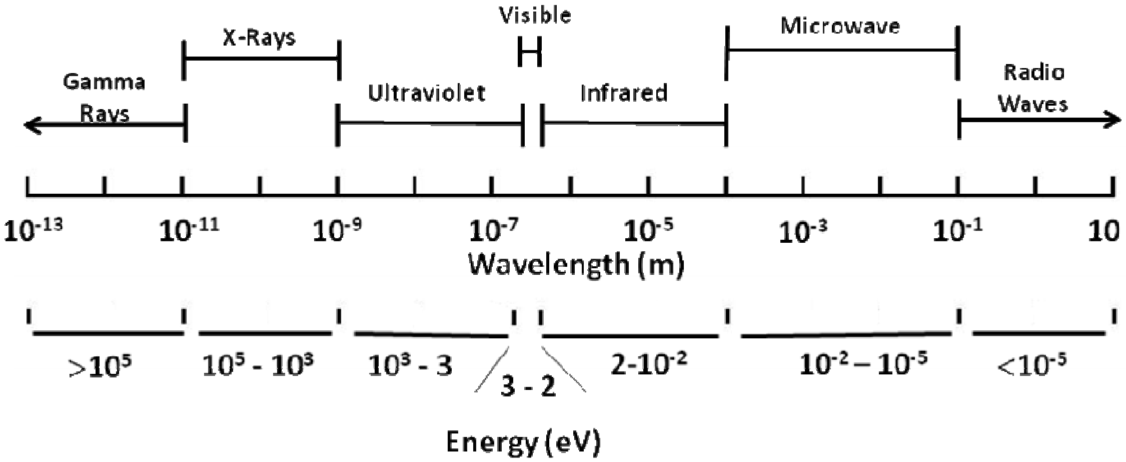

Figure 1.5: Energy diagram for electromagnetic spectrum

The initial ionization events results in formation and inhomogeneous distribution of highly reactive chemical species in sub-picosecond time scale. Radiation chemistry is different from photochemistry in one aspect i.e., interaction of ionizing radiation with atoms and molecules in their path is non-specific and non-selective in nature unlike in photochemistry where one can selectively excite, ionize or break a particular bond in a given molecule by choosing the energy of a photon. The interaction of ionizing radiation with material depends on the nature of radiation and properties of the material. The important parameters on which the interaction will depend are energy, mass and charge of the radiation, and atomic number or electron density of the material [67]. In this chapter the mechanisms of interaction of electromagnetic radiation and electrons are discussed in brief.

1.6.2. Interaction of electromagnetic radiation with medium

The electromagnetic radiations such as X-rays (extra nuclear origin) or gamma (γ) rays (produced from the atomic nuclei) belong to the class of ionizing radiation. The γ rays emitted by radioactive isotopes are mono-energetic, possessing one or more discrete energies. e.g.,

^{60}Co emits γ-photons of energy 1.332 MeV and 1.173 MeV. For a narrow beam, the intensity of gamma radiation transmitted through an absorber is given by,

$$I = I_0 e^{-\mu x} \tag{1.3}$$

Where, I_o is the incident radiation intensity, x is the thickness of material through which radiation has traversed and μ is the linear attenuation coefficient, which is the sum of a number of partial coefficients representing different processes occurring inside the absorber. These are (i)photoelectric effect, (ii)compton scattering, (iii)pair production, (iv)coherent scattering and (v)photonuclear reactions. The relative importance of each process depends on the photon energy and the atomic number (Z) of the absorbing material. Coherent scattering is of importance for low energy photons (<0.1 MeV), photonuclear reactions are possible with photons of energies in the range of 2 to 8 MeV for low Z materials and in the region of 7-20 MeV for high Z materials. Thus, for gamma radiation emitted by ^{60}Co source, only the first three interaction processes are of importance and are discussed below briefly.

i). Photoelectric effect*:* This process is the principal interaction process at low photon energies. In photoelectric process photon interacts with a bound electron in an atom and transfers all its energy and ejects it from the atom. The energy of the ejected electron (E_e) is equal to the difference between the energy of the photon (E_o) and the binding energy of the electron (E_b) (Equation 1.4).

$$E_e = E_0 - E_b \tag{1.4}$$

ii). Compton scattering: Compton scattering occurs when a photon with energy E_o interacts with a loosely bound or free electron. The resulting photon is deflected with reduced energy E_r at an angle θ to the direction of the incident photon and the electron gets accelerated at an angle φ with recoil energy E_e. The relation between the various parameters is given by equation (1.5). The energy of recoil electron is given by the Equation (1.6).

$$E_\gamma = \frac{E_0}{1 + (E_0/m_e c^2)(1 - \cos\theta)} \tag{1.5}$$

$$E_\gamma = E_0 - E_e \tag{1.6}$$

Compton scattering predominates for photon energies between 30 keV to 20 MeV for low Z materials.

iii). Pair production: This process is the reverse of electron -positron annihilation phenomenon and involves the complete absorption of a photon in the vicinity of an atomic nucleus resulting in the formation of two particles, an electron and a positron. Thus, this is an example of a physical process in which energy is converted into mass (Equation 1.7). Since the rest mass of an electron or positron is 0.511 MeV, for pair production to occur, minimum photon energy must be 1.02 MeV (i.e. $2m_ec^2$)

$$E_0 = E_e + E_{e+} + 2m_ec^2 \tag{1.7}$$

Thus depending on the incident photon energy, the photon gets attenuated and the total linear attenuation coefficient (μ) is given by Equation (1.8).

$$\mu = \tau + \sigma + \kappa \tag{1.8}$$

where, τ, σ, κ are the linear attenuation coefficient of photoelectric, compton and pair production process respectively.

1.6.3. Interaction of electrons with medium

Electron interacts with matter via four processes namely, emission of bremsstrahlung radiation, inelastic collision, elastic collision and Cerenkov emission. The relative importance of these processes depends mostly on the energy of the electrons and to a lesser extent on the nature of the absorbing material.

(i). Emission of bremsstrahlung radiation: High energy electrons passing close to the nucleus of an atom are decelerated due to their interaction with the electric field of the nucleus and radiate electromagnetic radiation called bremsstrahlung radiation. Bremsstrahlung emission is negligible below 100 KeV but increases rapidly with increasing energy, and is the dominant process at electron energy between 10 - 100 MeV.

(ii). Inelastic scattering: Inelastic scattering occurs when electrons interact with the electrostatic field of atomic electrons so that the atomic electrons are either raised to a higher energy level (excitation) or are ejected from the atom (ionization). Inelastic scattering is the only process that generates excited or ionized species in the absorber material and results in significant chemical or biological change. The incident primary electrons are slowed down and cascades of secondary and tertiary electrons are produced. The average amount of kinetic energy lost per unit length by electron through coulomb interaction with atomic electrons in a medium is defined as the specific energy loss or stopping power (S) of the medium and is defined by the Bethe's Equation (1.9).

$$S = -\frac{dE}{dx} = \frac{2\pi e^4 N_0 Z}{m_0 v^2}\left[\ln\frac{m_0 v^2 E}{2I^2(1-\beta^2)} - \left(2\sqrt{1-\beta^2} - 1 + \beta^2\right)\ln 2 + 1 - \beta^2 + \frac{1}{8}\left(1 - \sqrt{1-\beta^2}\right)^2\right] \tag{1.9}$$

Where, *e* and m_o represents the charge rest mass of electron, *v* is the velocity of electron, N_o is the number of atoms cm^{-3} in the medium, *Z* is the atomic number and *l* is the mean excitation potential of the electrons in the stopping material, β is the ratio of *v* to the speed of light *c*.

(iii). Elastic scattering: This is a quite frequent phenomenon because of the small mass of electrons and happens when electrons get deflected by the electrostatic field of an atomic nucleus. This essentially leads to a change in the direction of motion of electrons and is more probable for electrons with low energy and target with high atomic number.

(iv). Cerenkov emission: Electrons with velocity higher than that of light in a particular medium interacts and emits electromagnetic radiation, called Cerenkov radiation. This phenomenon is responsible for the blue glow observed around high intensity γ -sources stored under water.

The radiative emission is the predominant process at high electron energies and for high *Z* materials, whereas elastic and inelastic scattering predominates at low electron energies.

1.6.4. Distribution of primary reactive species in the medium

The electrons from compton scattering of ^{60}Co γ-rays have an average energy of 440 keV. These electrons, also termed as δ-rays, bring about further ionization and excitation. Such events along the main track or the branch track (δ-ray) are called isolated spurs. In water, the isolated spurs contain on an average 6 active species for about 100 eV energy absorbed. When δ-ray electron energy is < 5 keV, its penetration becomes very less and the spurs so formed in close vicinity overlap and take cylindrical shape, known as short tracks. As the electron energy becomes less than 500 eV, even denser regions of ionization, which look like large spurs, called as blobs, are produced (Figure 1.6) [67]. The typical energy distribution ratio for a 440 keV electron in water is spur (64%), short tracks (25%) and blobs (11%). In contrast to this, for heavy charged particles (high LET), more energy will be deposited in blobs and short tracks than in isolated spurs.

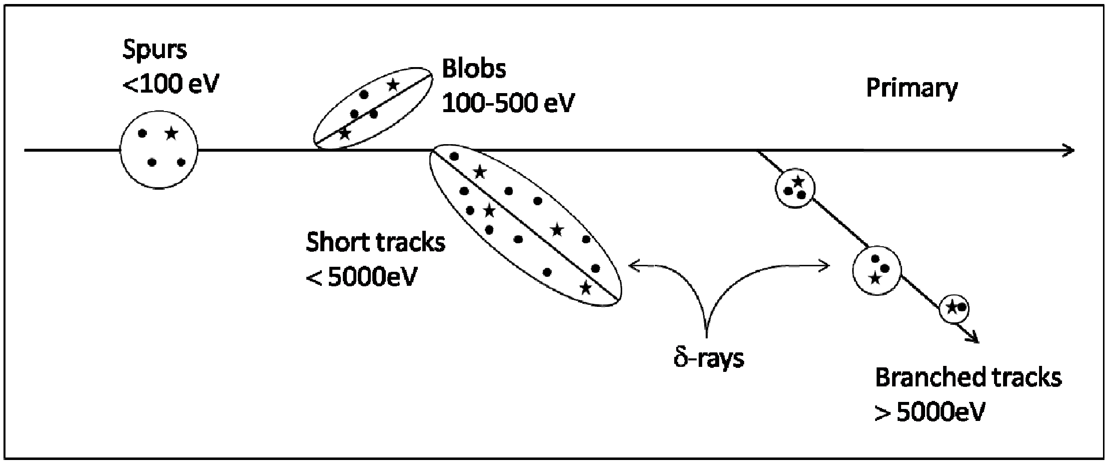

Figure 1.6: Distribution of ions and exited species along the track of fast electron; (•) represents the ions and (★) represents the exited species

1.6.5. Depth dose profiles for gamma radiation

When a beam of radiation interacts with the substrate, the secondary electron radiation builds upto a maximum at a distance below the impinging surface that is equal to the maximum range of secondary electrons. It falls off as the primary beam gets attenuated. The *depth-dose* distribution curves for γ-rays in water shows maximum for energy absorbed per unit shift to larger distance from the surface as the energy of photon increases. γ-rays from ^{60}Co having an average energy of 1.25 MeV show maximum *depth dose* at 0.5 cm from the surface in water. Typical depth dose curve for irradiation of water by electromagnetic radiation is shown in Figure 1.7.

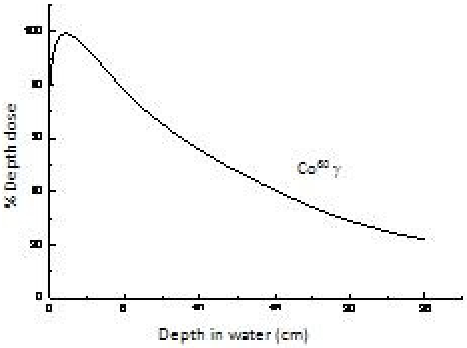

Figure 1.7: Percent depth dose curve for the irradiation of water by ^{60}Co γ radiation

1.6.6. Radiation-chemical yield

Conventionally, radiation chemical yields have been described in terms of G values, which represent the number of molecules of the product formed or starting material changed per 100 eV of energy absorbed. The SI unit of radiation chemical yield is defined as change in the number of moles of material formed or decomposed by energy absorption of 1 Joule. G-values reported in terms of number of species formed per 100 eV can be converted to SI units using the following relationship (1.10).

$$G\,(mol\,J^{-1}) = G\,(number\ per\ 100ev) \times 1.036 \times 10^{-7} \qquad (1.10)$$

1.6.7. Radiation chemistry of water

Understanding of radiation chemistry of water is of importance as water is present in most biological and chemical systems. For water, the sequence of events, like formation and solvation of the primary species, and the time scale of events initiated either by fast electrons from an accelerator or by ^{60}Co γ- rays is illustrated in Figure1.8 [68–70]. High energy radiation deposits energy in the medium in 10^{-16} seconds resulting in formation of “spurs” containing positively charged ions, electrons and excited species [67]. The term “spur” refers to a small volume of material in which the deposition of radiation energy has produced a small number of excited and ionized molecules. Energetically unstable positively charged ions (H_2O^+) undergo ion molecule reaction in 10^{-14} seconds producing $^{\bullet}OH$ radicals [71].

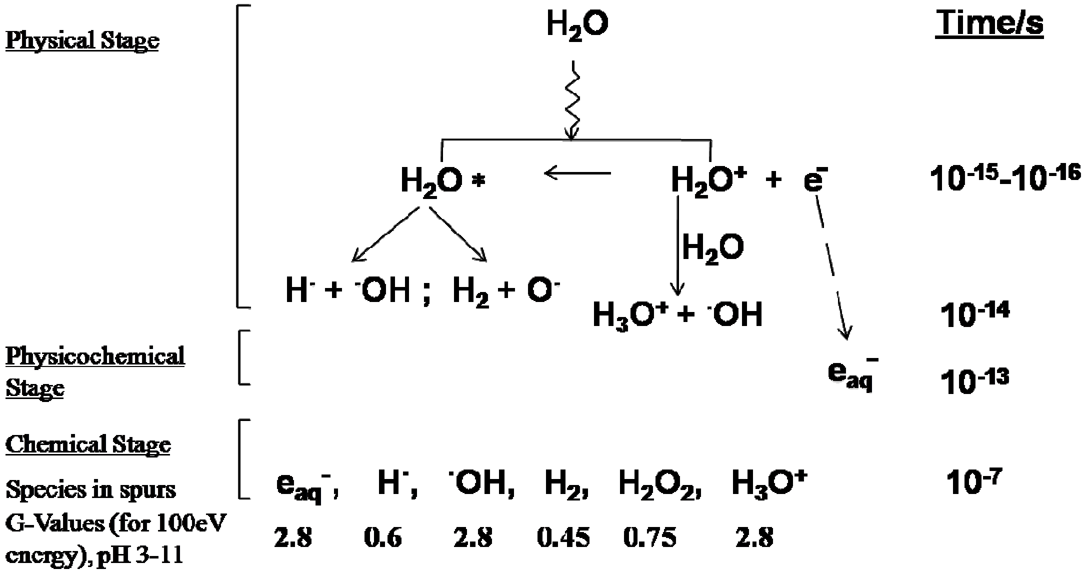

Figure 1.8: Sequence of events in water Radiolysis and formation of primary species from 10^{-16} to 10^{-7} second

The excited water molecules decompose in 10^{-14} seconds yielding $H^{\bullet}$ and $^{\bullet}OH$ radicals. The electron released during ionization can also bring about further ionization provided it has sufficient kinetic energy. Eventually, its energy will fall below the ionization threshold of water and then it dissipates rest of its energy by exciting vibrational and rotational modes of the solvent molecules. Finally, it would be localized in a potential energy well long enough to become solvated as a result of molecular dipoles rotating under the influence of the negative charge, and thus get stabilized [72]. The electrons get thermalised in about 10^{-13} seconds and subsequently get hydrated or solvated in less than 10^{-12} seconds and called hydrated electron (e_{aq}^{-}) [73]. These species, i.e. hydrated electrons, hydrogen atoms and hydroxyl radicals are formed in the spurs can react with one another to reform water or molecular products, H_2 and H_2O_2, while the remaining escape into the bulk solution. This spur expansion is complete in about 10^{-7}s. The reactions occurring during spur expansion are listed in Table 1.1. After about 10^{-7} second, the species homogeneously are known as primary species.Hence the overall reaction for generation of primary species by water radiolysis is given by Equation (1.11).

$$H_2O \overset{\gamma}{\rightsquigarrow} e_{aq}^{-} + H^{\bullet} + {}^{\bullet}OH + H_2 + H_2O_2 + H_3O^{+} \qquad (1.11)$$

Table 1.1: Spur reactions in water

Reaction			**Rate constant (10^{10} dm^3 mol^{-1} s^{-1})**
$e_{aq}^{-} + e_{aq}^{-}$	$\longrightarrow$	$H_2 + 2\,OH^{\bullet}$	0.54
$e_{aq}^{-} + OH^{\bullet}$	$\longrightarrow$	OH^{-}	3.0
$e_{aq}^{-} + H_3O^{+}$	$\longrightarrow$	$H^{\bullet} + H_2O$	2.3
$e_{aq}^{-} + H^{\bullet}$	$\longrightarrow$	$H_2 + OH^{-}$	2.5
$H^{\bullet} + H^{\bullet}$	$\longrightarrow$	H_2	1.3
$OH^{\bullet} + OH^{\bullet}$	$\longrightarrow$	H_2O_2	0.53
$H^{\bullet} + OH^{\bullet}$	$\longrightarrow$	H_2O	3.2
$H_3O^{+} + OH^{-}$	$\longrightarrow$	$2H_2O$	14.3

In the nanosecond time scale, different processes ultimately produce hydrated electrons (e_{aq}^{-}), $^{\bullet}OH$, $H^{\bullet}$ and molecular products H_2 and H_2O_2. These species can subsequently react with solutes present in the system. In water, 10^{-7} seconds is the lifetime of the radicals reacting at a diffusion-controlled rate with a solute whose concentration is 10^{-3} mol dm^{-3}.

Under these conditions the G-values of e_{aq}^{-}, $H^{\bullet}$ and ${}^{\bullet}OH$ radicals at 10^{-7} second are shown in the Figure 1.8 [65,69]. Classical kinetics is generally valid in this type of system.

1.6.8. Important reducing radicals in aqueous solutions

The hydrated electron (e_{aq}^{-}) and the hydrogen atom ($H^{\cdot}$) are the primary radicals which are reducing in nature. The redox-potential value E° = -2.9 V vs NHE for e_{aq}^{-} suggests that it is a powerful reducing agent (Table 1.2). Its reactions with solutes are best understood in terms of availability of a suitable vacant orbital in the solute molecule (S) for the electron to get localized [65,72]. A typical reaction is represented as in Equation (1.12) where the *n* represents the positive charge on the solute.

$$e_{aq}^{-} + S^{n} \longrightarrow S^{n-1} \qquad (1.12)$$

The rate constant values for typical hydrated electron reactions support the above requirement. For water, the rate constant, k is only 16 $dm^3\ mol^{-1}\ s^{-1}$ as a low-lying vacant orbital is absent in water. It also explains the sufficiently long half-life of e_{aq}^{-} in water. With solutes having low lying π^* orbital, the k value approaches the diffusion controlled limit.

Table 1.2: Properties of e_{aq}^{-}

Radius of charge distribution	0.25 – 0.30 nm
Diffusion coefficient	$4.9 \times 10^{-5}\ cm^2\ s^{-1}$
Spectral characteristics	$\lambda_{max} = 715nm$, $\varepsilon = 18400\ dm^3\ mol^{-1}\ cm^{-1}$
Reduction potential (vs NHE)	-2.9 V at pH 7
Half life (pH ≥ 7)	$6.6 \times 10^{-4}s$

In neutral and acidic pH, the $H^{\cdot}$ is an important reducing species with its redox potential value, E^0 = -2.3 V vs NHE (Table 1.3).

Table 1.3: Properties of $H^{\bullet}$ atom

Diffusion coefficient	$8.0 \times 10^{-5}\ cm^2\ s^{-1}$
Spectral characteristics	$\lambda_{max} = 200$ nm
Reduction potential (vs NHE)	-2.3 V at pH 0
pk_a	9.6

It can be thought of as a weak acid with pKa of 9.6. While it readily reduces substrates with more positive redox potential, the corresponding rates are slower than for e_{aq}^- reactions. With substrate having center of unsaturation, it is known to add readily to form H adduct. From a solute devoid of π- electrons, it abstracts hydrogen atom giving rise to a solute transient radical. Optical absorption of $H^\bullet$ lies around 200 nm with very low extinction coefficient, which is normally not accessible with the available experimental facilities. Thus, measurements of $H^\bullet$ reaction parameters are made by competition kinetics method or from the transient formation kinetics.

1.6.9. Important oxidizing radicals in aqueous solutions

Hydroxyl radical ($^\bullet OH$) is a strong oxidizing radical ($E^0 = 2.8$ V vs NHE) and like H·, it absorbs in the far UV, therefore, its kinetic parameters are also estimated by competition kinetics or transient formation kinetics. In strongly basic solution (pH > 11.9), it is deprotonated to give $O^{\cdot -}$. The properties of $^\bullet OH$ radical are listed in Table 1.4.

Table 1.4: Properties of $^\bullet$OH radical

Diffusion coefficient	2.2×10^{-5} cm^2 s^{-1}
Spectral characteristics	$\lambda_{max} = 235$ nm
Reduction potential (vs NHE)	+2.7V at pH 0, +1.9V at pH 7
pk_a	11.9

With organic compounds the hydroxyl radical can undergo mainly four types of reactions:

(i). Electron transfer

$$\mathbf{{}^\bullet OH + S^n \longrightarrow S^{n+} + OH^-} \qquad (1.13)$$

(ii). Hydrogen abstraction

$$\mathbf{{}^\bullet OH + RH \longrightarrow R^\bullet + H_2O} \qquad (1.14)$$

(iii). Addition

$$\mathbf{{}^\bullet OH + RH \longrightarrow RHOH^\bullet} \qquad (1.15)$$

(iv). Displacement

$$\mathbf{{}^\bullet OH + RX \longrightarrow X^\bullet + ROH} \qquad (1.16)$$

1.7. General method of synthesis of metal nanoparticles

Top-down and bottom-up are two approaches for the synthesis of nanomaterials [74,12]. Attrition or milling is an example of top-down method and the bottom approach basically consists of generation of colloidal dispersion by wet chemical synthesis method. The bottom up approach is preferred by researchers to obtain narrow size distribution of nanoparticles. This method of synthesis refers to build-up of a material from the bottom: atom-by-atom, molecule-by-molecule, cluster-by-cluster. As concerns the preparation of the colloidal metal nanoparticles from their precursors, various chemical reduction routes, including the use of chemical reductants in both aqueous and nonaqueous solvents, electrochemical method [75], sonochemical method [76], radiolytic [77] and photochemical [78] method have been widely studied for different purposes of application. Wet chemical methods to prepare metal colloids are usually based on the reduction of a suitable metal salt, in the presence of stabilizers. Synthesis of nanoparticles of metals using irradiation is now well established and the mechanism of production is reasonably understood. Spherical shape being thermodynamically most stable, the formation of spherical nanoparticles is more probable in any wet chemical synthesis method. Since the optical properties of clusters of metal nanoparticles are sensitive to size, shape, and composition, it is of importance to design a process that results in the formation of non spherical nanoparticles. Anisotropic metal nanoparticles have been synthesized in chemical method by using step wise growth method in presence of structure directing agent cetyl trimethyl ammonium bromide (CTAB) and nanoparticle seeds [79].

1.8. Brief discussion of chemical reduction method

The citrate reduction method proposed by Turkevich [80,81] consists of synthesis of spherical gold nanoparticles of ~20 nm diameter by reducing boiled aqueous hydrogen tetrachloro aurate/ chlorauric acid ($HAuCl_4$) solution with sodium citrate ($(H_2CCOOH)_2C(OH)COONa$).

$$3(H_2CCOOH)_2C(OH)COO^- + 2AuCl_4^- \rightleftharpoons \\ 3(H_2CCOOH)_2C(OH)C = O + 2Au + 8Cl^- + 3CO_2 + 3H^+ \qquad (1.17)$$

Other chemical methods involve reduction of metal ion precursor by reducing agents such as, sodium borohydride [82], hydrazine [83,84], formaldehyde [85,860] and ascorbic acid [87]. The synthesis steps for generation of metal nanoparticles by wet chemical method are given in the Figure 1.9.

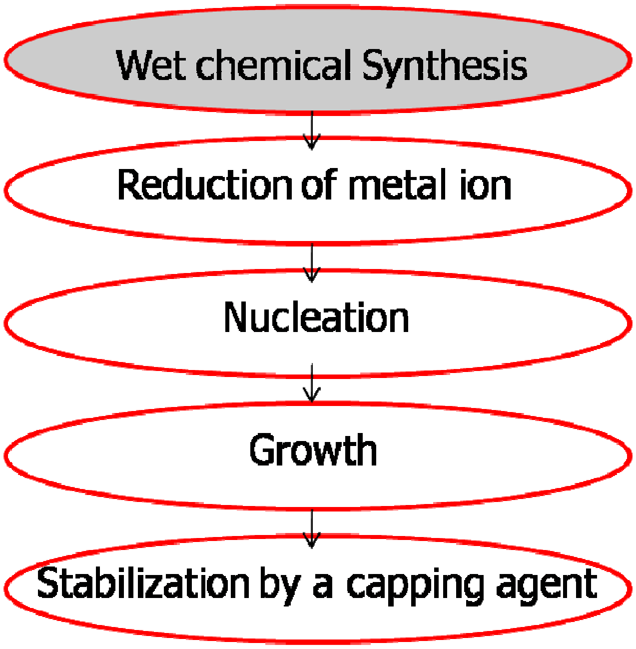

Figure 1.9: Synthesis step of metal nanoparticles in wet chemical method

Non-spherical metal nanoparticles are synthesized by template mediated method using surface active molecule cetyl trimethyl ammonium bromide (CTAB), a mild reducing agent such as ascorbic acid and metal nanoseeds. The synthesis of gold nanorods can be divided into two steps [88–92].

Step 1: Preparation of seed solution: A brownish yellow color Au nano seed solution is prepared by reducing chlorauric acid with ice-cold solution of sodium borohydride ($NaBH_4$) in presene of cetyltrimettyammonium bromide (CTAB: $C_{19}H_{42}NBr$). The seed solution was kept at room temperature to get rid of excess $NaBH_4$.

Step 2: Growth of nanorods: The gold nanorod is obtained by a stepwise growth method. Initially small amount of seed solution is mixed to a growth solution containing $HAuCl_4$, CTAB, Ascorbic acid ($C_6H_8O_6$) and a small amount of $AgNO_3$. In the next step this solution is used as seed and all other reagents will be same. In two to three steps nanorods having aspect ratio (length/width) ~ 3 are generated.

1.9. Synthesis of metal nanostructure by high energy radiation and advantages of radiolytic method

Primary radical species generated by radiolysis of water and their redox properties have been discussed in section 1.6.8. Irradiation of noble metal ion in aqueous solution results in reduction of metal ion by reducing radicals i.e., e_{aq}^- and $H^\cdot$ to generate metal atom [93–100]. These metal atom coalesce to produce nanoparticles in presence of a suitable stabilizer. The $^\cdot OH$ formed in water radiolysis are able to oxidize back the metal atoms into metal ions [101]. To prevent this oxidation, the solution is added with a scavenger of $^\cdot OH$ such as secondary alcohols or formate anions [102]. The secondary radicals formed, α -methyl-hydroxyethyl [$(CH_3)_2{}^\cdot C(OH)$] or formyl [$CO_2^{\cdot -}$] respectively are capable to reduce metal ions (Equation 1.20- Equation 1.22). The metal in zero valent state coalesce to form metal nanparticles in presence of a stabilizer (Equation 1.23- Equation 1.25).

$$\mathbf{CH_3CH(OH)CH_3 + {}^\cdot OH/H^\cdot \longrightarrow CH_3{}^\cdot C(OH)CH_3 + H_2O/H_2} \qquad (1.18)$$

$$\mathbf{HCO_2^- + {}^\cdot OH/H^\cdot \longrightarrow {}^\cdot CO_2^- + H_2O/H_2} \qquad (1.19)$$

$$\mathbf{M^+ + e_{aq}^- \longrightarrow M^0} \qquad (1.20)$$

$$\mathbf{M^+ + CH_3{}^\cdot C(OH)CH_3 \longrightarrow M^0 + CH_3COCH_3 + H^+} \qquad (1.21)$$

$$\mathbf{M^+ + {}^\cdot CO_2^- \longrightarrow M^0 + CO_2} \qquad (1.22)$$

$$\mathbf{M^0 + M^0 \longrightarrow M_2} \qquad (1.23)$$

$$\mathbf{M_m + M_n \longrightarrow M_{m+n}} \qquad (1.24)$$

$$\mathbf{M_{m+x}{}^{x+} + M_{n+y}{}^{y+} \longrightarrow M_{p+z}{}^{z+}} \qquad (1.25)$$

where m, n and p represent the nuclearities, x, y and z, the number of associated ions.

There are many advantages of irradiation method for generation of metal nanoparticles as compared to chemical reduction method. It is a room temperature process, hence capping agents, which are fragile to heat can be used in irradiation method unlike chemical method. The size shape and composition can be controlled by tuning radiation dose and dose rate. In chemical reduction method, the metal ion precursor is reduced by a chemical reducing agent such as sodium borohydride, hydrazine, aniline etc. In irradiation method reducing species like aqueous electron and hydrogen atom radical bring about the reduction reaction. The major advantage of irradiation method is that highly reactive species produced in-situ by the radiation, creates redox levels that are hard to achieve by other methods [95]. Since no chemical reducing agent is added externally it is a relatively clean method. The radiolytic synthesis methods not only have high potential to generate small clusters and metal nanoparticles of controlled size and shape, but also in studying the nucleation steps and clusters growth. Initial nucleation stage, which is very important to control the shape and size of final particles can be studied by pulse radiolysis techniques [103].

1.10. General characterization techniques

The stabilized metal nanoparticles are characterized by techniques such as UV-visible spectroscopy, X-ray diffraction technique (XRD), transmission electron miocroscopy (TEM), scanning electron microscopy (SEM), atomic force microscopy (AFM) etc (Figure 1.10) [12]. Some of the techniques have been discussed in the following section.

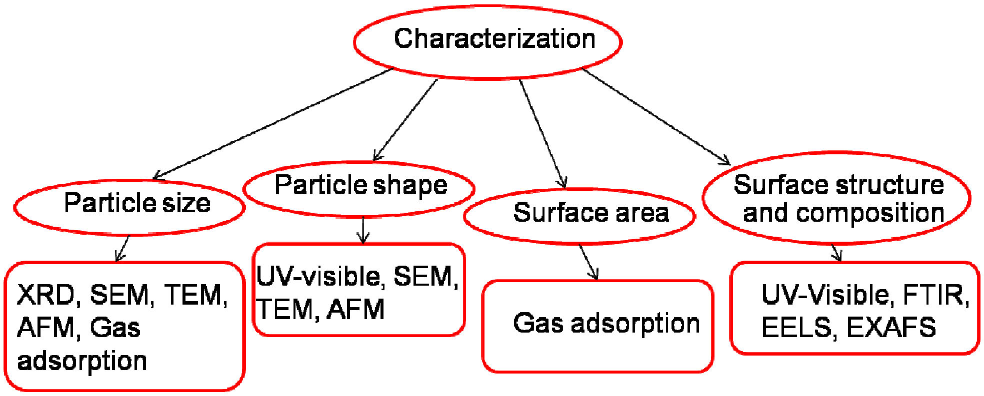

Figure 1.10: Common methods available for the characterization of nanoparticles

1.10.1. Absorbance spectroscopy

The uv-visible absorption spectroscopy is a useful technique especially to characterize noble metal nanoparticles [104], because they possess bright color visible by naked eye. These nanoparticle possess high extinction coefficient and their surface plasmon property is size and shape dependant. Hence qualitative information about the nanoparticle solution can be obtained by this technique. The absorbance is obtained by employing Beer's Law. The absorbance value (A) depends on nanoparticle concentration (c), path length (l) of measuring cell and extinction coefficient of nanopaticles (ε) (Equation 1.26).

$$A = \epsilon c l \qquad (1.26)$$

The position of the surface plasmon band depends several factors such as particle size, shape, nature of stabilising agent and temperature, extent of aggregation, presence of any adsorbate on the surface of nanoparticles as well as nature of the surrounding medium [105–108]. The plasmon bandwidth increases with decreasing size of nanoparticle in the intrinsic size region (mean diameter smaller than 25 nm), and also increases with increasing size in the extrinsic size region (mean diameter larger than 25 nm) [109]. The surface plasmon resonance shows a red- shift in the extrinsic size region and as the particle size increases [110]. The colour of gold nanoparticles changes from ruby red to purple and finally blue with increase in size. When the interparticle distances of nanoparticles become less that their average diameter the particles aggreagate, so that the plasmon resonances of each particle couple and their absobance is red shifted [5,6]. Sensors can be developed based upon these interesting optical properties on metal nanoparticles.

1.10.2. TEM

Particles smaller than 1 μm, cannot be observed by optical microscope due to diffraction effects. The amount of information a micrograph can provide depends on the resolution and the resolution mainly depends on the wavelength of the radiation beam selected for the imaging. High resolution can be achieved by a short wavelength beam.

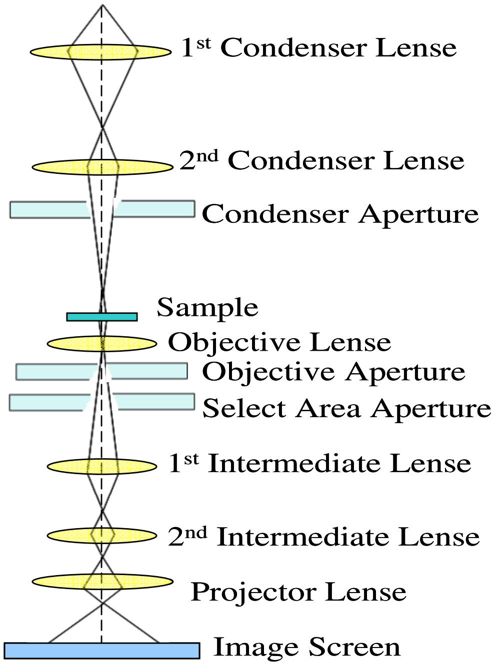

Figure 1.11: Schematic representation of TEM

Hence beyond this size imaging at higher resolution is possible by using shorter wavelength electron beam, called electron microscopy. Transmission electron microscope (TEM) is the most widely used technique to characterize metal nanoparticles. TEM machine works much like a slide projector except that they shine a beam of electrons (typically ~100-300 kV) and the transmitted beam is projected onto a phosphor screen for final image formation [Figure 1.11]. TEM machine equipped with other accessories can provide information regarding topography, morphology, dispersity, composition and crystallography of the sample. HRTEM (high resolution TEM) can go upto a magnification of ~10,00,000 with a resolution of ~1 A° [111].

1.10.3. SEM

In scanning electron microscope (SEM) the image of surface of specimen is obtained by scanning the surface with electron beam of accelerating voltage < 50kV [12]. The secondary electrons or the backscattered electrons are collected by the detector and analyzed for obtaining the image [Figure 1.12]. SEM gives information about the topography and morphology of the sample and it can go upto 1,00,000 magnification with a resolution of ~1.5 nm [112].

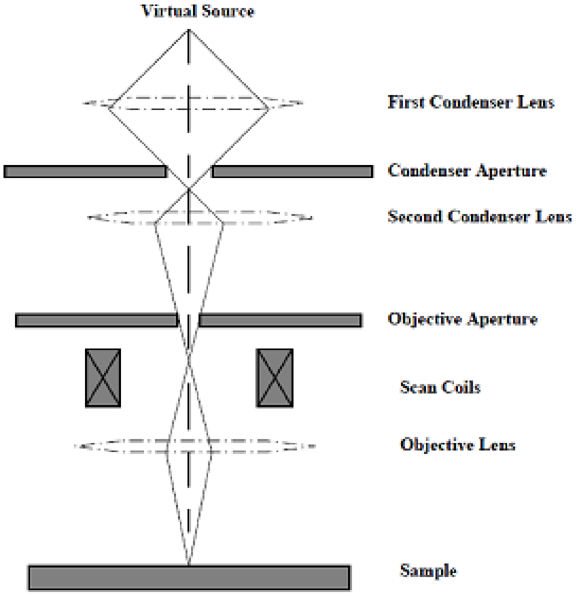

Figure 1.12: Schematic representation of SEM

1.10.4. AFM

AFM is a powerful analytical tool which gives information regarding the surface morphology and phase through the production of a 3D map of the sample surface. Typically, AFM instruments have vertical resolutions of less than 0.1 nm and lateral resolution of around 1 nm [113]. A schematic of AFM operation is shown in Figure 1.13. A cantilever with a very fine-pointed tip which is mounted perpendicular to the longitudinal direction of the cantilever is placed on the sample. A laser is reflected from the back of the cantilever into a position sensitive photodiode sensor which records any deflections of the cantilever induced by Van der Waals force between the tip and the sample. These signals are further processed to give the topographical information of the surface.

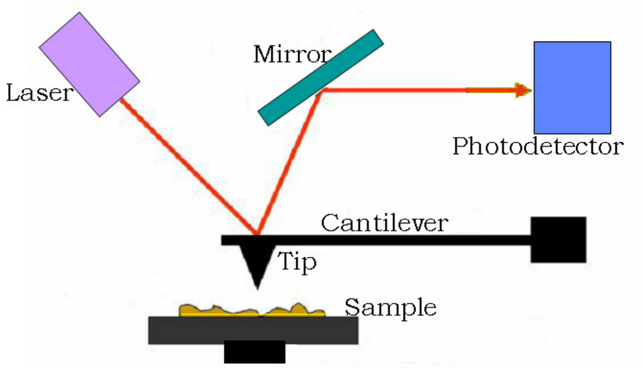

Figure 1.13: Schematic diagram of AFM

1.10.5. XRD

X-ray diffraction is a non destructive technique which can identify the crystal phase of nanoparticles. Powdered sample is placed on a sample holder and then illuminated with x-rays of a fixed wave-length and the intensity of the reflected radiation is recorded using a goniometer. This data is then analyzed for the reflection angle to calculate the inter-atomic spacing (*d* value in Angstrom units) by using Bragg's equation (Equation 1.27).

$$n\lambda = 2d\sin\theta \qquad (1.27)$$

where, *n* is an interger (1, 2, 3, ..., n), *l* the wavelength, *d* the distance between atomic planes, and *q* the angle of incidence of the x-ray beam and the atomic planes. XRD of metal nanoparticles give broad peaks [114,115]. The broadening provides information about crystallite size by Debye- Scherrer equation [116,117] (Equation 1.28).

$$d = \frac{\kappa\lambda}{\beta\cos\theta} \qquad (1.28)$$

where *K* is the shape factor (0.9), λ is the x-ray wavelength (1.5 A^0 for Cu k_α), *β* is the line broadening at half the maximum intensity (FWHM) in radians, and *θ* is the Bragg angle.

1.10.6. FTIR

Identification of specific types of chemical bonds or functional groups based on their unique absorption signatures is possible by infrared spectroscopy Chemical bond stretching and bending is possible by absorption of energy. This energy is in the IR range of electromagnetic spectrum. Fourier transform infrared spectroscopy (FTIR) offers several advantages from conventional IR spectroscopy [118−120] hence FTIR is widely adopted nowadays. Functional groups attached to the metal nanoparticle surface show different FTIR pattern than those of free groups [121], hence FTIR gives information about the surface chemistry of nanomaterials.

1.11. Scope of the Thesis

Metal nanoparticles (nps) especially noble metal nanoparticles are being explored for application in the areas of sensing, imaging, catalysis and antimicrobial applications. Generation of these metal nps by high energy radiation is promising because of several advantages offered by radiolytic method. The radiolytic method is an indirect method, where reactive reducing radicals are produced in-situ through water radiolysis. These radicals are utilized to reduce metal ion precursor to metal in zerovalent state and subsequently metal nps are formed. It is possible to generate spherical as well as nonspherical nps (nanorods, nanoplates) with controlled size by radiolytic route. Capping agents play very important role in stabilization of metal nps. Both natural polymer and synthetic polymers containing specific functional groups, like -OH, -NH_2, -COOH etc., can stabilize metal nps on their surfaces. The long polymer chain restricts agglomeration of the nps. In this work natural polymer, namely guar gum and synthetic polymer namely, poly methacrylic acid (PMA), poly vinyl pyrrolidone (PVP) have been explored for their stabilization property. Unlike spherical nps, anisotropic nps possess two absorption bands in the electromagnetic spectrum. Small changes in the shape of nanoparticle can have great effect on a variety of physical properties of the material. The key parameter to generate anisotropic nps is dose rate of irradiation along with presence of certain adsorbing molecule like surfactant and some metal ions. These molecules selectively adsorb upon certain facets of growing nanoparticle, blocking those facet and allowing directional growth. The nps were characterized by various techniques, such as uv-visible spectroscopy, XRD, TEM, TG and FTIR. Because of high surface area as well as high surface energy of metal nps, other molecules easily adsorb upon their surfaces. This property of metal nps helps in detection and estimation of chemical and biological analytes. Brief descriptions of the chapters in this thesis are presented below.

Chapter 2 describes about the materials, instrumentation and methods.

Chapter 3 depicts synthesis of spherical silver nanoparticles in a natural polymer, guar gum by using gamma radiation and characterization of these nanoparticles.

Chapter 4 describes synthesis and structural characterization of silver nps in polymethacrylic acid and investigation of these nps for estimation of biomolecule, dopamine.

Chapter 5 consists of three separate sections describing different methods to generate a variety of anisotropic shape gold nanoparticles. The role of kinetics in anisotropic metal np generation has been established. Section 5.2 presents the synthesis of short aspect ratio gold nanorods by controlling dose rate of gamma radiation. Section 5.3 describes the kinetics of np formation can be controlled by selectively producing mild reducing radical in water radiolysis. In this section gold nanorods are synthesized in milder reducing condition even at high radiation dose rate. In section 5.4 in-situ radiolytically generated seeds are used to provide surface for anisotropic plate like gold nps growth in presence of mild reductant, namely ascorbic acid.

Chapter 6 depicts synthesis and characterization of gold nanoparticles in poly vinyl pyrrolidone and their application in estimation of hydrogen peroxide.

Chapter 2: Materials and Methods

2.1. Chemical reagents

All reagents were of high purity and used as received. Prior to use, glassware was cleaned with aqua regia (volume ratio HNO_3/HCl = 1 : 3) and thoroughly rinsed with nano pure water. Aqueous solutions were prepared using nano pure water (resistivity =18 MΩ cm). $AgNO_3$ and ascorbic acid obtained from M/s Sarabhai Chemicals, Vadodara, India, hydrogen tetrachloroaurate trihydrate ($HAuCl_4.3H_2O$, 99.99%) from MV laboratories, o-phenylenediamine (o-PDA), horseradish peroxidase (HRP) (300 units/mg), hydrogen peroxide and poly(N-vinyl-2-pyrrolidone)s (PVPs) of molecular weights 40,000; 1,60,000 and 3,60,000 Da from Aldrich, isopropyl alcohol, acetone, sodium hydroxide, citric acid, sodium citrate, potassium dihydrogen phosphate and sodium hydrogen diphosphate from S. D. Fine Chemicals Ltd., Mumbai, India, guar gum from Sigma, cetyl trimethyl ammonium bromide (> 99%) from Fluka and methacrylic acid from CDH laboratories, Mumbai, India, dopamine hydrochloride (98%) from HiMedia Laboratories, Mumbai, India were used as received. A 0.125mg/10ml aqueous solution of horseradish peroxidase (HRP) was prepared for further use. High pure N_2 gas was used for saturating the reaction mixture before subjecting to gamma irradiation.

2.2. Gamma irradiator and dosimetry aspects

2.2.1. Gamma irradiator

A Gamma irradiation source, Gamma Chamber- 5000, supplied by the Board of Radiation & Isotope Technology (BRIT), Mumbai, INDIA was used for irradiation of reaction mixture solutions. Figure 2.1 shows the layout of gamma chamber used in these studies. Gamma chambers mainly consist of a set of stationary Cobalt-60 (^{60}Co) source placed in a cylindrical cage surrounded by a lead shield. The shield is provided around the source to keep external radiation field well within the permissible limits. The material for irradiation is placed in an irradiation chamber located in the vertical drawer inside the lead flask. The drawer can be moved up and down with the help of a system of motorized drive, which enables precise positioning of the irradiation chamber at the center of the radiation field. ^{60}Co radioisotope emits two γ rays of energy 1.33 and 1.17 MeV.

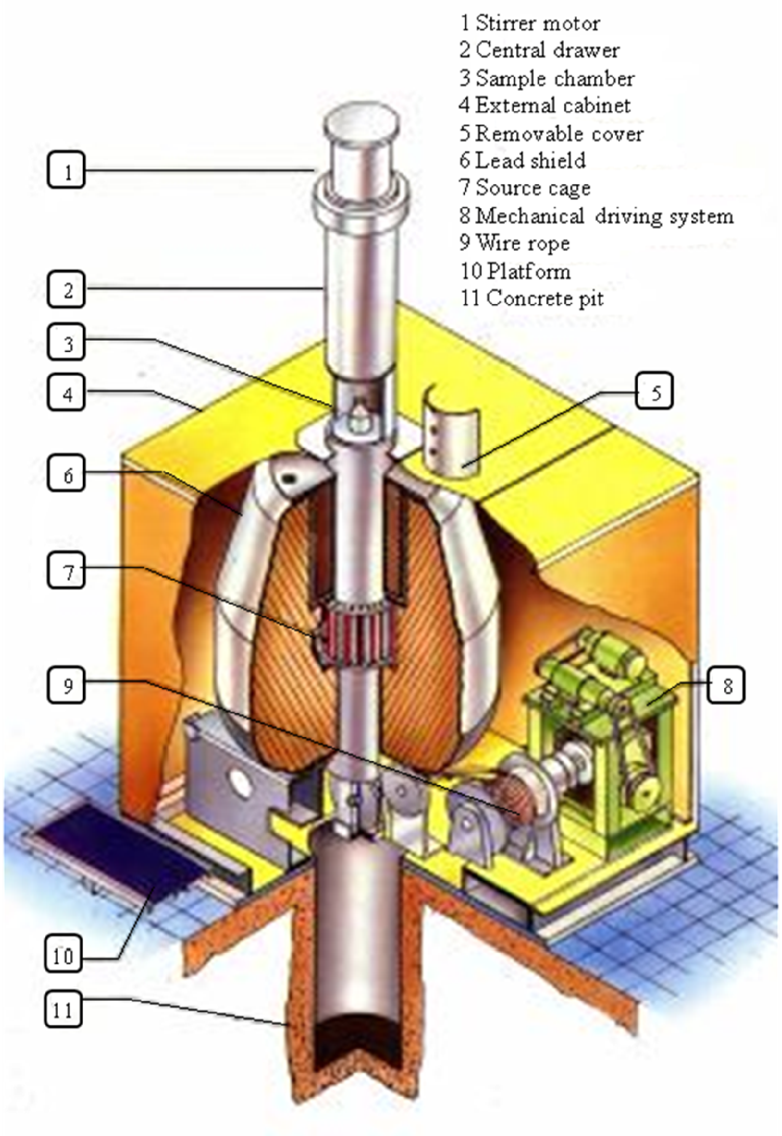

Figure 2.1: Layout of Gamma chamber 5000

2.2.2. Radiation dosimetry

To quantify the physical, chemical or biological changes produced by ionizing radiation, the knowledge of the amount of energy absorbed per unit mass and distribution of the absorbed energy in the absorbing material is necessary. Radiation dosimetry constitutes determination of these quantities.

(i). Absorbed dose: The absorbed dose is the amount of energy absorbed per unit mass of the irradiated material. The SI unit for the absorbed dose is Joules/kilogram (J kg^{-1}), which is known as gray (Gy) [122]. The old unit is rad (1 rad = 0.01 Gy) [123].

(ii). Absorbed dose rate: The absorbed dose rate is the absorbed dose per unit time.The unit for the absorbed dose is Gy s^{-1}.

(iii). Absorbed dose in samples

The absorbed dose measured by the dosimeter will represent the dose absorbed by the sample only when the following conditions are satisfied: (i) the dosimeter as well as the sample are both homogeneous, (ii) both have same size, density and atomic composition, and (iii) both are irradiated under same conditions. The simple and widely used method to achieve these conditions is to use equal volumes of dilute solutions of both sample and dosimeter, and irradiated them in turn using the same container at the same position in the radiation field. Therefore, experimental conditions must be suitably controlled for accurate measurement of the absorbed dose in the sample. However, these conditions do not match very often and in such cases a calculation must be carried out to obtain the absorbed dose in the sample using the Equations 2.1. For electromagnetic radiation like ^{60}Co γ-rays, the absorbed dose in the dosimeter (D_d) and sample (D_s) are related by equation (1.11).

$$D_s = \frac{D_d \times (Z/A)_s}{(Z/A)_d} \tag{2.1}$$

Where, Z/A is the ratio of the atomic number (Z) to the atomic weight (A) for an element and the ratio of the sum of the atomic numbers of the element present to the molecular weight for a compound.

(iv). Primary and secondary dosimeters

Dosimeters can be classified into two categories viz. primary dosimeters and secondary dosimeters. Primary dosimeters utilize a physical measurement such as temperature rise in a calorimeter, ionization produced in a gas or the charge carried by a beam of charged particles of known energy [123,124]. Secondary dosimeters are those dosimeters whose response to radiation has to be calibrated against a primary dosimeter. These include Fricke dosimeter, nylon film dosimeter, solutions of various dyes, perspex dosimeters [125]. The choice of a dosimeter for a particular application depends on many factors namely, (i) state of the system, (ii) dose range to be monitored and (iii) nature of radiation.

2.2.3. Dosimetry of gamma chamber

The dose rate delivered by gamma chamber 5000 was measured by Fricke dosimetry before carrying out any experiment. The oxidation of ferrous ions to the ferric ions in acidic aqueous solutions in presence of oxygen and under influence of radiation is the basic principle of Fricke dosimeter [126–129]. The standard Fricke dosimeter consists of an aerated solution of 1.0 x 10^{-3} mol dm^{-3} ferrous ammonium sulphate, 1.0 x 10^{-3} mol dm^{-3} NaCl and 0.4 mol dm^{-3} sulphuric acid (pH= 0.46). The reaction involved in the Fricke dosimeter is the radiation-induced oxidation of ferrous ion to ferric ion at low pH and in the presence of oxygen in accordance with the series of reactions (2.2) – (2.8).

$$H_2O \rightsquigarrow e_{aq}^-,\ H^{\cdot},\ {}^{\cdot}OH,\ H_2,\ H_2O_2,\ H_3O^+ \tag{2.2}$$

$$e_{aq}^- + H^+ \longrightarrow H^{\cdot} \tag{2.3}$$

$$H^{\cdot} + O_2 \longrightarrow HO_2^{\cdot} \tag{2.4}$$

$$Fe^{2+} + {}^{\cdot}OH \longrightarrow Fe^{3+} + OH^- \tag{2.5}$$

$$Fe^{2+} + HO_2^{\cdot} \longrightarrow Fe^{3+} + HO_2^- \tag{2.6}$$

$$HO_2^- + H^+ \longrightarrow H_2O_2 \tag{2.7}$$

$$Fe^{2+} + H_2O_2 \longrightarrow Fe^{3+} + OH^- + {}^{\cdot}OH \tag{2.8}$$

The yield of ferric ion is related to the primary radical and molecular yields by Equation (2.9)

$$G_{(Fe^{3+})} = 2G_{(H_2O_2)} + 3\left[G_{(e_{aq}^-)} + G_{(H^{\cdot})}\right] + G_{({}^{\cdot}OH)} \tag{2.9}$$

Since each molecule of hydrogen peroxide oxidizes two ferrous ions by reactions (2.8) and (2.5), while the reducing radicals each oxidize three ferrous ions by sequential reactions involving $HO_2^{\cdot}$, H_2O_2 and ${}^{\cdot}OH$ respectively. The number of moles of Fe^{3+} ions (M) produced upon irradiation is determined by absorption spectrophotometry employing Beer's law ($\Delta A = \Delta\varepsilon.c.l$) at 304 nm with $\varepsilon_{(Fe3+)} = 2205 \pm 3$ dm^3 mol^{-1} cm^{-1} and $\varepsilon_{(Fe2+)} = 1$ dm^3 mol^{-1} cm^{-1} at 25°C. The $G_{(Fe3+)}$ value accepted for electron and photon radiation in the range 1 to 30 MeV is 15.5 (or, 1.606×10^{-6} mol dm^{-3} J^{-1}) at 25°C and the density of Fricke dosimeter solution (ρ) is 1.024 gm ml^{-1}. The absorbed dose (D) is derived by following expression (2.10)

$$D = \frac{100 \times 1.602 \times 10^{-19} N_A M}{\rho G} Gy$$

$$\Rightarrow D = \frac{9.647 \times 10^{6} \nabla A}{\rho G \nabla \epsilon l} Gy$$

$$\Rightarrow D = 277 \times \frac{\nabla A}{l}\ Gy \qquad (2.10)$$

Where N_A= Avogadro's number and l is the path length in centimeters.

The Fricke dosimeter can be used to accurately determine dose only up to 400 Gy. Because of depletion of oxygen in the system beyond this dose $G_{(Fe3+)}$ does not remain constant. Fricke dosimeter is independent of dose rate between 0.2 to 2.0 x 10^6 Gy s^{-1}. A modified version of Fricke dosimeter, also called as super Fricke dosimeter, containing 10^{-2} mol dm^{-3} ferrous ions, oxygenated but without any sodium chloride, is dose rate independent up to absorbed dose rates of the order of 10^8 Gy s^{-1}. The upper limit of absorbed dose that can be measured using a super Fricke dosimeter is 2.0 kGy. Lead attenuators of suitable thickness were used for reducing the dose rates.

2.3. Characterization techniques

2.3.1. Ubbelohde viscometer

Viscosity measurement studies were carried out using an Ubbelohde viscometer from M/s Scam India having a flow time of 62 s for double-distilled water at 25 ^{0}C. The molecular weight of polymer was determined with the viscosity method from Mark-Houwink equation,

$$\eta = \kappa M_{\upsilon}^{\eta} \qquad (2.11)$$

Where, η is the intrinsic viscosity, M_v is the viscosity-average molecular weight, and κ and α are constants, whose values can be found from literature [130].

2.3.2. UV-visible spectrophotometer

The absorption spectra of aqueous silver nanoparticles in guar gum and short aspect ratio gold nanorods in CTAB were recorded on a Shimatzu model 4600 recording spectrophotometer in the wavelength region 250–900 nm. In all other cases the absorption spectra of gold nanoparticles were recorded on a Thermoelectron - Evolution 300 uv-visible spectrophotometer in the wavelength region of 250-900 nm.

2.3.3. TEM instrument

Transmission electron microscopy (TEM) of silver nanoparticles was performed on a Model JEOL 2000 FX transmission electron microscope with an accelerating voltage of 160 kV. Transmission Electron Microscopy (TEM) was of gold nanorod solution in CTAB performed on Libra 120 Zeiss cryoelectron microscope from TIFR with an accelerating voltage of 160 kV. Transmission Electron Microscopy (TEM) of other anisotropic gold nano particles in CTAB and gold nanoparticles in PVP were performed on a Model JEOL 2000 FX transmission electron microscope with an accelerating voltage of 120 kV. For the measurement of TEM a drop of dilute gold nanoparticle solution was placed on a carbon coated copper grid and dried before it was observed under the microscope. The solution of spherical nanoparticles in polymer was directly placed on a carbon coated copper grid allowing the water to evaporate at room temperature and then the grid was analyzed under TEM instrument. In case of anisotropic nanopartcle in surfactant solution the TEM sample was prepared by centrifuging the sample of nanorod twice at 15,000 rpm for 15 minutes in order to remove excess surfactant. Precipitates were collected and redispersed in a small amount of nanopure water, and 50 μl of the suspension was placed on a carbon coated copper grid and allowing the water to evaporate at room temperature.

2.3.4. FTIR spectrophotometer

Fourier transformed infrared spectroscopy (FTIR) measurements were performed on a FTIR spectrophotometer, FT/IR-610 from JASCO, Japan. Solid samples of metal-polynmer were thoroughly ground at liquid nitrogen temperature and mixed with KBr. The mixture was compressed to prepare disc for FTIR analysis. In case of liquid samples, like Ag/polymethacrylate, one drop of each sample solution was spread evenly on the ATR crystals window. The samples were air dried for water evaporation, the holder was mounted in the sample window of the spectrometer and the sampling window was scanned. FTIR spectra were recorded in the range from 400 to 4000 cm^{-1} with a resolution of 4 cm^{-1} and averaged over 25 scans.

2.3.5. X-ray diffractometer

The X-ray diffraction (XRD) patterns of powdered metal-polymer were recorded on a Philips XRD spectrophotometer (model PW 1729) in the range 2θ = 20^0-70^0. The size of metal nanoparticles were calculated from Debye- Scherrer equation,

$$d = \frac{\kappa\lambda}{\beta \cos\theta} \qquad (2.12)$$

where *K* is the shape factor (0.9), λ is the x-ray wavelength (1.5 A^0 for Cu k_α), *β* is the line broadening at half the maximum intensity (FWHM) in radians, and *θ* is the Bragg angle.

2.3.6. Thermo gravimetric instrument

Thermo gravimetric experiments were carried out under a N_2 flow with a TGA Mettler 3000 instrument at a heating rate of 10 ^{0}C/minute. The thermal stability of virgin polymer is different from metal nanoparticle incorporated polymer due to high thermal conductivity of metal.

2.3.7. Powder sample preparation

Powdered samples of Ag nanoparticles in guar gum for TG, XRD and FTIR analysis were prepared as follows. Ag/guar gum nanocomposite was precipitated by adding excess acetone to aqueous guar gum solution containing Ag nanoparticle. The precipitate was finally washed with acetone and then dried in a laboratory oven at 50 ^{0}C for 5 hrs under vacuum. The dried sample was grounded to fine powder by using a mortar and pestel.

Chapter 3: Synthesis of spherical silver nanoparticles in guar gum by gamma irradiation

3.1. Introduction

The study of metal nanoparticles is of interest in both research and technology, as metal nanoparticles possess specific properties not available in isolated molecules or bulk metals. These characteristics, namely, optical, magnetic, catalytic, and electrochemical properties, are dependant to a great extent on their dimensions, shape, and chemical surroundings and can be advantageously used for the purpose of the development of novel biosensors, chemical sensors, electrooptical devices, material for high-capacity data storage media [37–43] and substrates for enhanced Raman spectroscopy [137−142]. Noble metal nanoparticles, such as silver, gold, palladium, platinum etc. are preferably studied, because ease of their preparation and versatile applications of these colloidal particles. The synthesis of nanoparticles of metals involves the reduction of metal ion with a suitable reducing agent. The reduction can be achieved chemically [84], photochemically [78], by microwave heating [143], and by high-energy radiation [77,102,144], such as gamma and electron beam radiation. Among the various methods mentioned previously, the use of ionizing radiation for the synthesis of metal nanoparticles is promising; because of several advantages. Radiolytic methods are free from chemical reducing agents, as highly reactive species are produced in situ. It is a room temperature process and it provides flexibility of tuning the dose and dose rate for generating controlled size and shape metal nanoparticles.

Table 3.1: **Reduction potential values of primary radicals**

Radicals	Reduction Potential (E^0 / V_{NHE})
e_{aq}^-	-2.9 at pH 7
$H^\cdot$	-2.3 at pH 0
$^\cdot OH$	+2.8 at pH 0

The interaction of high-energy radiation with aqueous solution of metal ions induces ionization and excitation of the solvent, i.e., water molecule and leads to the formation of radiolytic molecular and radical species in the solution. Reactive transient radicals produced through water radiolysis are solvated electrons (e_{aq}^{-}), hydrogen atom ($H^{\bullet}$) and hydroxyl radical ($^{\bullet}OH$). The first two radicals are strong reducing agents (Table 3.1) capable to reduce metal ions to lower valences and finally to metal atoms. The later is oxidizing in nature, in presence of which the metal atoms thus formed can undergo back oxidation. To eliminate the later process a suitable $^{\bullet}OH$ scavenger, such as primary, secondary or tertiary aliphatic alcohol or formic acid are added to the system. The detailed mechanism has been discussed later in the text. The metal atoms coalesce to form small nuclei, which grow to metal nanoparticles (Figure 3.1). The formation of metal nanoparticles passes through three stages:

(i) supersaturation of metal atoms
(ii) nucleation to generate seeds
(iii) and finally the growth stage.

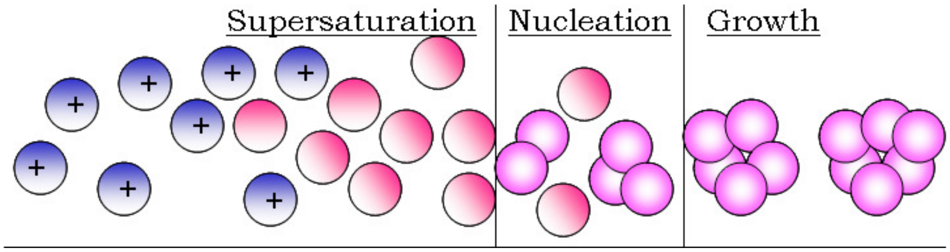

Figure 3.1: Pictorial representation of formation of metal nanoparticles

However, a capping agent is usually used in the synthesis of metal nanoparticles to both prevent the aggregation of the metal nanoparticles and impart useful chemical behavior to the final nanoscale product. It is now well established that polymers are excellent host materials for nanoparticles of metals. When the nanoparticles are embedded or encapsulated in a polymer, the polymer acts as a surface-capping agent. Various synthetic polymers, such as poly(vinyl alcohol) [84,85], poly(vinyl pyrrolidone) [27], polystyrene [115] and poly(methyl methacrylate) [145] have been used in the synthesis of metal nanoparticles. However, very few works have been reported in which a natural polysaccharide has been used as a capping agent for the stabilization of metal nanoparticles [146]. Natural polymers, because of their large abundance and the presence of reactive functional groups may show better ability to stabilize nanoparticles. Guar gum (GG) [147] is a naturally occurring edible carbohydrate polymer found in the seeds of guar plant (Cyamopsis tetragonoloba). It is a nonionic, branched-chain polymer, consisting of straight-chain β-D- mannose units joined by (1-4) linkages having α-D-galactose units attached to this linear chain by (1-6) linkages. The mannose: galactose ratio is approximately 2:1. Aqueous guargum solution is very stable in the pH 4.0-10.5 range. GG is an economical thickener and stabilizer used in food, pharmaceutical, paper and petroleum industries. It hydrates fairly rapidly in cold water to give highly viscous pseudoplastic solution. It is more soluble than other natural gums and a better emulsifier as it has more galactose branch units.The chemical structure of GG is shown in Figure 3.2. GG has several hydroxyl groups, which can effectively bind metal clusters on their surfaces. Being non ionic, it is not affected by ionic strength or pH of the solution.

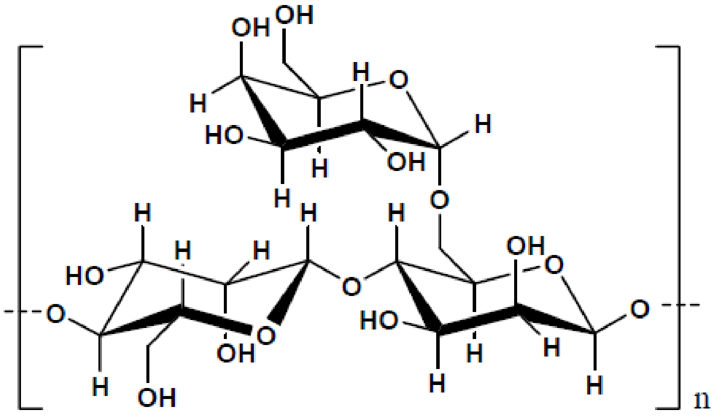

Figure 3.2: Chemical Structure of Guar gum

In the present chapter, silver (Ag) nanoparticles were synthesized in aqueous GG solution by using gamma radiation. The nanoparticles in solution were prepared by exposing aqueous solution of GG containing $AgNO_3$ and isopropyl alcohol to ^{60}Co gamma radiation. In aqueous solution water is the major component; hence most of the radiation energy is absorbed by water. The reducing radicals like e_{aq}^{-}, and $H^{\bullet}$ generated from water radiolysis are utilized for reduction of Ag^+ while the oxidizing $^{\bullet}OH$ radicals were scavenged with isopropyl alcohol to generate reducing isopropyl alcohol radical. The radiation dose delivered to the sample was adjusted in such a way so that entire Ag^+ was converted into Ag^0. The aim of this study was to investigate the optical and structural properties of silver nanoparticles as well as the influence of capping agent concentration, precuessor concentration along with effect of other parameters on nanoparticle size and size distribution.

3.2. Synthesis of Ag nanoparticles

A known concentration of $AgNO_3$ was dissolved in 0.5% (w/ w) aqueous GG solution containing 0.2 mol dm^{-3} isopropyl alcohol to prepare the reaction mixture. The solution was stirred until a viscous homogeneous solution was obtained. It was then purged with N_2 gas to eliminate the dissolved oxygen present in the solution. Then the reaction mixture was irradiated up to a desired dose. Irradiations were carried out in a ^{60}Co gamma chamber with a dose rate of 3.5 kGy h^{-1} determined with Fricke dosimetry [148]. With the course of irradiation silver nanoparticles were formed, indicated by bright yellow color solution, which was later confirmed by UV–visible spectroscopy. The radiation dose delivered to the sample for complete reduction of Ag^+ to Ag^0 was calculated as shown below.

$1 \text{ ev} = 1.6 \times 10^{-19}$ J

$100 \text{ ev} = 1.6 \times 10^{-17}$ J

In a total reducing condition, Net G value of transient reducing radicals is 6, which is the sum G values of e_{aq}^{-}, $H^{\cdot}$ and $^{\cdot}OH$.

⇒ As per definition of G value, 6 reducing radicals are produced by absorption of 100 ev energy.

⇒ 6 monovalent metal ions like Ag^+ are reduced by radiation energy of 1.6×10^{-17} J (or 100 ev).

1×10^{-3} mol dm^{-3} $Ag^+ = 6.023 \times 10^{20}$ number of Ag^+/dm^{-3}

To reduce 1×10^{-3} mol dm^{-3} Ag^+, energy required

$$
\begin{aligned}
&= [1.6 \times 10^{-17} \times 6.023 \times 10^{20}]/6 \quad J/dm^{-3} \\
&= 1.6 \times 10^{3} \quad J/dm^{-3} \\
&= 1.6 \times 10^{3} \quad J/Kg \text{ [Let density = 1]} \\
&= 1.6 \times 10^{3} \quad Gy \\
&= 1.6 \quad kGy
\end{aligned}
$$

Hence, for complete reduction of 1 millimolar Ag^+ 1.6 kGy radiation dose is required. Accordingly depending upon the concentration of metal ion total dose to be delivered is calculated.

3.3. Results and discussion

3.3.1. Determination of molecular weight of guar gum

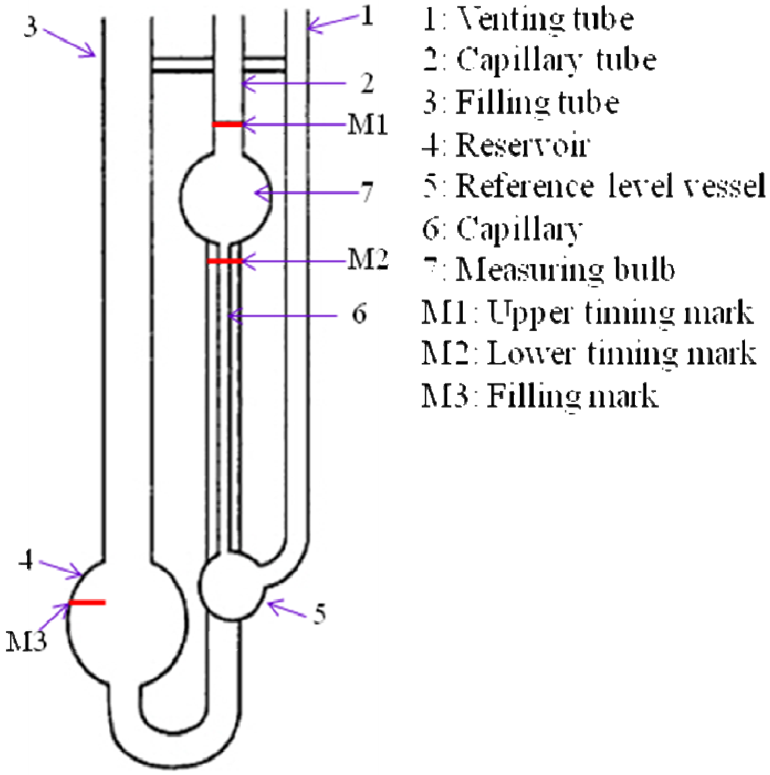

Figure 3.3: Schematic diagram of Ubbelohde viscometer

Molecular weight of guar gum was determined from their intrinsic viscosity values and its relation to molecular weight via Mark Houwink equation as reported earlier [149]. Using an Ubbelohde capillary viscometer [Figure 3.3] the relative viscosity (η_r) was measured [Equation 3.1].

$$\eta_r = \frac{T}{T_0} \qquad (3.1)$$

Where, T is the guar gum solution flow time and T_0 is solvent (water) flow time, which is 62 s at 25 ^{0}C.

From the above relation the specific viscosity (η_{sp}) and the reduced viscosity were calculated as follows,

$$\eta_{sp} = \eta_r - 1 \qquad (3.2)$$

$$\eta_{red} = \frac{\eta_{sp}}{c} \qquad (3.3)$$

Where, C is the concentration of guar gum solution.

The intrinsic viscosity (η) is was determined by measuring reduced viscosity, η_{red} at various concentrations of guar gum in dilute solution and extrapolating to concentration $C = 0$ as shown in Figure 3.4. The concentration dependence is often expressed in terms of the following relationship.

$$\frac{\eta_{sp}}{c} = [\eta] + K[\eta]^2 c \qquad (3.4)$$

Where, K is known as Huggins constant.

For flexible polymer molecules in good solvents K is often near to 0.35, although somewhat higher values occur in poor solvents. In the present work, a value of 0.35 was adopted in the above equation to calculate intrinsic viscosity. From the intrinsic viscosity, the viscosity-average molecular weight (M_v) was estimated by using the Mark-Houwink equation,

$$\eta = \kappa M_{u}^{\alpha} \qquad (3.5)$$

κ and α are constants, whose values are 3.8×10^{-4} and 0.732, respectively [150,130].

By employing above method the viscosity average molecular weight (M_v) of guar gum was found to be 1.9×10^{6}.

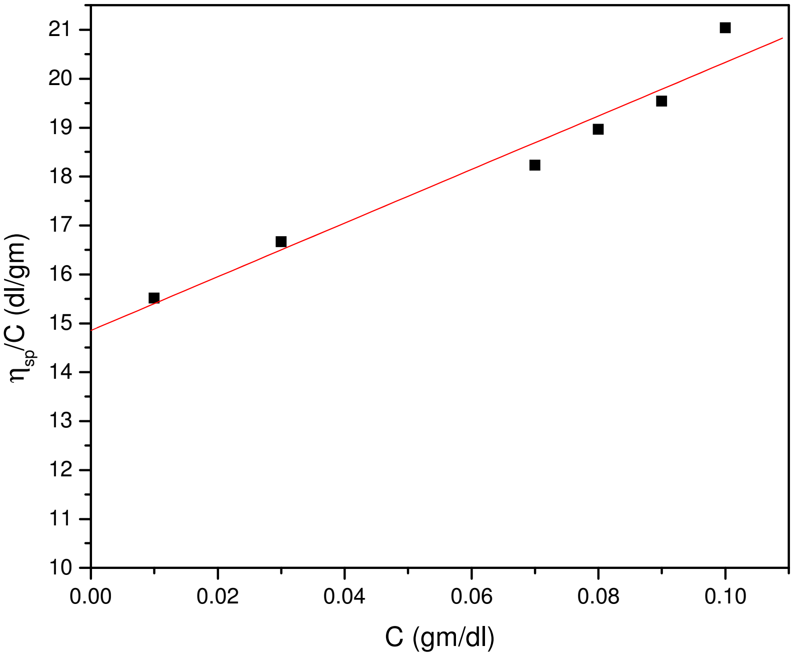

Figure 3.4: Plot of reduced viscosity vs concentration of dilute guar gum solution

3.3.2. Spectroscopic analysis of silver nanoparticles stabilized by guar gum

The reduction of silver ions in aqueous solutions in the presence of a polymeric stabilizer generally results in the formation of colloidal silver with a particle diameter of several nanometers. These particles have specific optical properties indicated by the presence of an intense absorption band at 390- 450 nm caused by the collective excitation of all the free electrons in the particle [104]. To investigate the ability of GG to stabilize the Ag clusters, the irradiation of an aqueous solution of GG in the presence of Ag^+ was carried out. The absorption spectra of aqueous solution of 0.5% GG containing 1×10^{-3} mol dm^{-3} Ag^+ and 2×10^{-1} mol dm^{-3} isopropyl alcohol irradiated with gamma radiation with various radiation doses are shown in Figure 3.5.

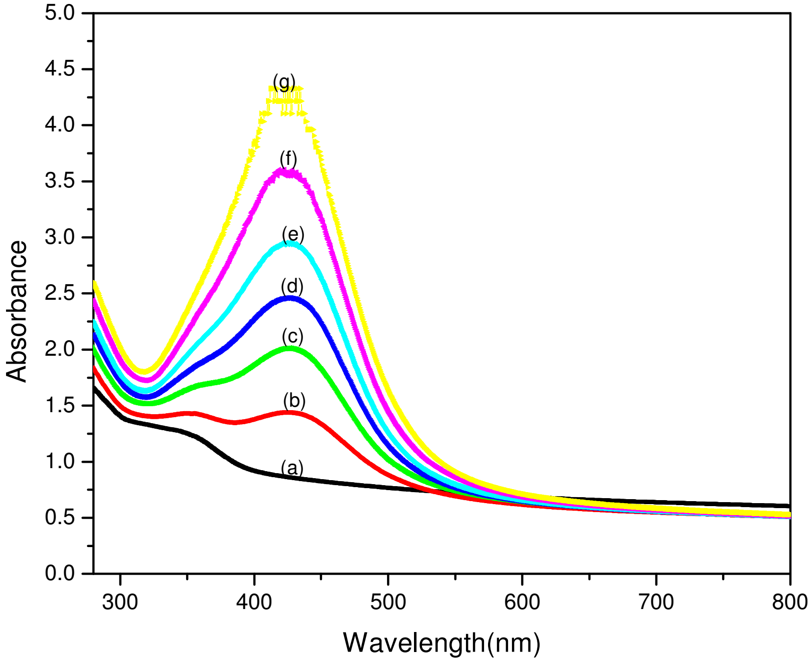

Figure 3.5: Absorption spectra of GG solutions irradiated at various doses: (a) unirradiated GG and GG irradiated with (b) 0.1, (c) 0.3, (d) 0.5, (e) 0.6, (f) 0.7, and (g) 0.9 kGy in the presence of 1 x 10^{-3} mol dm^{-3} Ag^+ and 0.2 mol dm^{-3} isopropyl alcohol

The un-irradiated GG solution showed a shoulder at 350nm without any peak in the visible region. With increasing radiation dose, the absorption in the region of 300- 600nm started to develop, with absorption maxima at 427 nm. Under the same experimental conditions, when irradiation was carried out in the absence of Ag^+, no absorption band in the region 300- 600 nm was observed. Thus, the absorption band observed at 427 nm was attributed to silver nanoparticles stabilized by GG. When Ag^+ dissolved in an aqueous solution of GG containing isopropyl alcohol was irradiated with gamma radiation, most of the energy was absorbed by water, which resulted in the generation of e_{aq}^- (hydrated electron), $H^\bullet$ (hydrogen atom), and $^\bullet OH$ (hydroxyl radical). Among these species, e_{aq}^- and $H^\cdot$ were very strong reducing agents having standard reduction potential, $E^0(H_2O/e_{aq}^-)= -2.87\ V_{NHE}$ and $E^0(H^+/H)= -2.3\ V_{NHE}$ respectively. These species reacted with Ag^+ and resulted in its reduction to Ag^0 [Equations (3.6) and (3.7)].

$$e_{aq}^- + Ag^+ \longrightarrow Ag^0 \qquad (3.6)$$

$$H^\cdot + Ag^+ \longrightarrow Ag^0 + H^+ \qquad (3.7)$$

The purpose of the addition of isopropyl alcohol was twofold:

(1) it reacts with the $^\bullet OH$ to form isopropyl radical, which thus prevents the oxidation of Ag^0 back to Ag^+ by the $^\bullet OH$.

(2) the isopropyl radical formed in Equation (3.8) is highly reducing in nature and it is capable of reducing Ag^+ to Ag^0 [Equation (3.9)].

$$^\cdot OH + (CH_3)_2CH\,OH \longrightarrow (CH_3)_2{}^\cdot C\,OH + H_2O \qquad (3.8)$$

$$Ag^+ + (CH_3)_2{}^\cdot C\,OH \longrightarrow Ag^0 + (CH_3)_2C=O + H^+ \qquad (3.9)$$

The silver atoms formed in reactions 3.6, 3.7, and 3.9 dimerize when they encounter each other or associate themselves with excess Ag^+ ions by a cascade of coalescence processes, and these species gradually grow into larger clusters, as shown in reactions (3.10) to (3.13).

$$Ag^0 + Ag^0 \longrightarrow Ag_2^0 \qquad (3.10)$$

$$Ag^0 + Ag^0 \longrightarrow Ag_2^0 \qquad (3.11)$$

$$Ag_n^0 + Ag^+ \longrightarrow Ag_{n+1}^+ \qquad (3.12)$$

$$Ag_{n+1}^+ + e_{aq}^-/H^\cdot \longrightarrow Ag_{n+1} + H^+ \qquad (3.13)$$

The growth of Ag clusters is arrested because of the presence of GG, which anchors these clusters on their surfaces. The -OH groups present on the backbone of GG bind with the growing Ag clusters. Also the long linear chain of mannose units containing side chain of galactose units provides steric stabilization to the anchored Ag nanoparticles most effectively. Evidence for the interaction of hydroxyl groups in the stabilization of the silvernanoparticles was obtained from the Fourier transform infrared (FTIR) spectra of the GG-containing Ag nanoparticles. The FTIR spectra of GG and Ag nanoparticles in GG are shown in Figure 3.6.

GG exhibited characteristics bands [151] at 3426 and 2926 cm^{-1} because of the O—H stretching vibrations and C—H stretching vibrations of the polymer associated. Additional characteristics absorption bands of GG appeared at 1418 and 1026 cm^{-1} because of C—H bending and O—H bending vibrations, respectively.

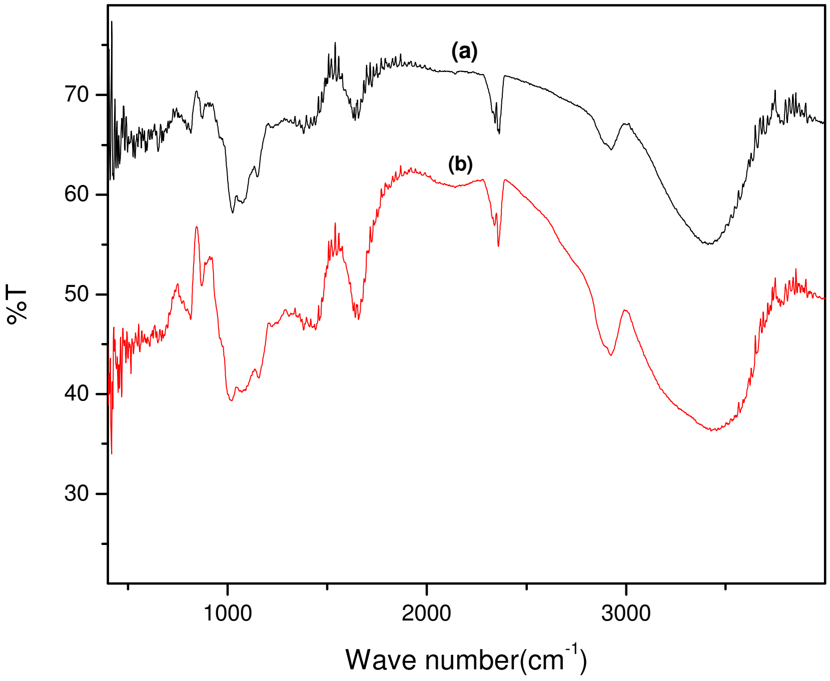

Figure 3.6: FTIR spectra of (a) GG and (b) Ag/GG

As shown in Figure 3.6, the band at 3426 cm^{-1} shifted to 3457 cm^{-1} in the presence of Ag and also, the band was broader in Ag/GG compared to GG. These observations clearly indicate the interaction of Ag with the —OH group of GG. Similar results were reported earlier in the synthesis of silver nanoparticles stabilized by Konjac Glucomannan, which is structurally similar to GG, by a photochemical reduction method [152].

3.3.3. Effect of the guar gum concentration on Ag nanoparticle formation

To obtain an optimum size and size distribution of Ag nanoparticles, a study aimed at controlling the reaction parameters was performed. This optimization process consists of the influence of the concentration of reactants like guar gum and $AgNO_3$ concentration, pH, and role of alcohol. The effect of the GG concentration on the formation of the Ag nanoparticles was studied by the irradiation of a solution containing 1×10^{-3} mol dm^{-3} Ag^+ and 2×10^{-1} mol dm^{-3} isopropyl alcohol and various GG concentrations. As mentioned earlier, the primary radiolytic species generated in aqueous solution are e_{aq}^{-}, $H^{\bullet}$, and $^{\bullet}OH$. Typically, in the presence of isopropyl alcohol, the yield of reducing species is 6 per 100 eV of absorbed energy [153]. In section 3.2 it has been calculated theoretically that for reduction of 1 millimolar Ag^{+} 1.6 kGy radiation dose is required. In other words, taking into account the random nature of absorption of radiation energy, a radiation dose of about 2 kGy in principle is sufficient to bring about the complete reduction of 1×10^{-3} mol dm^{-3} Ag^{+} to metallic silver. There is a possibility of GG reacting with the radicals generated from water radiolysis; hence a higher radiation dose of 3.5 kGy was selected to ensure the complete reduction of Ag^{+}. The absorption spectra recorded after irradiation at various concentrations of GG are shown in Figure 3.7. The spectrum at a low concentration of GG (0.1%) was very broad, with a shoulder at 520 nm and a maximum at 408 nm.

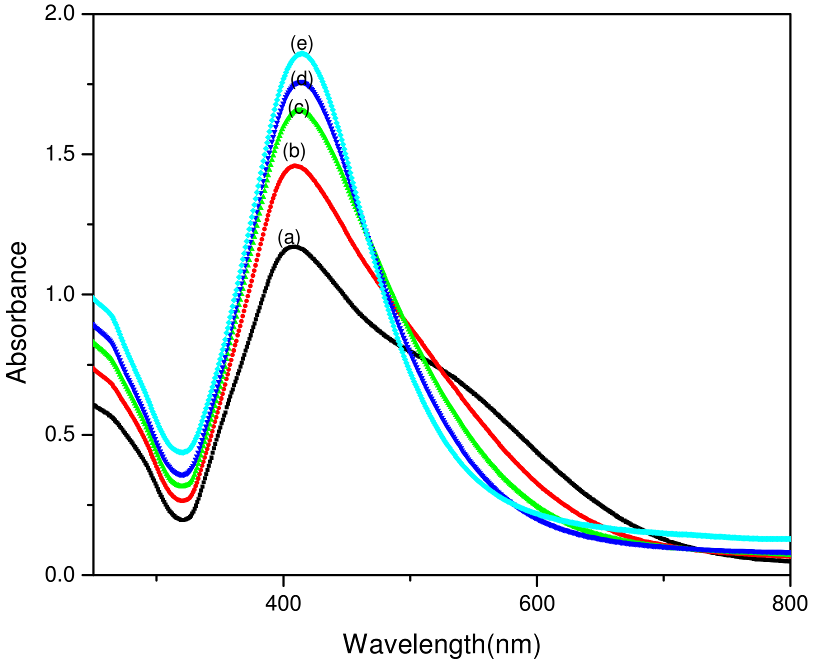

Figure 3.7: Absorption spectra of the Ag nanoparticles formed upon irradiation at various GG concentrations: (a) 0.1, (b) 0.2, (c) 0.3, (d) 0.4, and (e) 0.5% w/v

However, with increasing concentration of GG, the absorption spectrum became narrower, and the shoulder at 520 nm also disappeared. The narrowing of the absorption spectrum with increasing concentration of GG indicated that the nanoparticle size became more uniform. At low concentration, GG was not very effective in stabilizing the Ag nanoparticles, and therefore, there was less control over the particle size, as evident from the broad absorption spectrum.

3.3.4. Effect of Ag^+ concentration

The effect of Ag^+ concentration on the formation of Ag nanoparticles was studied by keeping the concentration of GG fixed (0.5%) and varying the concentration of Ag^+. The radiation dose delivered to sample was calculated on the basis of the concentration of Ag^+ (3.5 kGy per 1×10^{-3} mol dm^{-3} Ag^+). The absorption spectra of the irradiated solutions are shown in Figure 3.8. As shown in Figure 3.8, the intensity of the surface plasmon band of the Ag nanoparticles increases with increasing concentration of Ag^+, and the band was quite symmetrical up to a 2×10^{-3} mol dm^{-3} Ag^+ concentration. Further increases in the concentration affected the symmetry of the surface plasmon band, which became quite broad at Ag^+ concentration of 3×10^{-3} mol dm^{-3}, and a shoulder at 520 nm also appeared.

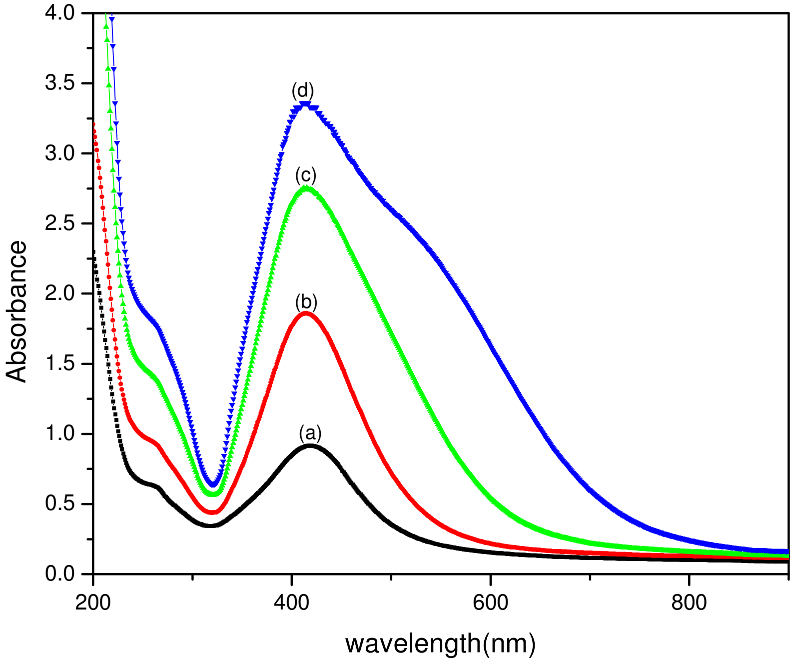

Figure 3.8: Changes in the surface plasmon resonance band of the Ag nanoparticles upon irradiation at various Ag^+ precursor concentrations: (a) 5×10^{-4}, (b) 1.0×10^{-3}, (c) 2.0×10^{-3} and (d) 3.0×10^{-3} mol dm^{-3}

At high Ag^+ concentrations, more nuclei were formed and the concentration of GG, which was kept constant at 0.5%, was not sufficient to control the growth and stabilization of the Ag nanoparticles. Hence, the size distribution was not uniform, as evident from the broadening of the surface plasmon band. Thus, it appears that cluster size was governed by both GG concentration and precursor Ag^+ concentration.

3.3.5. Effect of pH on the formation of Ag nanoparticles

It has been reported in the literature that the pH of the solution affects the formation of metal clusters in radiation-induced synthesis of Ag nanoparticles [154]. To understand the role of pH of the solution on the formation of GG-stabilized Ag nanoparticles, solutions of GG (0.5%) containing 1×10^{-3} mol dm^{-3} Ag^+ were irradiated at various pH values, which were varied by the addition of appropriate amounts of KH_2PO_4 or Na_2HPO_4 to the solutions before irradiation. The absorption spectra recorded after the irradiations are shown in Figure 3.9.

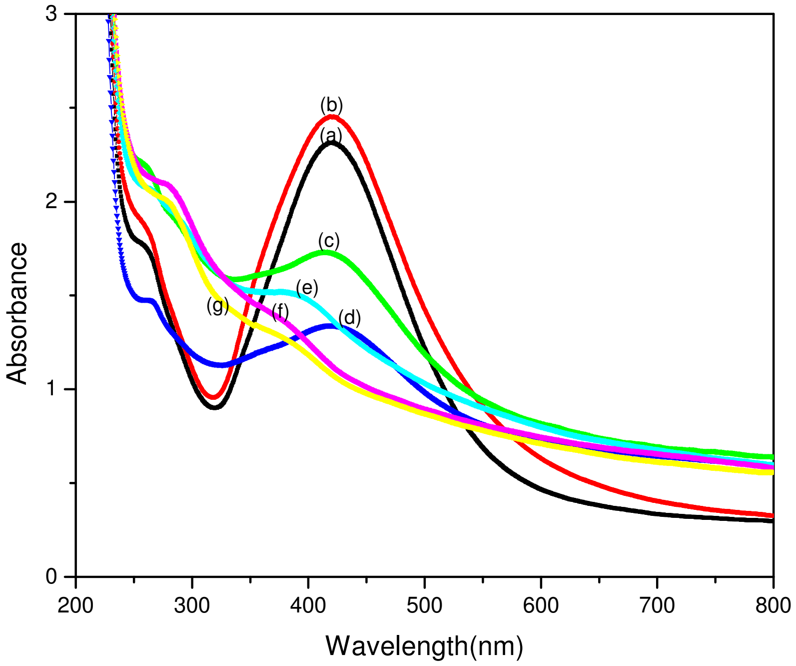

Figure 3.9: Absorption spectra of the Ag nanoparticles formed upon irradiation at various pH values of the solution: (a) 2.6, (b) 4.8, (c) 5.9, (d) 7.2, (e) 9.1, (f) 10.9 and (g) 11.4

The surface plasmon resonance band was obtained to be symmetrical and had very low absorbance at wavelengths beyond 600 nm at pH values of 2.6 and 4.8. This indicated narrow size distribution of the nanoparticles. However, at a pH above 5, the symmetry of band was lost, and it became broad with enhanced absorption at wavelengths above 600 nm. In the alkaline region at pH above 10, no surface plasmon resonance band was observed. In the radiation- induced synthesis of copper nanoparticles [155] in alkaline media, a yellow precipitate of $Cu(OH)_2$ was obtained. During the chemically induced reduction of silver ions by formaldehyde [85] in aqueous media, in alkaline medium, silver nanoparticles were not stable. Thus, it appears that silver clusters stabilized by GG are stable in acid media and that alkaline media are not desirable for the synthesis.

3.3.6. Role of alcohol in the formation of Ag nanoparticles

Although isopropyl alcohol was used as an $^{\bullet}OH$ scavenger throughout this study, the ability of other alcohols to scavenge the $^{\bullet}OH$ and the subsequent reactions of alcohol radicals in the reduction of Ag^+ to metallic silver were also investigated. We studied this by irradiating a 0.5% aqueous solution of GG containing 1×10^{-3} mol dm^{-3} Ag^+ and 2×10^{-1} mol dm^{-3} of various alcohols, including methanol, ethanol, isopropyl alcohol, butanol, and tertiary butyl alcohol. The solutions were purged with N_2 to eliminate oxygen.

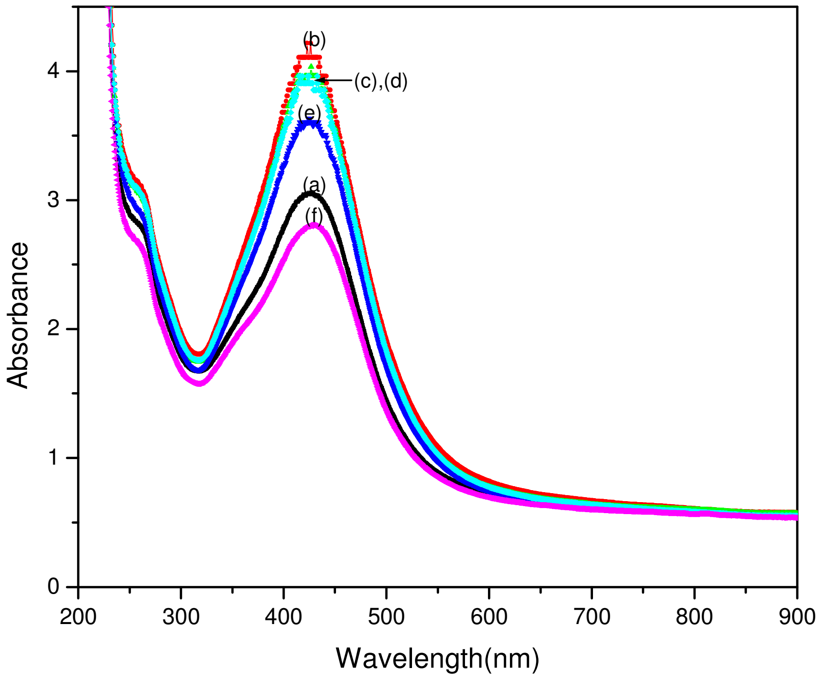

Figure 3.10: Formation of the Ag clusters in the presence of various alcohols used for scavenging OH radicals: (a) no alcohol, (b) methanol, (c) ethanol, (d) isopropyl alcohol, (e) n-butanol, and (f) tertiary butanol (concentration of alcohol 0.2 mol dm^{-3})

The UV- visible spectra of the irradiated samples are shown in Figure 3.10. As shown in this figure, the intensity of the surface plasmon resonance band in the case of all alcohols except tertiary butyl alcohol was higher compared to that in the absence of alcohol. This indicates that radicals generated from the reaction of all these alcohols with the $^{\bullet}OH$ are effective in reducing Ag^+ to metallic silver. Another very important observation that can be made from Figure 3.10 is that the intensity of the surface plasmon band in the presence of tertiary butyl alcohol was lower than that in the absence of alcohol. It is known from the literature that the radical produced from the reaction of $^{\bullet}OH$ with tertiary butyl alcohol is highly unreactive [156] and cannot reduce Ag^+ to Ag^0, and therefore, in both of the cases, e_{aq}^- and $H^{\bullet}$ bring about the reduction of Ag^+ to Ag^0. In that case, the intensity of the surface plasmon band should have been same in both the cases. The only difference between these two cases was the fate of the $^{\bullet}OH$ in the absence of alcohol where it can react with GG. Therefore, it appears that the radical generated from the reaction of $^{\bullet}OH$ with GG was able to reduce Ag^+ to Ag^0. Because of this, the intensity of the plasmon band was higher in the absence of alcohol.

3.3.7. Characterization of Ag nanoparticles by XRD and TEM

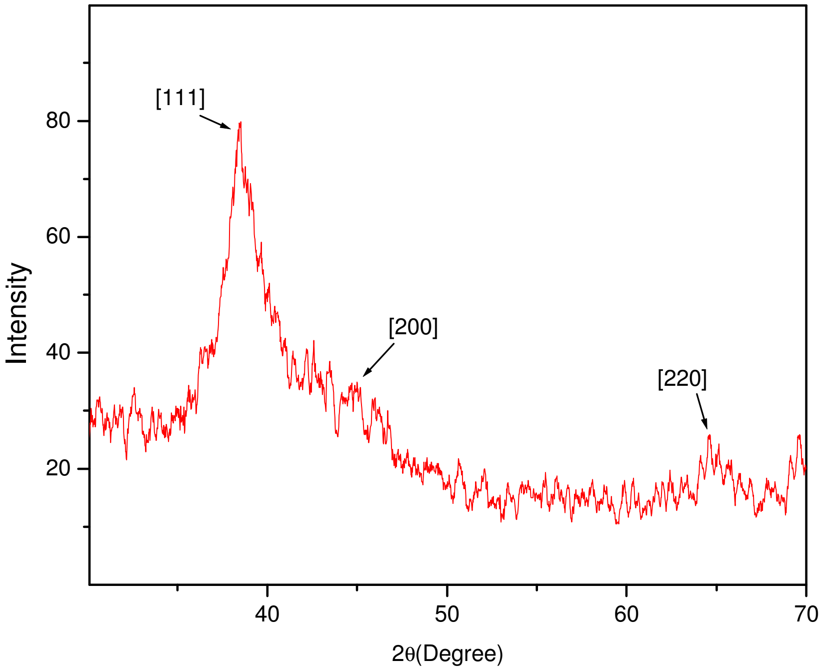

Figure 3.11: XRD pattern of Ag/GG

Formation of Ag nanoparticles stabilized by guar gum using gamma radiation as a tool for the reduction has been successfully demonstrated from the absorption spectra which showed the characteristics surface plasmon band of Ag nanoparticles in the region of 400-450 nm. These nanoparticles were further characterized by several physical techniques such as XRD, TEM and Thermogravimetry. The XRD pattern recorded in the 2θ region of $20\text{-}70^0$ is shown in Figure 3.11. In the XRD pattern, peaks at 2θ value of 38.1, 44.25 and 64.54 were observed, which confirmed the formation of metallic silver [157]. The broad bandwidth of main peak at 2θ value of 38.1 indicates that the size of clusters is small which was confirmed from the TEM analysis. The TEM picture of Ag/guar gum is shown in Figure 3.12. It shows spherical particles with size distribution in the range of 10-30 nm.

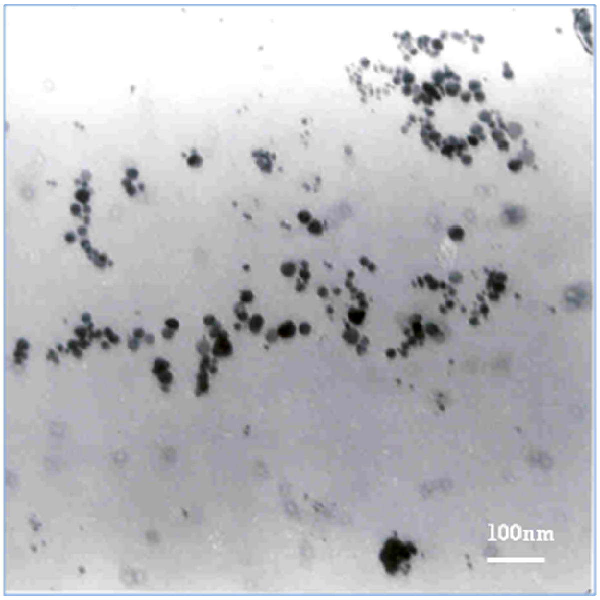

Figure 3.12: TEM images of the Ag clusters formed upon irradiation in aqueous GG solution (bar length= 100 nm)

3.3.8. Thermal studies of Ag nanoparticles stabilized by guar gum

The thermal stability of silver nanoparticles is of importance as these are being considered to be utilized for high temperature applications specifically in catalysis. Further it is well known that guar gum like other naturally occurring polymer undergoes chain scission when exposed to ionizing radiation, resulting in the decrease in the molecular weight [158]. The changes occurring in thermal properties of guar gum upon irradiation and after forming composite with Ag were studied using thermogravimetric analysis. For this a sample containing 5% loading of Ag nanoparticles in the guar gum was prepared by irradiating 50 ml of 5% aqueous solution of guar gum containing 220 mg of $AgNO_3$ to a radiation dose of 56 kGy. The 5% loading of Ag was chosen so as to get noticeable changes in the thermogram.

The radiation dose was selected to achieve complete conversion of Ag^+ to metallic silver. The irradiated solution was precipitated by adding to acetone followed by washing with acetone to eliminate radiolytic products. Finally it was dried at 50 ^{0}C under vacuum. Similarly 5% solution of guar gum was also irradiated in the absence of Ag^+. The thermogram of unirradiated guar gum, irradiated guar gum and guar gum irradiated in the presence of Ag^+ is shown in Figure 3.13. The decomposition of unirradiated guar gum starts at 278 ^{0}C whereas guar gum irradiated in the absence of Ag^+ starts decomposing at much lower temperature ~237 ^{0}C. The observed decrease in the decomposition temperature is due to the degradation of guar gum upon irradiation. As mentioned earlier, guar gum belongs to the class of natural polymers, which undergo depolymerization when exposed to ionizing radiation such as gamma rays. The reduction in the molecular weight is responsible for the decrease in the observed decomposition temperature.

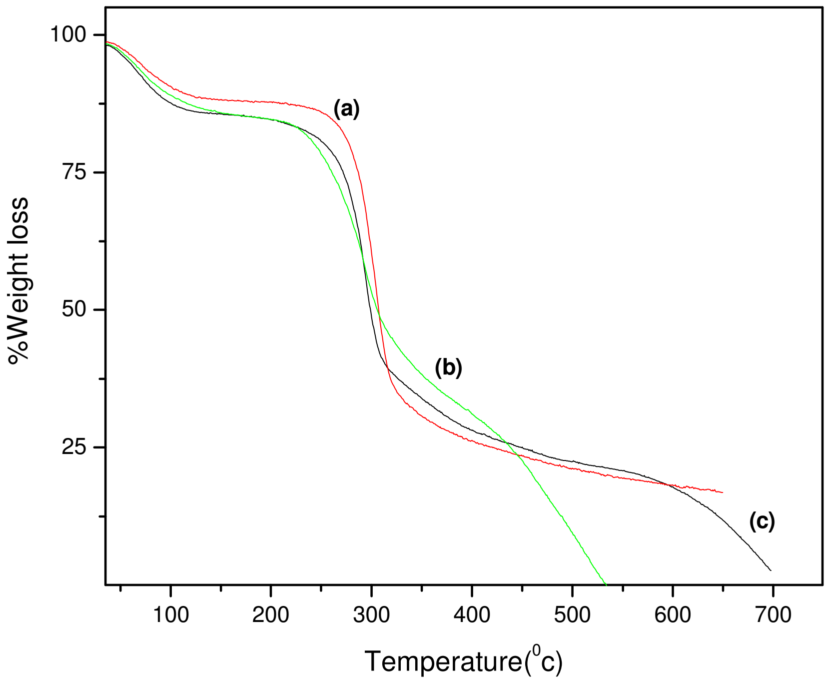

Figure 3.13: Thermograms of (a) GG, (b) irradiated GG, and (c) GG irradiated in the presence of Ag^+

Alternatively, when guar gum was irradiated in the presence of Ag^+ that resulted in the formation of Ag/GG nanocomposite, the decomposition of resultant Ag/guar gum composite starts at 258 ^{0}C which is higher than the one observed for guar gum irradiated in the absence of Ag^+. In both the cases i.e. in the absence and the presence of Ag^+, the radiation dose delivered to the guar gum solution was same. Thus it appears that presence of nano size silver in the irradiated guar gum is responsible for improvement in its thermal properties, which acts as a filler. The analysis of later part of thermogram also indicates that the thermal properties of irradiated guar are improved upon incorporation of Ag. As can be seen from the Figure 3.13, the complete decomposition of irradiated guar gum in the absence of Ag^+ is over at much lower temperature ~ 530 ^{0}C unlike the one irradiated in the presence of Ag^+, where complete decomposition is not even over at 700 ^{0}C. Similar results were also reported for Ag/PVA nanocomposites synthesized using chemical reduction method [84].

3.4. Conclusions

Guar gum is a very effective stabilizer for Ag nanoparticles generated by gamma radiation. Acid medium is the best medium for generating Ag nanoparticles in the presence of guar gum. The radiation dose required to produce 1×10^{-3} mol dm^{-3} nanosilver was found to be 3.5 kGy. In the present work the size distribution of Ag nanoparticles synthesized is 10-30 nm as found from the TEM image. The Ag nanoparticles embedded in guar gum has good thermal stability up to 258 ^{0}C and the complete degradation occurs at 700 ^{0}C.

Chapter 4: Synthesis of silver nanoparticles in methacrylic acid by radiolytic method and studying its application as sensor

4.1. Introduction

Noble metal nanoparticles possess absorption band in the whole visible region of electromagnetic spectrum, hence it is convenient to use them for analytical and biochemical sensing. These metal nanoparticles can be easily dispersed in water and their optical property is very sensitive to their size, shape, nature of surface adsorbed molecules and dielectric property of the surrounding medium. Nanoparticles of silver and gold have been explored by researchers because of uniqueness in their optical properties and facile synthesis [159,58,160]. These nanoparticles have absorption at certain wavelength in the visible spectrum with extremely large molar extinction coefficients (of the order of 10^{11} dm^{3} mol^{-1} cm^{-1}) [161] allowing higher sensitivity in optical detection of biomolecules. Spectrophotometric detection of various molecules/ species based on the optical properties of metal nanoparticles has recently been reported [162–167]. Based on the characteristic changes in the absorption spectra of metal nanoparticles with change in their size, shape or size distribution, optical sensors has been fabricated [168]. Change in the spectral position, FWHM or intensity of absorption spectra of nanoparticles due to interaction of metal nanoparticles with biological analyte is the basis of widely applicable colorimetric sensing [169–172].

Most of colorimetric methods previously reported employed gold nanoparticles as sensing elements. In this work, attempt has been made to develop a colorimetric sensor using silver nanoparticles (Ag np). Though there are several other methods exist in the literature for synthesis of metal nanoparticles [173–177], but gamma radiation induced synthesis method has proved to be effective [178–180,95,102]. In this method, as the aqueous solution of metal salt is exposed to γ-radiation, the radiolysis of water generates species, namely hydrated electron (e_{aq}^{-}) hydrogen atom ($H^{\cdot}$) and hydroxyl radical ($^{\cdot}OH$). The e_{aq}^{-} and $H^{\cdot}$ are strong reducing reagents and they reduce the metal ion (Ag^{+}) to zero valent state (Ag^{0}) [181]. The Ag^{0} coalesce to form Ag nanoparticles in presence of a stabilizer, polymethacrylate (PMA). The $^{\cdot}OH$ radicals produced by water radiolysis were utilized to bring polymerization of methacrylic acid (MA). The radiolytic method is advantageous compare to the chemical method due to *in situ* generation of reducing radicals in the former case, so that the system is free from by-products from external reducing agent. Apart from this the radiolytic reduction method allows a control of the reduction process by tuning the dose and dose rate. Use of polymers as surface capping agents in the synthesis of metal nanoparticles is a well established technique [182,183]. Earlier reports on the synthesis of nanoparticles of silver in poly methyl methacrylate [184–186,145] have described use of sodium salt of acrylic acid for their preparation by radiolysis method. In the first part of this work Ag nanoparticles were synthesized in polymethacrylate by gamma irradiation method. Effect of various experimental parameters on nanoparticle formation has been investigated. The peak maxima (λ_{max}) as well as the absorbance of the surface plasmon resonance spectrum of noble metal nanoparticles (Ag, Au) is highly sensitive to the nanoparticle size, shape and external dielectric environment. This property of silver nanoparticles helps in developing a new class of nanoscale affinity biosensors. Dopamine (DA) belongs to class of catecholamines, which are compounds with a dihydroxyphenyl group and an amine group [187] (Figure 4.1).

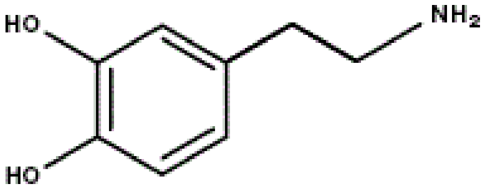

Figure 4.1: Chemical structure of dopamine

These biomolecules act as neurotransmitters in the function of brain and nerve signal transduction. Lack of dopamine cause diseases such as parkinsonism, schizophrenia. Therefore, monitoring of dopamine concentration is essential and important technique. In recent years, many methods have been reported for the determination of neurotransmitters in pharmaceutical preparations and biological samples such as electrochemistry [188,189], chemiluminescence [190], spectrofluorimetry [191,192], high performance liquid chromatography (HPLC) with different detectors [193,194] and mass spectrometry [195]. Wang et al. reported the determination of DA by flourophotometry in a linear range 0.02-0.60 mg L^{-1} with a lower upper limit [192]. Many current techniques for neurotransmitter detection in spite of good sensitivity require expensive and sophisticated instrumentation or complicated sample preparation and time consuming processes. Thus, the development of new sensitive, fast and practical method for neurotransmitter detection still remains a great challenge. In the present work a simple, sensitive and inexpensive spectroscopic method has been developed to estimate DA in aqueous solution in a linear range of 5.27×10^{-7} to 1.58×10^{-5} mol dm^{-3} DA (0.1-3 mg L^{-1}). The silver nps have been synthesized in polymethacrylate (PMA) by means of gamma irradiation. The effects of different parameters on formation of nanoparticles have been studied. It was observed that the spectral behaviour of PMA stabilized silver nanoparticles changes in response to addition of a small quantity of DA and the change is gradual with respect to DA concentration variation. DA concentration in the range of 5.27×10^{-7} to 1.58×10^{-5} mol dm^{-3} shows very good linear response in the plot of absorbance value versus DA concentration with the correlation factor, R=0.9977 and the detection limit 5.27×10^{-7} mol dm^{-3}. Ascorbic acid (AA) is present in millimolar concentration along with DA (nanomolar to micromolar) in biological fluid [196,197]. Conventionally DA was estimated by electrochemical analysis. In electrochemical detection of DA, AA imposes major problem, because the redox potential of AA is close to DA. This affects the selectivity due to overlapping of signal of AA with the signal of the compound of interest, DA. In this study the interference of AA in estimation of DA has also been studied. AA concentration up to to 1.0×10^{-4} mol dm^{-3} does not interfere in the estimation of DA in the range of 5.27×10^{-7} to 1.05×10^{-5} mol dm^{-3}.

4.2. Result and discussions

4.2.1. Synthesis of Ag nanoparticle solution

Aqueous solution containing 1×10^{-3} mol dm^{-3} $AgNO_3$, 1×10^{-1} mol dm^{-3} methacrylic acid (MA) and various concentrations of NaOH was purged with N_2 and irradiated in a ^{60}Co gamma chamber having dose rate 2.2 kGy h^{-1}. Total dose delivered to this solution was 2 kGy. The order of addition of reagents was MA, NaOH and $AgNO_3$ and this order was strictly followed in all the experiments. After irradiation the appearance of yellow color is because of formation of Ag nps and the same was further confirmed by uv-visible and TEM measurements.

When aqueous solution of $AgNO_3$, MA and NaOH was subjected gamma irradiation at different absorbed dose, dark yellow colored solution of Ag nps were obtained. The absorption spectrum of this solution is shown in Figure 4.2. During irradiation polymerization of MA and Ag nanoparticle formation take place simultaneously. Polymerization of MA results in formation of polymethacrylate (PMA) in presence of NaOH, which subsequently stabilizes the Ag nanoparticles. Generally in radiolytic synthesis of metal nps isopropanol is added to scavenge oxidizing ${}^{\bullet}OH$ radicals to create total reducing environment. But in this work the addition of isopropyl alcohol has been avoided because the ${}^{\bullet}OH$ radicals produced by water radiolysis were utilized to bring polymerization of MA. Polymers provide more effective capping to metal nanoparticles compared to their respective monomers because the steric stabilization is more pronounced in case of the polymers.

The interaction of γ-radiation with aqueous solution of metal ions leads to radiolysis of water and subsequently generates reactive radical species throughout the solution (Equation 4.1).

$$H_2O \xrightarrow{\gamma} e_{aq}^{-} + H^{\bullet} + {}^{\bullet}OH \tag{4.1}$$

$$e_{aq}^{-} / H^{\bullet} + Ag^{+} \longrightarrow Ag^{0} + /H^{+} \tag{4.2}$$

$${}^{\bullet}OH + MA \longrightarrow PMA \tag{4.3}$$

The e_{aq}^{-} and $H^{\bullet}$ are strong reducing agents, which can reduce Ag^{+} to Ag^{0} (Equation 4.2). Though ${}^{\bullet}OH$ radical produced is oxidising in nature, this radical does not hinder in reduction of metal ion. Because the ${}^{\bullet}OH$ radicals are known to induce polymerization in methacrylic acid type of monomers [198,199]. Hence in presence of ${}^{\bullet}OH$, MA polymerizes to form PMA (Equation 4.3). The Ag^{0} atoms being unstable in solution coalesce to form Ag nanoparticles in presence of capping agent, PMA.

4.2.2. Characterization of Ag/methacrylic acid

The Ag nanoparticles solution prepared from 1×10^{-3} mol dm^{-3}Ag^{+}, 1×10^{-1} mol dm^{-3} MA and 1×10^{-1} mol dm^{-3} NaOH shows absorption band at ~450 nm as shown in Figure 4.2. The intensity of absorption band increases and it becomes narrower with increase in absorbed radiation dose. This is because at lower dose, less amount of Ag^{+} are reduced, which results in formation of smaller size and lower concentration of Ag nps. At very small size Ag nps shows broad absorption peak. With increase in absorption dose the yield of nps increases, hence the intensity of absorption band increases.

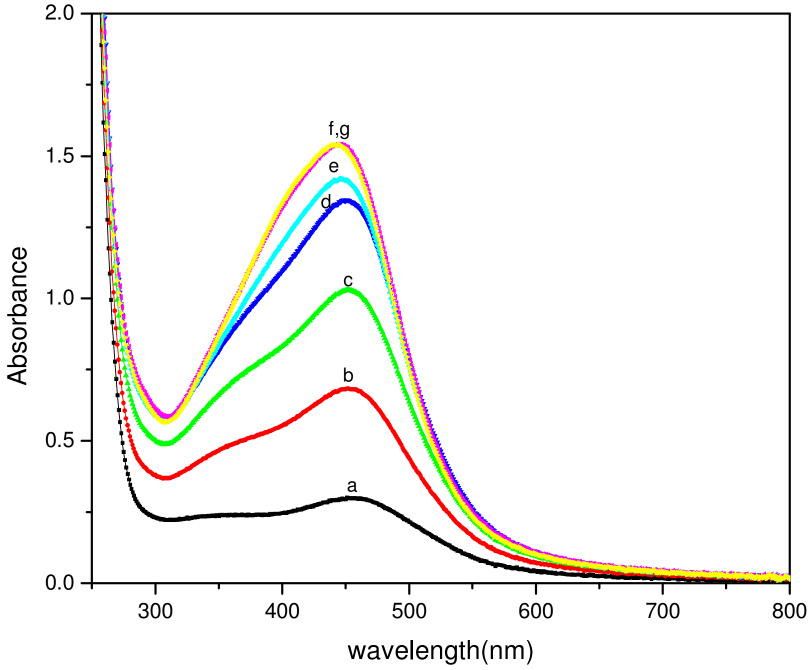

Figure 4.2: Absorption spectra of aqueous Ag nanoparticle solution at different radiation dose: (a) 0.5 kGy, (b) 1.1 kGy, (c) 1.7 kGy, (d) 1.8 kGy, (e) 2.0 kGy, (f) 2.2 kGy, (g) 2.4 kGy. [Ag^+= 1 x 10^{-3} mol dm^{-3}, MA= 0.1 mol dm^{-3}, NaOH= 0.1 mol dm^{-3}, Dose= 2.2 kGy h^{-1}, Solution was diluted in ratio 1:4 with water before taking spectra]

The average size of Ag nps known from the TEM image shown in Figure 4.3 was found to be 6 nm.

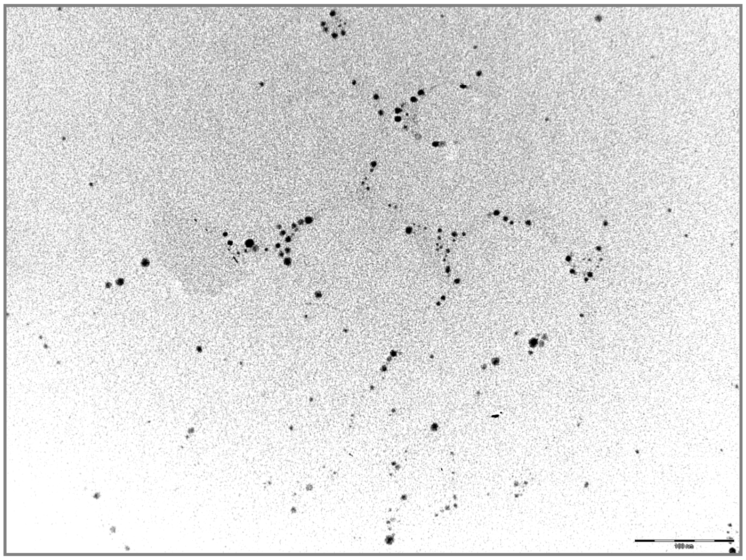

Figure 4.3: TEM image of Ag nanoparticles stabilized by poly methacrylate

The pH of solution containing 1 × 10^{-1} mol dm^{-3} NaOH and 1 × 10^{-1} mol dm^{-3} MA (NaOH : MA= 1:1) was measured and found to be 12.8, which is much above than pKa of MA, i.e., 4.7. At this composition of MA and NaOH, MA will remain in deprotonated form. This particular ratio of NaOH: MA has been maintained in all other experiments for synthesis of Ag nps unless it has been mentioned. Hence in the final step of synthesis, deprotonated form of polymethacrylic acid, i.e., polymethacrylate (PMA) stabilizes Ag nps. The detail mechanism is given in Figure 4.4. Ag^+ ions are reduced to Ag^0 by γ-radiolysis and subsequently Ag^0 atoms coalesce to form Ag nps. The methacrylic acid gets polymerized in presence of $^{\bullet}OH$ radicals and NaOH to form polymethacrylate (PMA). Then as formed Ag nps are stabilized by PMA by surface capping. The anionic carboxylate functional groups are known to stabilize smaller size metal nanoparticles due to stronger electrostatic stabilization. Hence the np size obtained in this study is only 6 nm. Similar results have been obtained by Nishimura and his co-workers in case of Ag nps stabilized by sodium acrylate [200]. In their work also the size of Ag nps obtained was 6 nm.

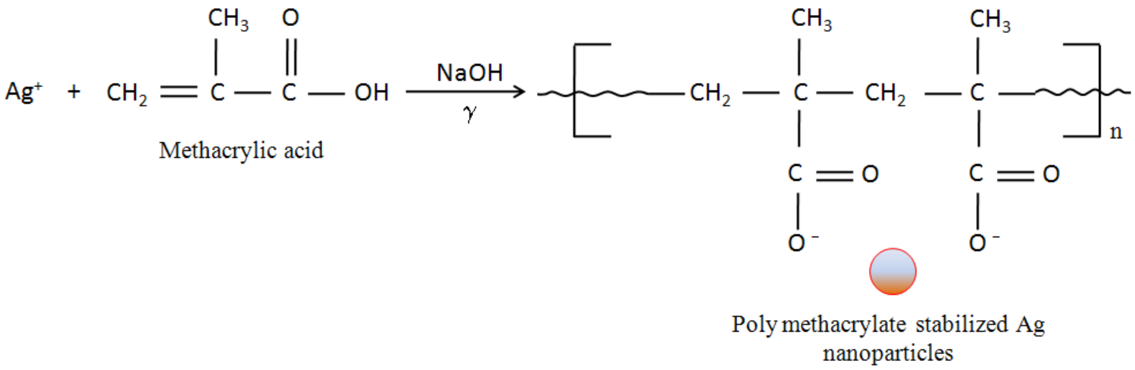

Figure 4.4: Mechanism of Ag nanoparticle formation and stabilization by polymethacrylate

During irradiation along with formation of Ag nps MA polymerizes to form PMA, which subsequently stabilizes the nps. This can be confirmed from the FTIR spectra of monomer (MA) and polymer stabilized Ag nanoparticles (Ag/PMA) as shown in Figure 4.5. The IR peaks corresponding to different functional groups in both the cases are listed in Table 4.1. In case of pristine MA the IR peak at 1697 cm^{-1} is due to C=C double bond. This peak is absent in case of final sample after irradiation (Ag-PMA), which is an indication of polymerization of MA during irradiation. The peak at1630 cm^{-1} in both the spectra is due to >C=O stretching of carboxylate group. In case of Ag–PMA the peak at 1630 cm^{-1} is a little broader. The broadening may be due to interaction of carboxyllate group with Ag nps. IR peak at 1540 cm^{-1} in case of Ag nps/PMA is for 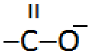 $-\overset{\parallel}{\mathrm{C}}-\mathrm{O}^{-}$ stretching of carboxylate group. Since NaOH is present in the solution and the pH is around 12.8, polymethacrylic acid exists in deprotonted form.

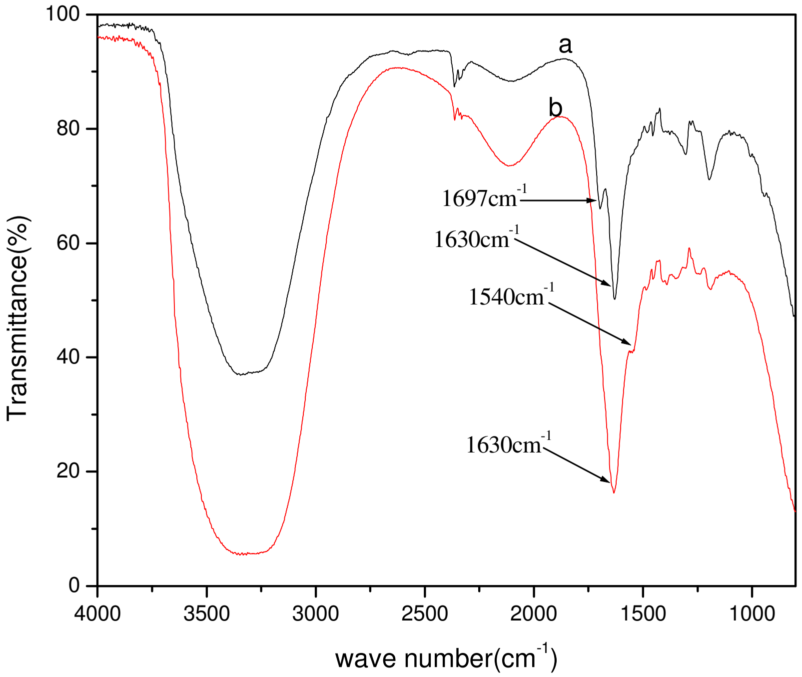

Figure 4.5: FTIR spectra of (a) Methacrylic acid, (b) Ag nanoparticles stabilized by polymethacrylic acid sodium salt [Ag nanoparticles in methacrylic acid synthesized by taking 1 x 10^{-3} mol dm^{-3} AgNO3, 0.2 mol dm^{-3} MA and 0.15 mol dm^{-3} NaOH , dose rate = 2.2 kGy h^{-1}, dose = 2.4 kGy]

Table 4.1: FTIR peaks of methacrylic acid and Ag/polymethacrylate

FTIR peak of MA (cm^{-1})	Functional group in MA	FTIR peak of Ag-PMA (cm^{-1})	Functional group in Ag-PMA	Remarks (in case of Ag-PMA)
1697	>C=C<	(1697) Absent	-	Double bond does not exist due to polymerization of methacrylic acid
1630	>C=O	1630, broad	>C=O	Carboxyllic group interaction with Ag np
(1540) Absent	-	1540	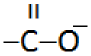 $-\overset{\parallel}{\mathrm{C}}-\mathrm{O}^{-}$	Carboxylate group of PMA is in deprotonated form

4.2.3. Effect of the methacrylic acid concentration

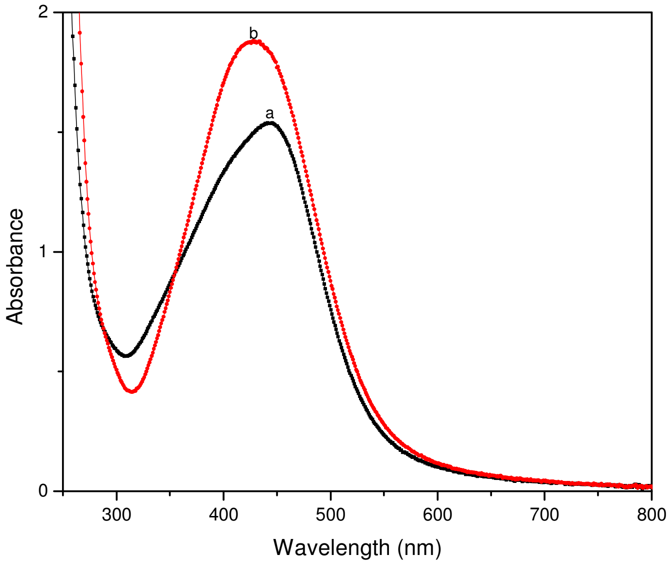

Figure 4.6: Absorption spectra of Ag nanoparticles at different methacrylic acid concentration MA= (a) 0.1 mol dm^{-3}, NaOH= 0.1 mol dm^{-3} (b) 0.2 mol dm^{-3}, NaOH= 0.2 mol dm^{-3} [Ag^{+}= 1 x 10^{-3} mol dm^{-3}, dose rate= 2.2 kGy h^{-1}, dose = 2.4 kGy, Solution was diluted in ratio 1:4 with water before taking spectra]

The effect of MA concentration on Ag np formation was studied by varying MA concentration from 1×10^{-1} mol dm^{-3} to 2×10^{-1} mol dm^{-3} (for [NaOH] = 1×10^{-1} mol dm^{-3} and 2×10^{-1} mol dm^{-3} respectively) keeping Ag^{+} concentration constant to 1×10^{-3} mol dm^{-3}. For lower MA concentration the spectrum is broad and for higher MA concentration a narrow spectrum has been obtained as shown in Figure 4.6. This is because higher concentration of capping agent (MA) will more effectively confine the np size in a certain range leading to formation of narrow size distribution of nps.

4.2.4. Effect of the Ag^{+} concentration

Aqueous solution containing 2×10^{-1} mol dm^{-3} MA, 2×10^{-1} mol dm^{-3} NaOH and different amount of Ag^{+} was irradiated for total dose of 2.4 kGy and the absorption spectra is shown in Figure 4.7. It has been observed that as the concentration of Ag^{+} increases from 1×10^{-3} mol dm^{-3} to 2×10^{-3} mol dm^{-3} there is broadening in the absorption spectra. As the Ag^{+} concentration increases, 2×10^{-1} mol dm^{-3} MA is not sufficient to stabilize nps at this concentration. Hence the particle size becomes large and polydispersed, which causes broadening of absorption spectra.

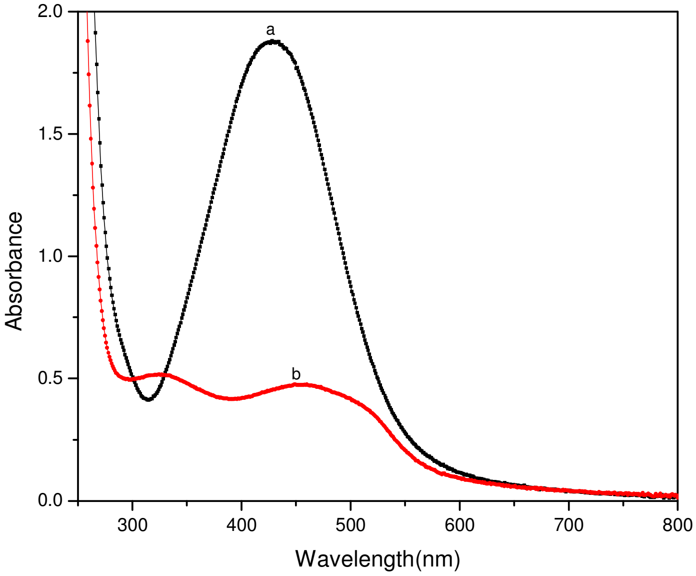

Figure 4.7: Absorption spectra of Ag nanoparticles at different $AgNO_3$ concentration Ag^+= (a) 1 x 10^{-3} mol dm^{-3}, dose = 2.4 kGy (b) 0.2 mol dm^{-3}, dose = 4.8 kGy, [MA= 0.2 mol dm^{-3}, NaOH= 0.2 mol dm^{-3}, Dose rate= 2.2 kGy h^{-1}, Solution was diluted in ratio 1:4 with water before taking spectra]

4.2.5. Estimation of dopamine concentration

For estimation of DA Ag nps were synthesized by different experimental set up and these nanoparticle solutions were examined to obtain uniform and gradual change in the spectral characteristic with varying DA concentration. The optimum experimental condition for synthesis of Ag nps derived was 1×10^{-3} mol dm^{-3} $AgNO_3$, 2×10^{-1} mol dm^{-3} methacrylic acid and 1.5×10^{-1} mol dm^{-3} of NaOH. Aqueous solution containing these reagents was purged with N_2 and irradiated for a dose of 2kGy in ^{60}Co gamma chamber having dose rate 2.2 kGy h^{-1}. Measured amount of as prepared Ag nps in PMA solution was added to aqueous solution containing different amount of DA, so that the final concentration of nps was maintained 5×10^{-4} mol dm^{-3} (in terms of Ag^+) in each measurement. Then this solution mixture was kept for 5 hours to attain equilibrium before measuring the absorption spectra. The color change from light yellow to dark yellow with increase in DA concentration could be easily distinguished.

The chemical name of DA is 3,4 dihydroxy phenyl ethyl amine and it contains a dihydroxyphenyl group and an amine group (Figure 4.1). When DA was added to Ag np solution prepared by gamma radiolysis the change in color of the nanoparticle solution could be recognized visibly. This phenomenon was quantified by recording the absorption spectra of np solution in presence of various amount of DA. The absorption spectra of np solution in presence of different DA concentration are given in Figure 4.8. From the spectra it is observed that with increase in DA concentration the intensity of the absorption band increases. The mechanism proposed for the effect of dopamine addition to the Ag np is explained as follows. The Ag np solution prepared through gamma irradiation contains some unreduced Ag^+ ions. DA is a two electron mild reductant [201]. In this system the Ag^+ ions are adsorbed on the surface of Ag nps, so that the chemical potential of these ions are shifted to more positive value than their bulk form [202]. As a result these Ag^+ ions are easily reduced by DA. Also in presence of NaOH the dihydroxy phenyl group of DA loses H^+ and the de-protonated form of DA has more negative reduction potential [203]. Hence in alkaline solution and in presence of Ag nps the reduction of Ag^+ by DA is more facilitated. As more and more DA was added to the reaction solution more Ag^+ are reduced and the Ag^0 formed are either deposited on previously present Ag nps or can form new Ag nps.

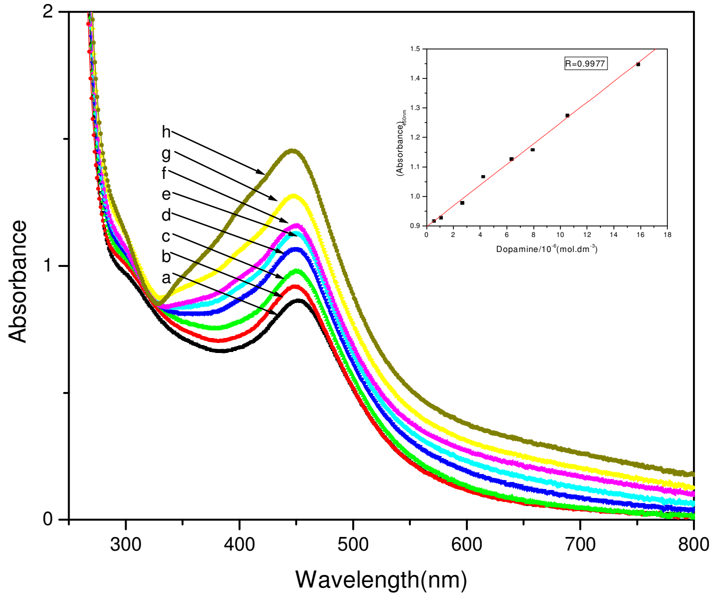

Figure 4.8 Absorption spectra of Ag nanoparticle solution in presence of various dopamine concentration (a) 0, (b) 5.27 x 10^{-7}, (c) 2.63 x 10^{-6}, (d) 4.21 x 10^{-6}, (e) 6.32 x 10^{-6}, (f) 7.9 x 10^{-6}, (g) 1.05 x 10^{-5}, (h) 1.58 x 10^{-5} mol dm^{-3}
(Inset): Linear plot of absorbance at 450nm versus DA concentration in the range 5.27 x 10^{-7} to 1.58 x 10^{-5} mol dm^{-3}.

As a result there is a possibility of increase in Ag np size and size distribution, which is indicated by increase in intensity and broadening of absorption band of Ag np solution. There is no shift in the peak position, because for spherical nps small change in particle size does not affect the plasmon band position. The increase in absorbance at 450nm was plotted against DA concentration. The plot is linear in the range 5.27×10^{-7} to 1.58×10^{-5} mol dm^{-3} of DA concentration with the correlation factor, R=0.9977 and the detection limit 5.27×10^{-7} mol dm^{-3}.

4.2.6. Estimation of dopamine in presence of ascorbic acid

Conventionally DA was estimated by electrochemical analysis. A common problem in electrochemical analyses at unmodified electrodes is the lack of selectivity due to the presence of interfering compounds that overlap with the signal of the compound of interest. For example, ascorbic acid (AA) oxidizes at nearly the same potential as DA. Also AA coexists with DA in the extracellular fluids of mammalian brain. Hence in this study the interference of AA in DA estimation was also investigated.

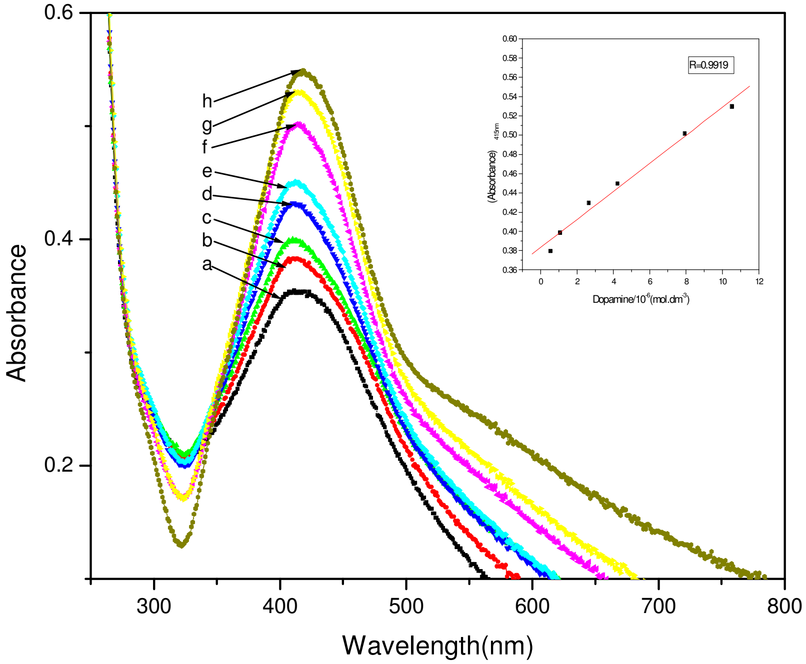

Figure 4.9: Absorption spectra of Ag nanoparticle solution in presence of various dopamine concentration (a) 0, (b) 5.27 x 10^{-7}, (c) 1.05 x 10^{-6}, (d) 2.63 x 10^{-6}, (e) 4.21 x 10^{-6}, (f) 7.9 x 10^{-6}, (g) 1.05 x 10^{-5}, (h) 1.58 x 10^{-5} mol dm^{-3} in presence of 1.0 x 10^{-4} mol dm^{-3} ascorbic acid
(Inset): Linear plot of absorbance at 415 nm versus DA concentration in the range 5.27 x 10^{-7} to 1.05 x 10^{-5} mol dm^{-3}: (Spectra taken with 0.2 cm path length cuvet)

The interference of AA on DA estimation was studied by adding 1×10^{-4} mol dm^{-3} AA to the aqueous solution containing Ag nps in PMA and different concentrations of DA were added after addition of AA. The absorption spectra of all the samples with varying DA concentrations were measured after 5 hours of mixing all the reagents. As shown in Figure 4.9 the absorbance of Ag np solution gradually increases with DA concentration at ~415 nm even in presence of AA. Figure 4.9: Inset shows linear plot of absorbance at 415 nm versus DA concentration in presence of 1.0×10^{-4} mol dm^{-3} AA. After optimization of experimental parameters it was obtained that AA concentration up to 1.0×10^{-4} mol dm^{-3} does not interfere in the estimation of DA in the range of 5.27×10^{-7} to 1.05×10^{-5} mol dm^{-3}. It has been observed that in presence of AA the Ag nanoparticle absorption peak intensity increases as well as the spectra is shifted to lower wavelength (spectra taken with 0.2 cm path length cuvet) even before addition of DA as compared to that in absence of AA. The increase in intensity is assigned to reduction of Ag^+ by AA so that there is an increase in yield of Ag nps. AA has also stabilization property towards metal nanoparticles. In millimolar concentration it may affect the stabilization of Ag nanoparticles in this particular case.

4.3. Conclusions

Silver nanoparticles have been synthesized in polymethacrylate by gamma radiolysis technique. Effects of different experimental parameters, such as $AgNO_3$ concentration, methacrylic acid concentration on formation of silver nanoparticles have been investigated. The nanoparticles were characterized by UV-visible spectroscopy, FTIR and TEM analysis. The polymerization of MA and interaction of Ag np with PMA was confirmed by FTIR analysis. Experimental set up was standardized to estimate dopamine using the radiolytically synthesized Ag nanoparticles. The anionic carboxylate functional groups from deprotonated PMA helps in formation of smaller size metal nanoparticles by providing stronger electrostatic stabilization. This was confirmed by measuring the nanoparticle size by TEM, which was found to be ~6 nm. Dopamine concentration in the range of 5.27×10^{-7} to 1.58×10^{-5} mol dm^{-3} can be estimated by the proposed method. The detection limitof this method is 5.27×10^{-7} mol dm^{-3}. The interference of ascorbic acid in dopamine estimation was investigated. Ascorbic acid concentration up to 1.0×10^{-4} mol dm^{-3} does not interfere in the estimation of dopamine in the range 5.27×10^{-7} to 1.05×10^{-5} mol dm^{-3}.

Chapter 5: Radiation induced synthesis of anisotropic gold nanoparticles and their characterization

5.1. Introduction

Fine metal particles with nanometer scale dimensions are of current interest due to their unusual properties [169,204,205]. The applications of nanomaterials depend strongly on the particle size, the interparticle distance and the shape of the nanoparticles. The morphology of metal nanoparticles is important in the field of scientific research, because small changes in the shape of nanoparticles can have great effect on a variety of physical properties of the material [92,206–212,110]. Nanoscale particles of gold are being investigated for potential applications in the field of catalysis, chemical and biological sensors and biomedical applications [205,92,10,101,213–217]. Therefore controlled preparation of nanomaterials is very important and significant. Many physical and chemical approaches have been developed to obtain special shaped nanomaterials such as nanorods, ellipsoids, cubes, etc. The physical methods produce nanomaterials from bulk materials with the help of exact and sophisticated equipments, while the chemical approach prepares nanomaterials from the atoms and molecules through simple chemical routes. In the past decade, many research groups have dedicated themselves to the preparation of metal nanomaterials following chemical approach. Several chemical synthesis methods based on colloid chemistry have been developed for the production of metal nanoparticles with different shapes [209–211,85,87,215,219–223] using CTAB as a structure directing capping agent. Chen et al. (2006) have reviewed in detail the account of chemical approach for preparing special shaped nanomaterials. Usually, chemical approaches are classified as (i) selfstructure confinement approach, (ii) hard or soft template approach, (iii) physical chemistry approach and (iv) soft solution approach. Among these the soft solution method, which is based on the reduction in the solution by mild reducing agents in the presence of additives like polymers [224,225], surfactants [213,226–229] and dendrimers [230–233], is widely used. In the case of special shaped metal nanoparticles, these additives adsorb on the precursor metal ions first and then create anisotropic confinements by selective passivation of certain facets to induce and maintain anisotropic crystal growth. This approach enables to generate special shaped nanostructures with highly crystalline and well-controlled composition in a high yield. The ability of ionizing radiation to bring about ionization and excitation in the medium through which they travel results in the formation of reactive species, which can be utilized to reduce metal ions into metal atoms to generate metal nanoparticles. Radiolysis of water/ aqueous solution results in generation of reactive species such as hydrated electron (e^{-}_{aq}) and hydrogen atom ($H^{\cdot}$) and hydroxyl radical ($^{\cdot}OH$). The first two radicals can easily reduce metal ions down to zero valent state [95,234]. As mentioned in chapter 3 (section 3.1) the hydroxyl radicals produced in the course of radiolysis are oxidizing in nature. To scavenge this radical, isopropyl alcohol is added to the reaction system, which subsequently forms isopropyl radical. Hence a total reducing atmosphere is created. The difference between gamma radiation method and soft solution method is that in the former the reducing species are generated in situ, whereas in later the reducing agent is incorporated in to the system from an external source. Further in radiation method, reduction is carried out at room temperature, so that additives sensitive to heat, such as polymeric systems that are not suitable for chemical reduction under heating may also be used in the radiolytic method. A particular advantage of radiolysis method is that the reduction rate is controlled by selected dose rate, which offers a wide range of conditions from slow to quasi-instantaneous atom production unlike chemical method where the local concentration of reducing species is very high and cannot be controlled very easily. The literature survey reveals that only a few articles are available on generation of anisotropic metal nanoparticles by using high energy radiation [235]. Preparation of non spherical gold nanoparticles by means of chemical route is a multi step process and requires optimization of many experimental factors, such as Au^{III} precursor ion concentration, the surface directing agent namely cetyl trimethyl ammonium bromide (CTAB) concentration and most importantly the seed concentration [213,221,88,236,237]. Chemical method for the synthesis of gold nanorods was proposed by Murphy et al., in 2001[227]. It is a seed mediated growth procedure, in which metal salts (Au^{III}) are reduced initially with a strong reducing agent (sodium borohydride), in water, to produce ~4nm seed particles. Then in another set, metal salts (Au^{III}) are reduced by a weak reducing agent (Ascorbic acid) in the presence of structure-directing additives (CTAB and Ag^{+}) and previously synthesized Au seeds to generate Au nanorods [213,227,88]. In present work initially attempt has been made to design a system for synthesis of gold nanorods similar to chemical method. This is a two step seeded growth method, but instead of using ascorbic acid as a reductant, gamma radiation has been used to generate reducing radicals. Radicals generated by imparting gamma energy radiation are strong reducing species. A milder reducing enviroment is expected to be suitable for formation of anisotropic shaped nanoparticles. Hence low dose rate condition had been chosen to control the reaction rate for generation of Au nanorods.

The above method has been further modified to design a simple and convenient synthesis process, in which the seed solution synthesis step and external addition of seed has been eliminated. In this method a total reducing environment containing a single type of reducing species has been created by carefully choosing the nature and concentration of reactants. It is a one-pot synthesis method, in which even at high dose rate gold nanorods generation has been achieved.

In another approach, anisotropic gold nanoplates have been synthesized by combining both radiolytic and chemical methods. Au seeds are generated in-situ by radiolysis and the Au nanoparticles are allowed to grow on these seeds by ascorbic acid reduction method.

In section 5.2, synthesis of different anisotropic shaped metal nanoparticle by means of gamma-radiation based method has been discussed. Initially short aspect ratio gold nanorods were synthesized by controlling the dose rate of gamma radiation. In this method previously prepared gold seed solution and CTAB were used for nanorod synthesis, where these two play important role to induce anisotropy. Here the reducing agents used were e^{-}_{aq} and $H^{\cdot}$ and isopropyl radical. The effect of absorbed dose and dose rate and reactant concentration in controlling the growth of particles has also been investigated.

In section 5.3 development of a modified method for producing gold nanorods has been described. Here a single type of reducing species, namely isopropyl radical has been employed unlike earlier methods where hydrated electron, $H^{\cdot}$ and isopropyl radicals were used as reducing agents. Also under the present experimental protocol, synthesis of gold nanorods has been achieved without using any gold seed solution. The effect of dose, dose rate, precursor metal ion concentration and the concentration of CTAB on the formation of nanorod have also been investigated.

Section 5.4. provides details of rectangular gold nanoplates synthesized by employing both radiation and chemical method. The rectangular gold nanoplates have been formed in a single step by irradiating the growth solution containing 4×10^{-4} mol. dm^{-3} gold precursor ion

(Au^I), 0.1 mol dm^{-3} cetyl trimethyl ammonium bromide (CTAB), 0.2 mol dm^{-3} isopropanol, 6 × 10^{-5} mol dm^{-3} Ag^+ and 7.2 × 10^{-4} mol dm^{-3} ascorbic acid for short duration of time at a dose rate of 3.4 kGy h^{-1} so that appropriate amount of nanoparticle seeds are generated *in situ*. These seeds provide the site for nanoparticle growth and the anisotropy of the nanoparticles is controlled by the capping agent, namely CTAB and Ag^+ as mentioned in the literature [79,236,238]. Hence, unlike chemical method the seed preparation step has been avoided in the present method, so that the complexity of the process and wastage of reagents in the unused seed solution has been minimized. The evolution of nanoparticle with time and the effect of experimental parameters such as absorption dose, ascorbic acid/ Au^{III} ratio, precursor Au^{III} concentration, $AgNO_3$ concentration, the concentration of CTAB and pH on the formation of nanoparticles has also been investigated.

5.2. Synthesis of short aspect ratio anisotropic gold nanorods in CTAB by using gamma radiation

5.2.1. Synthesis of Au seed solution

The Au seeds were prepared by a method similar to that described in the literature [213]. In a typical protocol, 4ml of 1×10^{-3} mol dm^{-3} Au^{III} solution, 5ml of 0.2 mol dm^{-3} CTAB solution and 1ml of 1×10^{-2} mol dm^{-3} ice cold sodium borohydride were mixed in the same order as mentioned. The solution was shaken vigorously for 2 minutes and kept aside for 2 hours before use. The color of the solution changed from light yellow to light brown after the addition of sodium borohydride. The formation of Au seeds is schematically represented in Figure 5.1. The resultant Au seeds have particle size in the range 3.5– 4.0 nm as determined by TEM analysis [213].

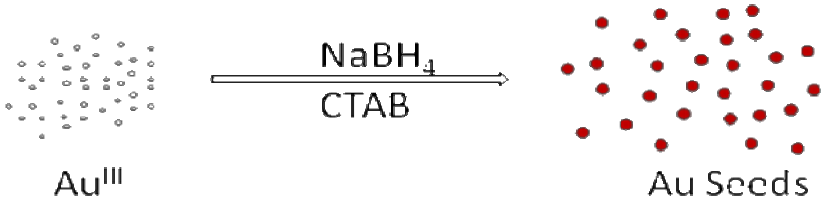

Figure 5.1: Cartoon picture of synthesis of Au seeds from Au^{III} ions in presence of $NaBH_4$ and CTAB

5.2.2. Synthesis of Au^I solution

The aqueous solution of 4×10^{-4} mol dm^{-3} $HAuCl_4$ containing 0.2 mol dm^{-3} isopropyl alcohol and 0.1 mol dm^{-3} CTAB was irradiated in the gamma chamber at a dose rate 3.4 kGy h^{-1} after purging with high pure N_2 gas till the solution turned colorless. The colorless solution is due to formation of Au^I as shown in Equations (5.1- 5.3). This solution contains Au^I and was used as a precursor for gold in the synthesis of gold nanorods. The concentrations of different reagents mentioned in this section were kept constant throughout the study in section 5.2 unless it is mentioned.

$$Au^{III} + e_{aq}^{-} / (CH_3)2^{\bullet}C\text{-}OH \longrightarrow Au^{II} + (CH_3)_2C{=}O + H^+ \quad (5.1)$$

$$Au^{II} + Au^{II} \longrightarrow (Au^{II})_2 \quad (5.2)$$

$$(Au^{II})_2 \longrightarrow Au^{III} + Au^{I} \quad (5.3)$$

5.2.3. Results and discussion

5.2.3.1. Irradiation at higher dose rate

The chemical method for synthesis of gold nanorods involves the reduction of Au^{III} by weak reducing agent such as ascorbic acid in the presence of Au seeds and Ag^+, the surfactant CTAB is used as a structure directing agent [239,211,88]. In the present method reducing species, which are generated *in situ* by gamma radiolysis, are used for the reduction of Au^I to metallic Au in aqueous medium. 6×10^{-5} mol dm^{-3} of $AgNO_3$ and 1.2×10^{-6} mol dm^{-3} of seed solution (in terms of Au^{III}) were added to aqueous solution containing 4×10^{-4} mol dm^{-3} of Au^I, 0.2 mol dm^{-3} of isopropanol and 0.1 mol dm^{-3} of CTAB (prepared as per mentioned in section 5.2.2.) and it was irradiated with gamma rays at a dose rate= 3.4 kGy h^{-1}. Under these conditions most of the energy is absorbed by water resulting in the formation of highly reactive species such as e^-_{aq}, $H^\bullet$ and $^\bullet OH$. Among these radicals e^-_{aq} (E^0 H_2O/e^-_{aq} = -2.87 V_{NHE}) and $H^\bullet$ (E^0 H^+/H= -2.3 V_{NHE}) are highly reducing in nature. Both these radicals bring about the reduction of Au^I to Au^0. However, in the presence of isopropyl alcohol the $^\bullet OH$ radical is scavenged and isopropyl radical is generated [Equation 5.4]. The isopropyl radical thus generated is reducing in nature (E^0= -1.5 V_{NHE}) and is capable of reducing Au^I to Au^0 as shown in Equation 5.5.

$$(CH_3)_2CH(OH) + {}^\bullet OH \longrightarrow (CH_3)_2\,{}^\bullet C(OH) + H_2O \quad (5.4)$$

$$(CH_3)_2\,{}^\bullet C(OH) + Au^I \longrightarrow (CH_3)_2CO + Au^0 + H^+ \quad (5.5)$$

The Au atoms generated by radiolysis undergo coalescence resulting in the formation of Au nanoparticles, which get stabilized by CTAB. The absorption spectra of irradiated solution at various times of irradiation are shown in Figure 5.2.

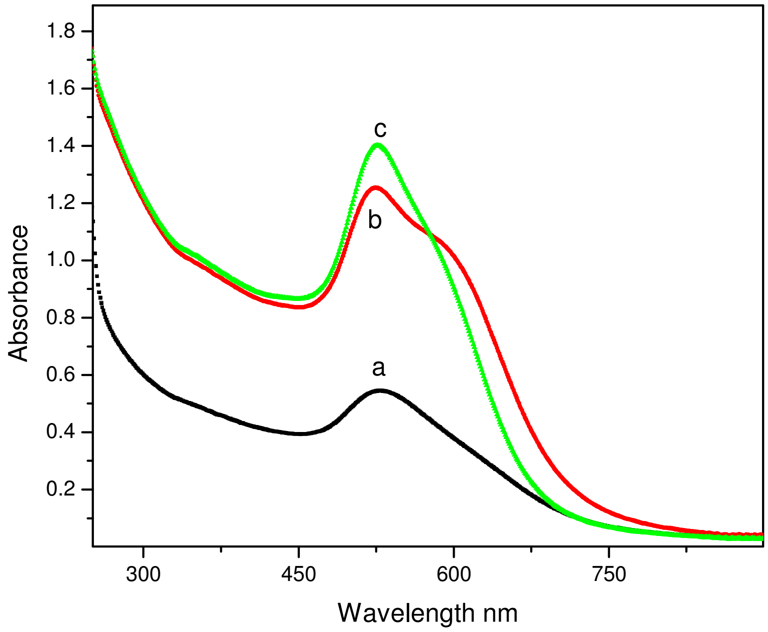

Figure 5.2: Absorption spectra of irradiated solution containing 4 x 10^{-4} mol dm^{-3} of Au^{I}, 0.2 mol dm^{-3} isopropanol, 6x10^{-5} mol dm^{-3} of $AgNO_3$, 0.1 mol dm^{-3} of CTAB and 1.2 x 10^{-6} mol dm^{-3} seed at various absorbed doses (a) 0.8, (b) 1.7 and (c) 2.6 kGy. Dose rate =3.4 kGy h^{-1}

As can be seen from Figure 5.2, only a single peak at 527 nm, which is the characteristic surface plasmon resonance band of Au spheres, is observed. The intensity of this band increases with increase in dose. Under similar conditions, in the synthesis of Au nanoparticles by chemical method employing ascorbic acid as a reducing agent [211], two absorption bands, one at 522 nm and the other at higher wavelength region (650– 800 nm), were observed which were attributed to the formation of gold nanorods. The position of second absorption band at higher wavelength region, also known as longitudinal surface plasmon band, varies with the length of the rod. It is red shifted with increase in the length of the rod [88]. The appearance of single absorption band at 527 nm after the radiolysis indicates the formation of nanoparticles in spherical form. Although, there was an indication of formation of second absorption band during the radiolysis as evident from the appearance of shoulder at 590 nm; however, it did not grow with increasing dose and finally only a single absorption peak at 527 nm was observed. It is known from the literature that during the synthesis of gold nanorods using chemical method the kinetics of the addition of Au^I to the growing seeds governs the shape and size of the nanoparticle [88]. The radiolytic method offers wide ranges of dose rates and therefore the rate of generation of reducing species can easily be governed. The radiolysis was carried out at lower doses and the results obtained are described below.

5.2.3.2. Irradiation at lower dose rates

To investigate the effect of dose rate on the formation of Au nanoparticles, irradiation of aqueous solution containing Au^I, isopropanol, $AgNO_3$, CTAB and seed solution at concentrations same as mentioned in section 5.2.3.1 at various dose rates was carried out. The absorption spectra of solution irradiated at a dose rate 1.7 kGy h^{-1} at various intervals of irradiation are shown in Figure 5.3.

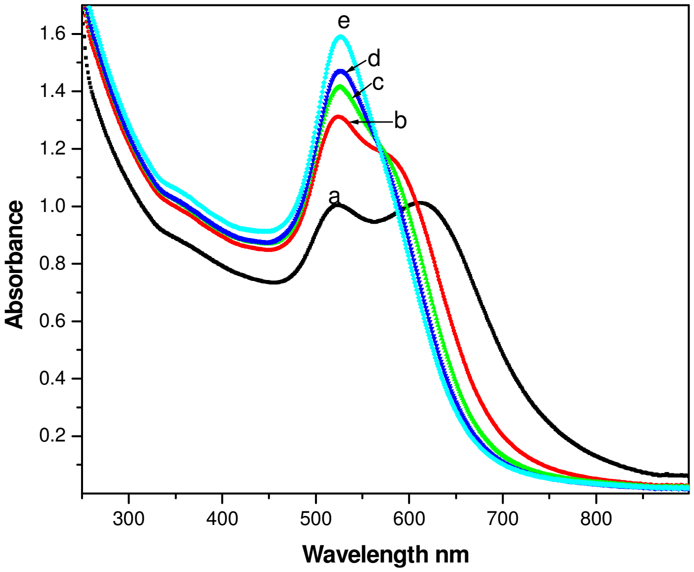

Figure 5.3: Absorption spectra of irradiated solution containing $4x10^{-4}$ mol dm^{-3} of Au^I, 0.2 mol dm^{-3} isopropanol, $8x10^{-5}$ mol dm^{-3} of $AgNO_3$, 0.1 mol dm^{-3} CTAB and 1.2 x 10^{-6} mol dm^{-3} seed at various absorbed doses (a) 1.7, (b) 2.6 (c) 3.0, (d) 3.5 and (e) 4.5 kGy. dose rate = 1.7 kGy h^{-1}

At lower absorption dose two absorption maxima at 523 and 610 nm were observed (Figure 5.3a) that disappeared with further increase in radiation dose and finally only a single peak at 528 nm was observed. The appearance of two absorption maxima at 522 and 610 nm in the beginning (Figure 5.3a) indicated the tendency for formation of anisotropic shape particle. However with increase in dose the absorption maxima at 610 nm disappears and finally only a single peak at 527 nm is observed indicating that the net result is the formation of spheres.

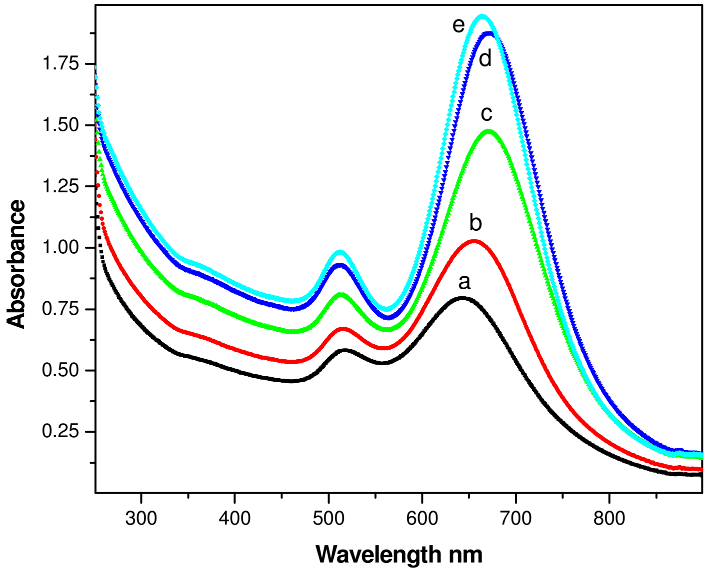

Figure 5.4: Absorption spectra of irradiated solution containing 4 x 10^{-4} mol dm^{-3} of Au^{+1}, 0.2 mol dm^{-3} isopropanol, 8 x 10^{-5} mol dm^{-3} of $AgNO_3$, 0.1 mol dm^{-3} of CTAB and 1.2 x 10^{-6} mol dm^{-3} seed at various absorbed doses (a) 1.2, (b) 1.6 (c) 2.0, (d) 2.3 and (e) 2.6 kGy. Dose rate = 0.8 kGy h^{-1}

When, radiolysis of the above solution was carried out at still lower dose rate, i.e, 0.8 kGy h^{-1}, the absorption spectra of solutions irradiated to various absorbed doses showed two absorption maxima as shown in Figure 5.4.

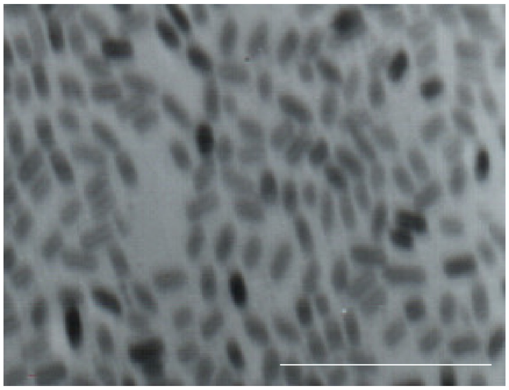

Figure 5.5: TEM of gold nanorods synthesized by radiolytic method. Bar length = 50 nm

The two bands are attributed to the formation of Au nanorods. The first absorption maximum, which is centered at 513 nm did not shift with increasing radiation dose, whereas the second one is red shifted from 643 to 670 nm with increase in radiation dose. This shift of absorption maxima by 27 nm with increasing radiation dose may be due to increase in aspect ratio caused by the growth of nanorods. The formation of nanorods was further confirmed from transmission electron microscopy results (Figure 5.5). The TEM image showed uniform sized nanorods without presence of any spheres. The aspect ratio of nanorods was estimated to be 2.4 by measuring the length and breadth of 100 particles using ocular lens.

5.2.3.3. Suggested mechanism

The anisotropic shape generation in case of gold nanoparticles requires three most important parameters:

i) surfactant, CTAB, which provides tubular template in aqueous solution

ii) Au seed particles, which have facets to grow anisotropic nanoparticles

iii) Adsorbate ions, like Ag^+, which block certain facets thereby facilitating directional growth

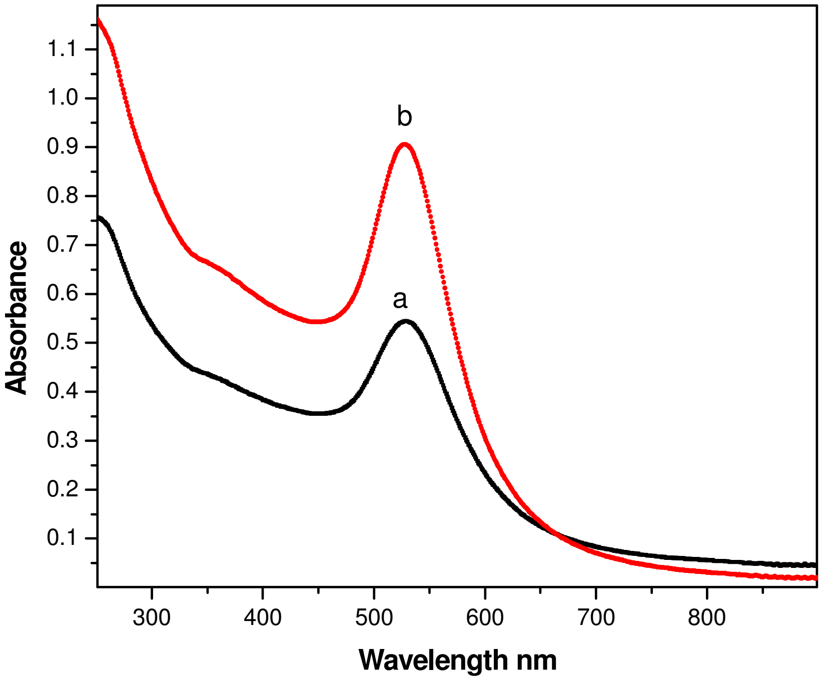

Figure 5.6: Absorption spectra of irradiated solution in absence of Ag^+ (a) 1.7 and (b) 6.8 kGy. All other conditions are same as mentioned in Figure 5.3

In chemical method of synthesis of gold nanorods [211,227,88] it has been postulated that the presence of Ag^+ in the growth solution is a must for getting nanorods in high yield. It was found to be true for the radiation method of synthesis of nanorods also. Keeping all other parameters same, when irradiation was carried out in absence of Ag^+, the absorption spectra at various doses are shown in Figure 5.6. Appearance of only single absorption maxima at 527 nm clearly indicates that only spheres were formed thus confirming that Ag^+ are essential for the synthesis of nanorods by radiolytic method also. The role played by Ag^+ in the synthesis of Au nanorod is not yet fully understood. The proposed mechanism for gold nanorod formation suggests that the surfactant forms a soft cylindrical template, with a certain size that depends on surfactant concentration. Nikoobakht and El-Sayed proposed that the silver ions located between the head groups of the capping surfactant (CTAB) can be considered as Ag–Br pairs, decreasing the charge density on the bromide ions, and therefore, the repulsion between neighboring headgroups on the gold surface, and resulting in CTAB template elongation [227,236,240]. This possibility is supported by the stronger affinity of CTAB monomers for the side facets compare to the end facets [241].

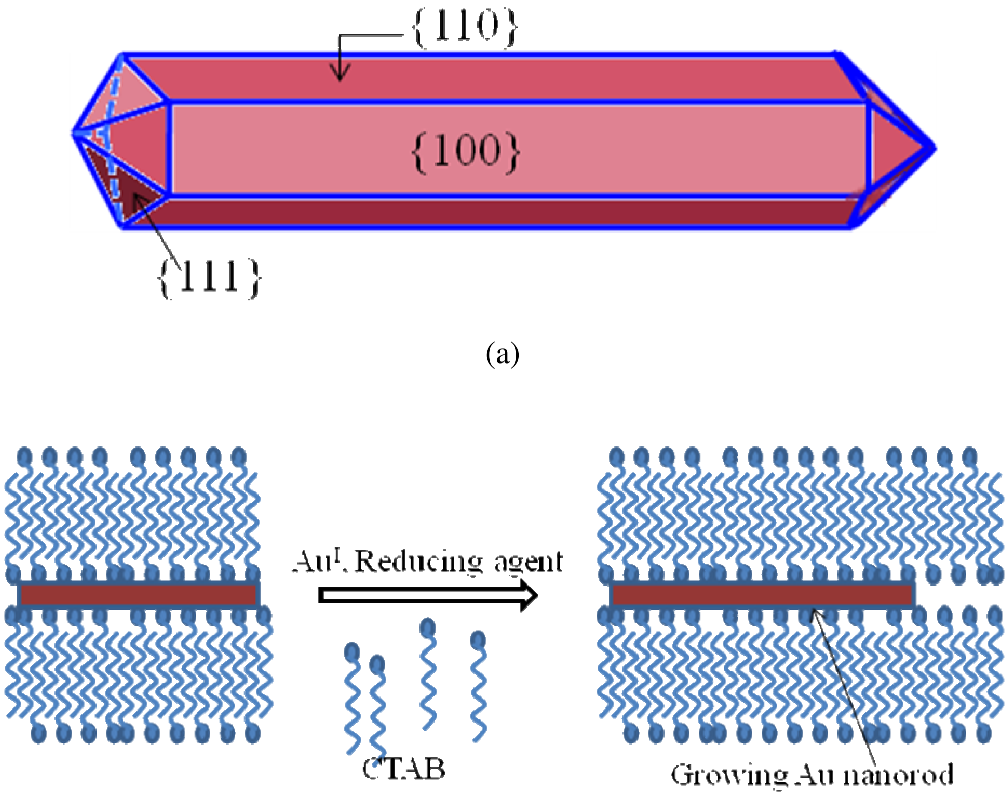

(a)

(b)

Figure 5.7: (a) Cartoon picture of gold nanorod showing (100), (110) side faces and (111) end faces
(b) Schematic representation of zipping mechanism for the growth of gold nanorods in CTAB bi-layer template

High-resolution TEM images show that nanorods have four facets [242]. According to the proposed mechanism Ag^+ ions get adsorbed on the side facets, i.e., (100) and (110) thereby blocking these facets. So that the tip of growing nanorod, which contains (111) facets are free for adsorption of Au atoms [212] and growth of nanorod (Figure 5.7 a). Johnson et al, proposed a zipping mechanism [213] for rod elongation considering CTAB monomer as rigid structure (Figure 5.7 b). The concentration of Ag^+ in the solution also plays an important role in the synthesis of Au nanorods. The radiolysis was carried out at various concentrations of Ag^+ keeping Au^I concentration constant (4×10^{-4} mol dm^{-3}). The best and reproducible results were obtained at Ag^+ concentration of 6×10^{-5} mol dm^{-3} and the same was used throughout this study. Thus in the radiolytic method nanorod formation occurs when the concentration ratio of Au: Ag is ~7. Similar results were also obtained in the seed mediated method for the synthesis of short aspect ratio Au nanorods [212] in aqueous medium using ascorbic acid as reducing agent. Ascorbic acid, which is a mild reducing agent, is used in the chemical method of synthesis of nanorods. When ascorbic acid was added to the aqueous solution containing Au^{III}, Au seeds and surfactant (CTAB), Au^{III} is reduced to Au^I.

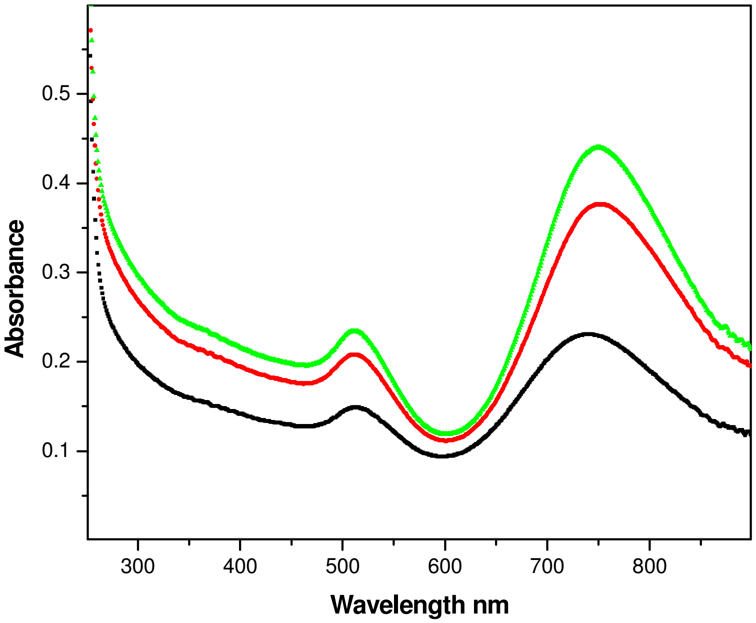

Figure 5.8: Absorption spectra of irradiated solution containing 1 x 10^{-4} mol dm^{-3} of Au^{+1}, 0.2 mol dm^{-3} isopropanol, 8 x 10^{-5} mol dm^{-3} of $AgNO_3$, 0.1 mol dm^{-3} of CTAB and 1.2 x 10^{-6} mol dm^{-3} seed at various absorbed doses (a) 0.85, (b) 1.06 and (c) 1.2 kGy. Dose rate = 0.8 kGy h^{-1}

The ascorbic acid cannot reduce Au^{III} down to Au^0 due to its low reducing power. However in the presence of Au seed, Au^I gets adsorbed on the surface of seed and the adsorbed Au^I can be reduced by ascorbic acid to atomic Au. This results in the growth of seed; however in the presence of CTAB, which preferentially binds to the growing seed along the long axis forming a bilayer [88], the addition of Au^I takes place along the short axis that results in the growth in one direction. This anisotropic addition of Au results in the formation of nanorod. In the present method as mentioned earlier in the text, the radicals namely e_{aq}^- and isopropyl radical generated during radiolysis are highly reducing in nature and can bring the reduction of Au^I to atomic Au in the solution unlike chemical method where ascorbic acid cannot reduce Au^I to Au. Therefore, in the chemical method when seeds are not added to the growth solution, nanorods formation does not occur. But in the present radiolytic method when seeds were not added to the solution, the reduction of Au^I to Au still occurs as the solution after irradiation turned pink.

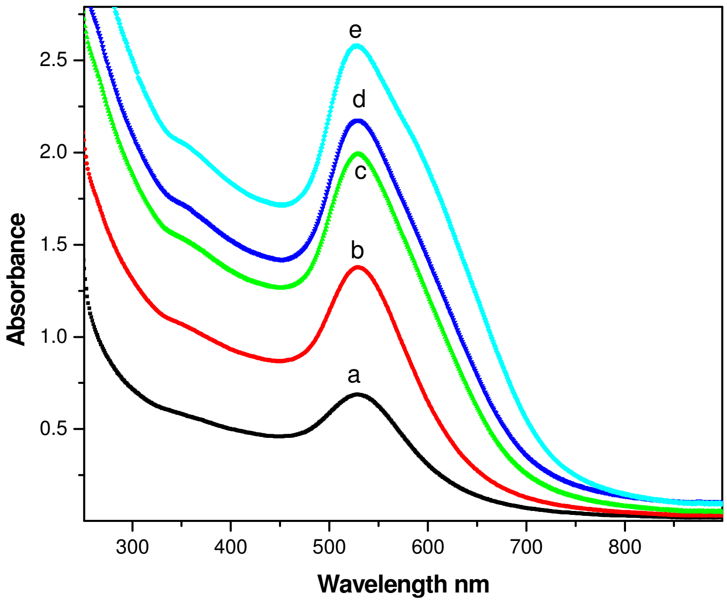

Figure 5.9: Absorption spectra of irradiated solution containing 1 x 10^{-3} mol dm^{-3} of Au^{+1}, 0.2 mol dm^{-3} isopropanol, 8 x 10^{-5} mol dm^{-3} of $AgNO_3$, 0.1 mol dm^{-3} of CTAB and 1.2 x 10^{-6} mol dm^{-3} seed at various absorbed doses (a) 1.28, (b) 2.12 and (c) 3.0, (d) 3.4 and (e) 4.25 kGy. Dose rate = 0.8 kGy h^{-1}

The irradiated solution showed only one absorption maximum at 527 nm, which is the band for spherical Au nanoparticles. Thus, in radiation method the growth of particles takes place by the addition of Au atoms formed in the solution upon radiolysis on the growing seed. When aqueous solution is subjected to gamma radiolysis, there is a steady- state concentration of radicals in the solution. The steady-state concentration of radicals depends on the dose rate. In the present case all these reducing radicals, namely e_{aq}^{-} and isopropyl radical, react with Au^I in the solution. Therefore, the rate of formation of Au^0 in the solution is equal to the product of steady-state radical concentration of reducing radicals and the concentration of Au^I. At high dose rate (3.4k Gy h^{-1}) no nanorods are formed but only spheres are obtained as evident from single absorption maxima at 527 nm (Figure 5.2). It appears that when the formation rate of Au^0 in the solution is high, the rate of addition of Au^0 to growing particle is high and under these conditions addition takes place isotropically which results in the formation of spheres. When dose rate is reduced by a factor of 4, the steady-state concentration of Au^0 in the solution is also correspondingly reduced and in turn the rate of addition of Au to the growing particle is reduced by a factor of 4. The results show that under slower kinetics conditions addition of Au to the growing particles takes place in anisotropic manner leading to the formation of rod. The evidence for the role of kinetics in governing the final shape of particle is further substantiated by the experimental observation where the concentration of Au^I used for the synthesis is reduced by a factor of 4. When aqueous solution containing 1×10^{-4} mol dm^{-3} of Au^I, 0.2 mol dm^{-3} of iso- propanol, 6×10^{-5} mol dm^{-3} of $AgNO_3$, 0.1 mol dm^{-3} of CTAB and 1.2×10^{-6} mol dm^{-3} of seed solution was irradiated with gamma rays at 0.8 kGy h^{-1} dose rate, the absorption spectra obtained at various irradiation times are shown in Figure 5.8. Under these conditions the formation of gold nanorods takes place as evident from the appearance of two absorption maxima at 513 and 750 nm (Figure 5.8c). The second absorption maximum, which was centered at 670 nm when the concentration of Au^I was 4×10^{-4} mol dm^{-3} (Figure 5.4), was red shifted to 750 nm at lower Au^I concentration of 1×10^{-4} mol dm^{-3}. It is reported that the longitudinal plasmon band is red shifted as the length of nanorods increases. At lower precursor concentration, the length of rod increases indicating that the addition of Au takes place in a more directional manner, i.e. on the tip of the growing rod. Under this condition the steady-state concentration of Au^0 in the bulk is 4 times lower compared to the condition where Au^I concentration is 4×10^{-4} mol dm^{-3}. This clearly indicates that the formation of nanorod is controlled by kinetics, i.e. lower the steady-state concentration of Au in the bulk, lower is its addition rate to the growing rod and in turn higher is the probability of its addition in a particular direction, which results in the formation of nanorod. This hypothesis was further confirmed when synthesis of gold nanorod was carried out at high concentration of Au^I (1×10^{-3} mol dm^{-3}) at the same dose rate of 0.8 kGy h^{-1}. Under these conditions no nanorods formation was observed as absorption spectra shows only single absorption maxima at 530 nm whose intensity increases with increase in dose as shown in Figure 5.9. Thus by proper choice of Au^I concentration and dose rate, nanorods of gold can easily be generated in the aqueous medium using gamma radiolysis technique.

5.3. Modification of synthesis method for preparation of gold nanorods at high dose rate and in absence of Au seeds

5.3.1. Synthesis of Au^I solution

The Au^I solution was synthesized as mentioned in section 5.2.2. Aqueous solution containing 4×10^{-4} mol dm^{-3} $HAuCl_4$, 0.2 mol dm^{-3} isopropyl alcohol and 0.1[1] mol dm^{-3} CTAB was purged with high pure N_2 gas and it was irradiated in the gamma chamber at a dose rate 3.4 kGy h^{-1} till the solution turned colorless. This solution was used as a precursor for gold in the synthesis of gold nanorods. The concentrations of different reagents mentioned in this section were kept constant throughout the study in section 5.3 unless it is mentioned.

5.3.2. Synthesis of rod-shaped gold nanoparticles

To the Au^I solution prepared by gamma radiolysis 2.75×10^{-2} mol dm^{-3} of acetone, 0.2 mol dm^{-3} isopropyl alcohol and 6×10^{-5} mol dm^{-3} of Ag^+ were added, the final solution was purged with N_2 and it was subjected to gamma irradiation. The concentration of Au^I was adjusted by diluting the solution with appropriate amount of water. The solution was irradiated in the gamma chamber and the resulting colored solution containing gold nanorods was first analysed by UV-visible spectroscopy.

5.3.3. Results and discussion

5.3.3.1. Reaction of isopropyl radical with Au^I

When the precursor solution containing 4×10^{-4} mol dm^{-3} Au^I, 2.75×10^{-2} mol dm^{-3} acetone, 0.2 mol dm^{-3} isopropanol and 6×10^{-5} mol dm^{-3} of Ag^+ was subjected to gamma irradiation at a dose rate = 3.4 kGy h^{-1}, the primary radicals of water radiolysis namely e_{aq}^-, $H^{\bullet}$ and ${}^{\bullet}OH$ undergo the following two reactions:

$$^{\bullet}OH/H^{\bullet} + (CH_3)_2CH\text{-}OH \longrightarrow (CH_3)_2{}^{\bullet}C\text{-}OH + H_2O/H_2 \quad (5.6)$$

$$e_{aq}^- + (CH_3)_2C{=}O \longrightarrow (CH_3)_2{}^{\bullet}C\text{-}OH + OH^- \quad (5.7)$$

Table 5.1: Rate constant for the reaction of radicals of water radiolysis with acetone and isopropanol [70]

S. No.	Reactant	Radical	Rate constant ($dm^3 mol^{-1} s^{-1}$)
1	Acetone	e_{aq}^-	$7.7x10^9$
2	Acetone	$H^{\bullet}$	$2.0x10^6$
3	Acetone	${}^{\bullet}OH$	$1.3x10^8$
4	Isopropanol	e_{aq}^-	$\sim10^3$
5	Isopropanol	$H^{\bullet}$	$9.0x10^7$
6	Isopropanol	${}^{\bullet}OH$	$1.6x10^9$

The rate constant for the reaction of radicals of water radiolysis with acetone and isopropyl alcohol is given in Table 5.1. In the present system the concentration of acetone has been kept almost seven times lower than that of isopropyl alcohol to minimize the possibility of reaction of acetone with $OH^{\bullet}$. At the same time the concentration of acetone has been kept higher than the precursor Au^I concentration, so that the e_{aq}^- and $H^{\bullet}$, instead of reacting with Au^I, preferably react with acetone to generate isopropyl radical. Thus, in the present method all the primary radicals of water radiolysis are converted into a single type of radical namely isopropyl alcohol radical, which reduces Au^I present in the solution into Au^0 as shown in Equation (5.2). The absorption spectrum of irradiated solution is shown in Figure 5.10. As can be seen from Figure 5.10, two absorption maxima one at 511 nm known as transverse surface plasmon absorption band and other in higher wavelength region known as longitudinal surface plasmon absorption band at 701 nm are observed, which are characteristic of gold nanorod thus confirming the formation of nanorod upon irradiation.

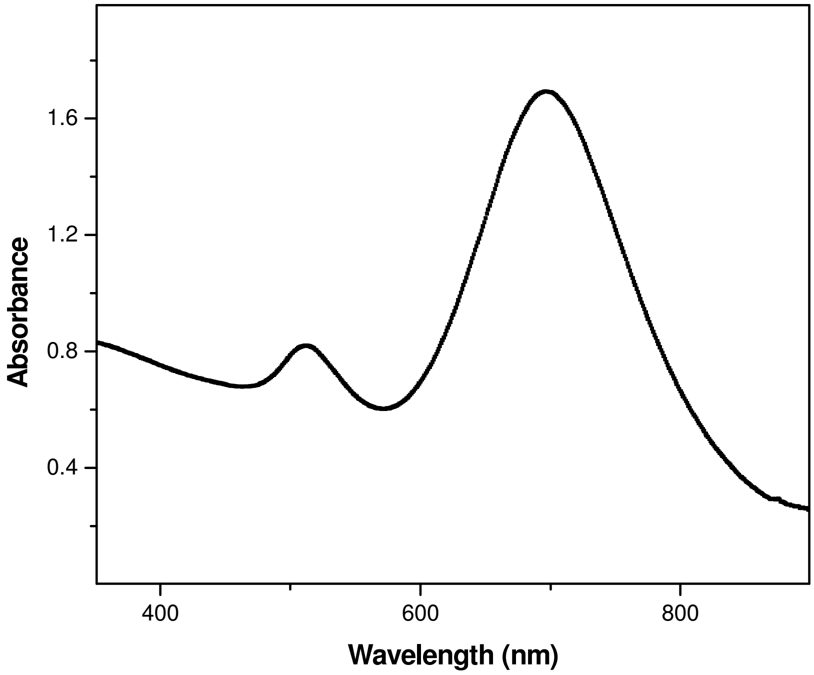

Figure 5.10: Absorption spectrum of gold nanorods synthesised by the reaction of Au^I with isopropyl radical in the presence of CTAB. Concentration of $Au^I = 4 \times 10^{-4}$ mol dm^{-3} and dose = 2.8 kGy, Dose rate = 3.4 kGy h^{-1}

5.3.3.2. Effect of precursor Au^I concentration

In order to understand the role of the concentration of precursor Au^I on the formation of nanorod, gamma radiolysis of solution containing 2.75×10^{-2} mol dm^{-3} acetone, 0.2^1 mol dm^{-3} isopropanol and 6×10^{-5} mol dm^{-3} of Ag^+ and varying concentration of Au^I was carried out. The dose delivered to sample was based on the concentration of Au^I used. The theoretical calculation of dose required to reduce a certain concentration of metal ion has been mentioned in section 3.2 of chapter 3. The absorption spectra of the irradiated solution are shown in Figure 5.11. At Au^I concentration of 4×10^{-4} mol dm^{-3} the absorption maxima (λ_{max}) of longitudinal band is positioned at 701 nm and with decrease in concentration of Au^I the λ_{max} is red shifted as shown in Figure 5.11.

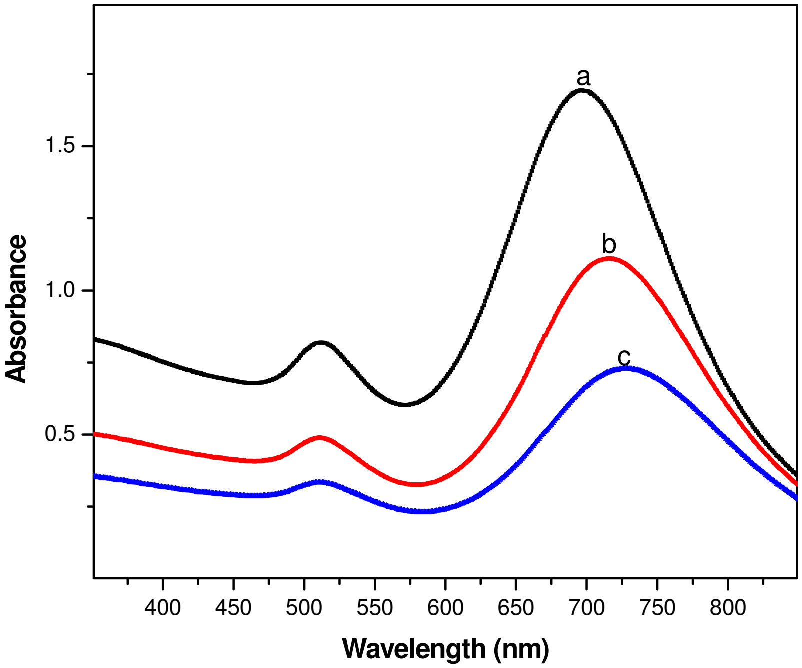

Figure 5.11: Effect of Au^I concentration on nanorod formation: (a) 4 x 10^{-4} mol dm^{-3}, λ_{max} = 701 nm (b) 3 x 10^{-4} mol dm^{-3}, λ_{max} = 715 nm and (c) 2.5 x 10^{-4} mol dm^{-3}, λ_{max} = 729 nm. Absorbed dose (a) 2.8 kGy, (b) 2.3 kGy and (c) 1.4 kGy, Dose rate = 3.4 kGy h^{-1}

5.3.3.3. Effect of CTAB concentration

In the chemical method it has been reported that concentration of CTAB plays an important role for obtaining nanorods in high yield [243]. Therefore in the present study effect of CTAB on nanorod formation was investigated. The absorption spectra of irradiated solution containing varying concentration of CTAB are shown in Figure 5.12. At CTAB concentration of 0.1 mol dm^{-3}, absorption maxima is observed at 729 nm whereas decrease in the concentration of CTAB resulted in the blue shift of the absorption maxima with considerable broadening of peak as shown in Figure 5.12. The blue shift clearly indicates that shorter rods are formed with decreasing CTAB concentration and also broadening of absorption peak indicates that size distribution is non uniform. Therefore, for getting uniform sized nanorods in higher yield, the concentration of CTAB should be not less than 0.1 mol dm^{-3}. The results are similar to those obtained by chemical methods reported earlier [243].

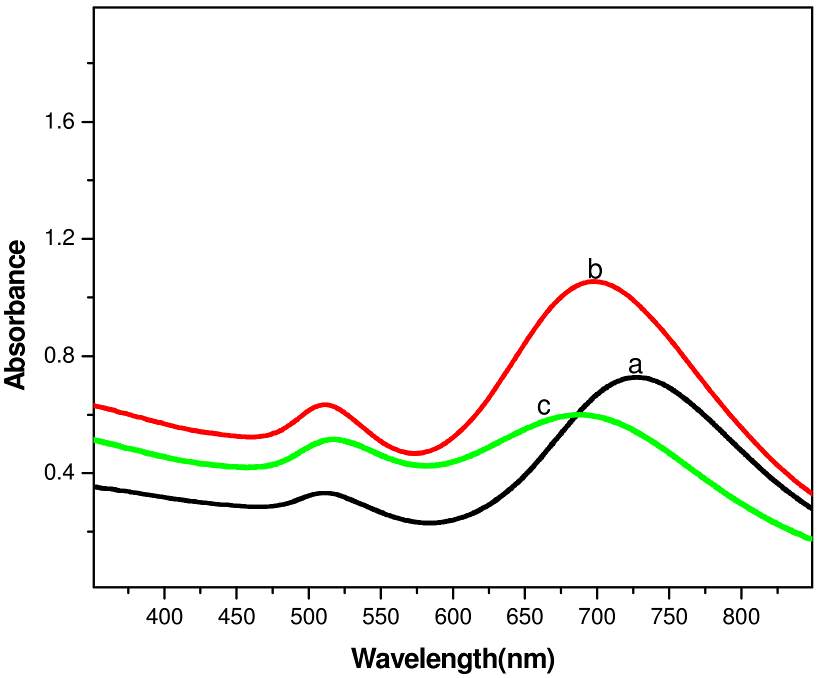

Figure 5.12: Effect of CTAB concentration on nanorod formation: (a) 0.1 mol dm^{-3}, λ_{max} = 729 nm (b) 8 x 10^{-2} mol dm^{-3}, λ_{max} = 699 nm and (c) 5 x 10^{-2} mol dm^{-3}, λ_{max} = 680 nm, Dose rate = 3.4 kGy h^{-1}, [Au^{I}] = 2.5 x 10^{-4} mol dm^{-3}

5.3.3.4. Mechanism of rod formation

The mechanism of Au nanorod formation is similar to as explained in section 5.2.3.3. The optimized concentration of Ag^+ (6×10^{-5} mol dm^{-3}) was used in the present study also. In our previous work (section 5.2.3.) under similar conditions of dose rate and precursor concentration, as used in the present study, nanorod formation was not observed and only Au spheres were obtained. There are two major differences between the experimental procedure in the present and the earlier method i.e.,

i) the nature of reducing radical

ii) the presence/absence of Au seed.

It is known that isopropyl radical (E^0 = –1.5 V vs. NHE) is milder reducing agent as compared to e_{aq}^- (E^0 = –2.9 V vs. NHE) and $H^\bullet$ (E^0 = –2.3 V vs. NHE). The rate constants for the reaction of isopropyl radical with Au^I are not reported in the literature, however with other metal ions such as Ni^{2+}, the rate constant (7.2×10^8 dm^3 mol^{-1} s^{-1}) for the reaction of isopropyl radical [244] is 50 times lower in magnitude as compared to hydrated electron [245], which reacts with Ni^{2+} with rate constant equal to 3.5×10^{10} dm^3 mol^{-1} s^{-1}. The Au atom formed upon radiolysis is unstable in the aqueous medium and undergoes coalescence with other Au atoms resulting in the growth of particle. The kinetics of the growth of the particle will depend on the rate at which Au is produced in the system. Since in the present study isopropyl radical used to reduce Au^I to Au is expected to react slowly as compared to other reducing radical such as hydrated electron and $H^\bullet$, the rate of growth of particle is slow. Thus by using the milder reducing radical i.e., isopropyl radical the nanorod formation takes place at higher dose rate and in the absence of any seed. This observation supports the role of the kinetics in governing the shape of Au nanoparticles as reported in the literature [225]. In our previous work (section 5.2.3.) the kinetics of formation of nanorods was controlled by reducing the dose rate. At lower dose (0.8 kGy h^{-1}) nanorod formation occurred while irradiation at higher dose rate resulted only in the formation of spheres.

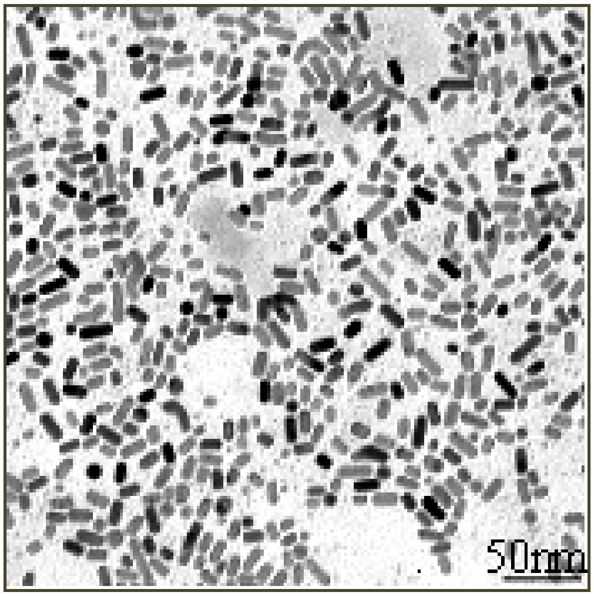

Figure 5.13: TEM image of gold nanorods prepared by the reduction of Au^I using isopropyl radical generated by gamma radiolysis

The modified method to synthesize gold nanorods is simpler and more convenient as compared to earlier developed methods. In the earlier method the longitudinal absorption band was positioned at 671 nm at dose rate 0.8 kGy h^{-1} when the precursor Au^I concentration was 4×10^{-4} mol dm^{-3}. In the current method for the same Au^I concentration, the longitudinal band has been observed at 701 nm even at a dose rate of 3.4 kGy h^{-1}, indicating the formation of longer rod. It is known from the literature that as the length of rod increases, the longitudinal plasmon band is red shifted [5]. Thus the shift in the longitudinal plasmon band by 30 nm is due to the formation of longer nanorods. This is further confirmed from the TEM image, which is shown in Figure 5.13. From this figure average aspect ratio is calculated as 3 by measuring the length and width of 100 nanorods. In principle the seeds are not required in the radiation method unlike chemical method. In the later case the synthesis of nanorods cannot be achieved without the presence of seeds. In the present method, isopropyl radical generated during radiolysis is reducing in nature and bring the reduction of Au^I to atomic Au in the solution unlike chemical method where ascorbic acid cannot reduce Au^I to Au^0. The Au^0 formed in the solution undergo coalescence with other atoms that results in the formation of small clusters of Au_n in the solution. Thus in radiolytic method seeds are generated in-situ and their subsequent growth results in the formation of nanoparticles. The final shape of the particles depends on the rate at which the particle growth takes place. The slower growth rate results in the formation of gold nanorod. The slower kinetic condition is achieved in the present method by using isopropyl radical to bring about the reduction of Au^I to Au^0. The role of kinetics is also evident from the results obtained when the concentration of precursor Au^I is varied as shown in Figure 5.11. The result shows with decreasing Au^I concentration, there is an increase in aspect ratio of nanorods. With decreasing concentration of Au^I, the rate of formation of Au in the solution is also reduced, which results in the slower growth of nanorod. Thus, when the growth kinetics of rod is slow the material addition takes place more anisotropically that result in longer rod formation. Therefore the kinetics of the rod formation may also be controlled by changing the concentration of precursor Au^I.

5.3.3.5. Irradiation in the presence of Au seeds

The effect of addition of Au seeds to the solution prior to irradiation on nanorod formation was investigated. The results are shown in Figure 5.14, wherein the absorption spectrum of irradiated solution recorded in presence and in absence of seeds is presented. As can be seen from this figure, in both the cases nanorod formation takes place, however when seeds are present the absorption spectra is red shifted by 15 nm (λ_{max} = 700 nm) as compared to the one in the absence of seed (λ_{max} = 685 nm). This is because the seeds act as well-defined site for Au atoms formed from radiolytic reduction process, so that the final nanorods become longer and more uniform in size distribution. Whereas, when seeds are not added externally, seeds are generated in-situ by radiolysis of Au^I, which is a random process, so that the seeds have wide size distribution, hence the nanorods formed are shorter as compared with, in presence of seed.

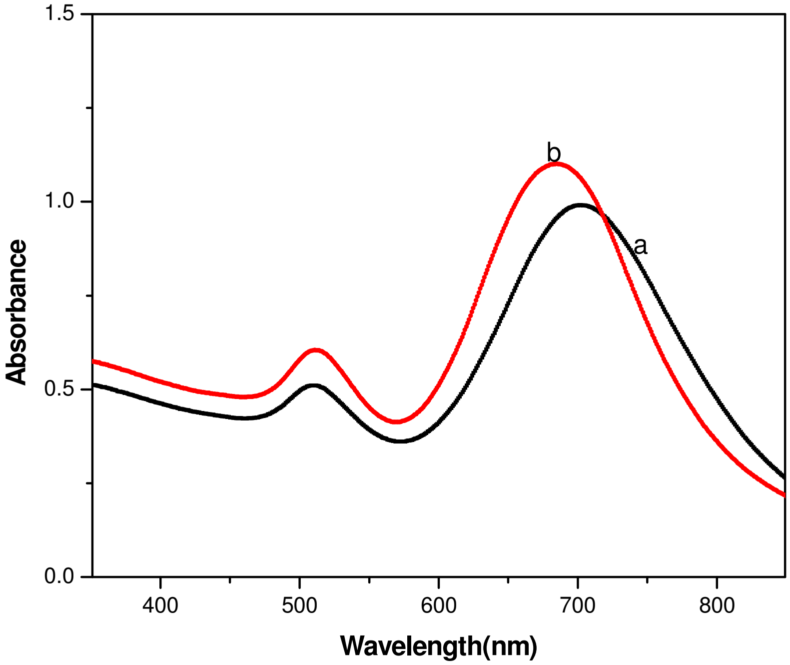

Figure 5.14: Effect of seed on nanorod formation: (a) in presence of seed [1.28×10^{-6} mol dm^{-3}], λ_{max} = 700nm and (b) in absence of seed, λ_{max} = 685 nm, Dose rate = 3.4 kGy h^{-1}, [Au^{I}] = 4 x 10^{-4} mol dm^{-3}

5.3.3.6. A comparison of radiolytic method with chemical method

The radiolytic method for the synthesis of nanorod is carried out in the absence of Au seed whereas in chemical method seeds have necessarily to be added to the system. As known from the literature, the seed solution that is prepared by the reduction of Au^{III} by sodium borohydride is stable only for few hours and cannot be used, thereafter, which results in the loss of precious gold metal. Due to the availability of a large number of reactive reducing species and wide range of dose rates, the radiolytic method offers several ways to control the kinetics of the growth process, which cannot be achieved in the chemical method. In radiolytic method since the reactive reducing species are generated in situ, the reaction can be stopped at any stage by simply removing the system from the radiation zone whereas in chemical method does not offer this convenience as reducing agent is added externally and cannot be removed from the system. Thus the radiolytic method reported in this section is very simple, easy and effective way of generating short aspect ratio gold nanorods in a one-pot. The schematic of generation of Au nanorods by radiolytic and chemical methods have been represented in Figure 5.15 and Figure 5.16 respectively.

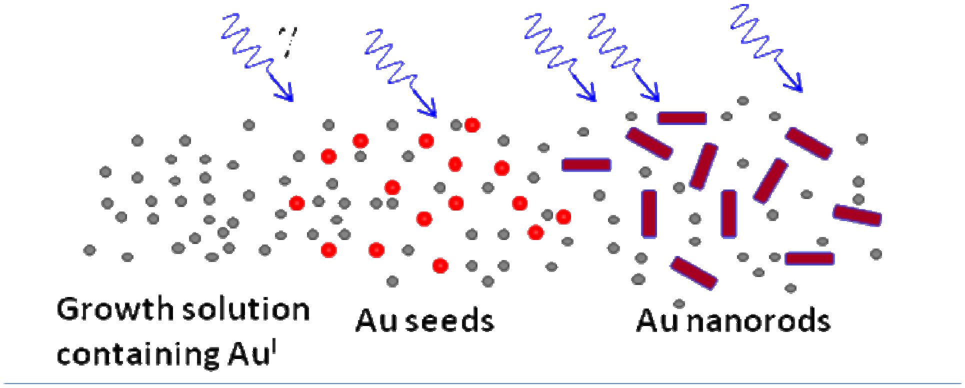

Figure 5.15: Cartoon picture depicting one-pot synthesis of gold nanorods through *in situ* generation of Au seeds in gamma radiation method

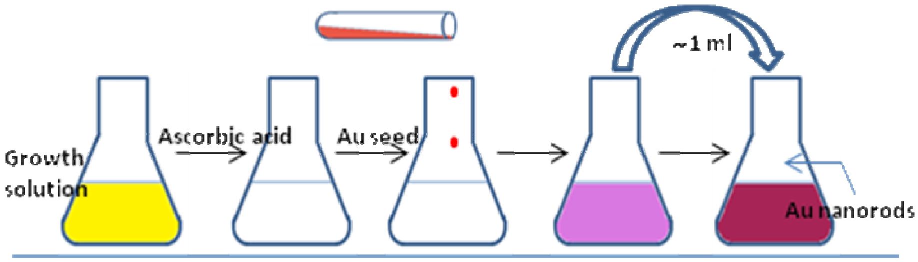

Figure 5.16: Cartoon picture depicting stepwise synthesis of gold nanorods by external addition of Au seeds in chemical method

5.4. A facile method to synthesize anisotropic plate like gold nanoparticles by combining radiation and chemical methods

The chemical methods for synthesis of gold nanoplates reported in the literature are high temperature polyol methods [246,247] in which Polyols are used as media and also reducing agent. In some other methods polyols are used as media and an appropriate reducing agent is used to reduce gold at higher temperature. The methods include microwave induced [248], UV light induced [249], and electrochemical processes [250] to reduce gold ions. In most of these methods Poly(vinylpyrrolidone) (PVP) is used as a stabiliser. Other than polyols, mild reducing agent, such as ascorbic acid [211] has also been used to reduce gold to achieve gold nanoplates. It is well known that certain reducing agents or stabilisers can control the crystallization of gold, and consequently yield a special form of gold crystals [211]. In this work gold nanoplates have been synthesized by using radiolytically synthesized Au seeds in one pot. The milder reducing agent like ascorbic acid has been used here to generate Au nanoplates. The morphology and dimension of the Au nanoparticles depend on the concentrations of the seed particles and surfactant, CTAB, in addition to the reactants (Au^{III} and Ascorbic acid) [211].

5.4.1. Synthesis of Au^{I} in solution phase

In order to reduce Au^{III} to Au^{I}, 7.2×10^{-4} mol dm^{-3} ascorbic acid was added to yellow colored aqueous solution containing 4×10^{-4} mol dm^{-3} of Au^{III}, 0.1 mol dm^{-3} CTAB, 0.2 mol dm^{-3} propanol and 6×10^{-5} mol $dm^{-3}Ag^{+}$. After addition of ascorbic acid the solution turned colorless, which indicate reduction of Au^{III} to Au^{I}. Although ascorbic acid was present in excess in the reaction medium, but being a mild reducing agent, it could not reduce Au^{I} to Au^{0} in solution. The Au^{I} obtained by this method was used as a precursor for gold in the synthesis of rectangular gold nanoparticles.

5.4.2. *In situ* generation of Au seeds

The above solution containing Au^{I} was subjected to gamma irradiation at a dose rate of 3.4 kGy h^{-1}. As soon as the reaction medium was exposed to gamma radiation, the reduction of Au^{I} to Au^{0} took place by transient species generated from water radiolysis (Equation 5.5 and Equation 5.8).

$$e_{aq}^{-} + Au^{I} \longrightarrow Au^{0} \qquad (5.8)$$

Subsequently Au^{0} atoms coalesce to form Au seeds in situ [101]. The seed particle size was controlled by the high concentration of capping agent CTAB, which does not allow the seed to grow beyond a particular size. By controlling the exposed radiation dose the concentration of seeds in the system can be controlled.

5.4.3. Synthesis of rectangular plate like gold nanoparticles

The irradiated solution was kept undisturbed for 2h for subsequent growth of gold nanoparticles. As it is known from the literature, in the presence of Au seed, Au^{I} gets adsorbed on the surface of seed and the adsorbed Au^{I} can be reduced by ascorbic acid to atomic Au, which subsequently grows to form nanoparticles. Although the formation of maximum amount of gold nanoparticles was over within 35 minutes after irradiation (confirmed by spectral measurement), for complete conversion the UV–visible spectra were recorded after 2 hour of irradiation.

5.4.4. Results and discussion

5.4.4.1. Spectroscopic and microscopic characterization of Au nanoplates

The anisotropic nature of the gold nanoparticles was confirmed by the presence of two distinct peaks in the visible region of UV- visible spectra of the irradiated sample (Figure 5.17) and from the transmission electron microscopy (TEM) results. The optical properties of anisotropic gold nanoparticles are mainly governed by the longitudinal dipolar mode, i.e., the peak at higher wavelength in the UV- visible spectra.

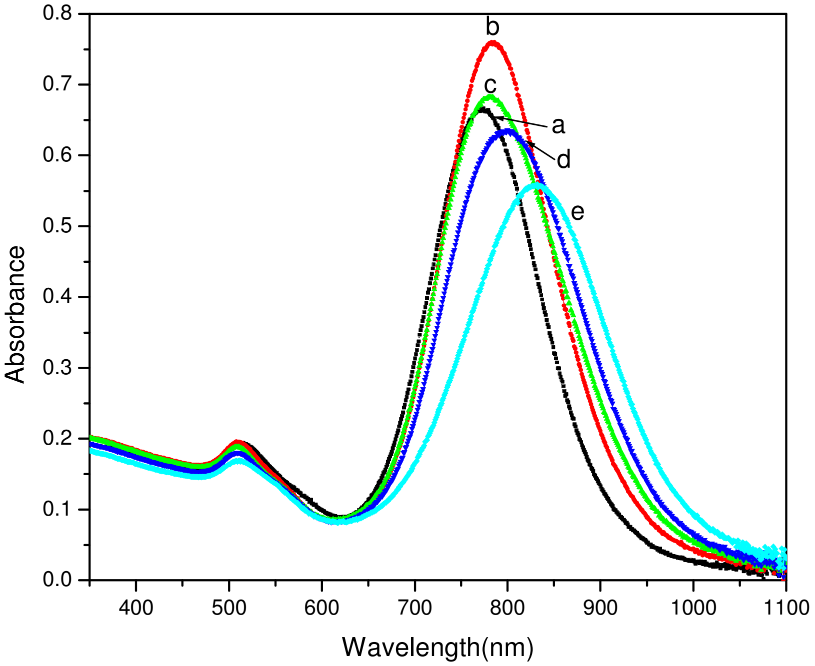

Figure 5.17: Absorption spectra of gold nanoparticle solutions irradiated at various absorption doses : dose (Gy) = (a) 28.3, (b) 56.6, (c)85, (d) 113.3, (e) 170 for 4 x 10^{-4} mol dm^{-3} Au^{III}, 7.2 x 10^{-4} mol dm^{-3} ascorbic acid, 0.1 mol dm^{-3} CTAB, 6 x 10^{-5} mol dm^{-3} Ag^{+}, 0.2 mol dm^{-3} isopropanol and dose rate of 56.6 Gy/min

The TEM picture (Figurte 5.18) confirmed the formation of rectangular plate like gold nanoparticles. The average aspect ratio of these rectangular nanoplates was estimated to be 2.5 by measuring the length and breadth of 100 nanoparticles using ocular lens.

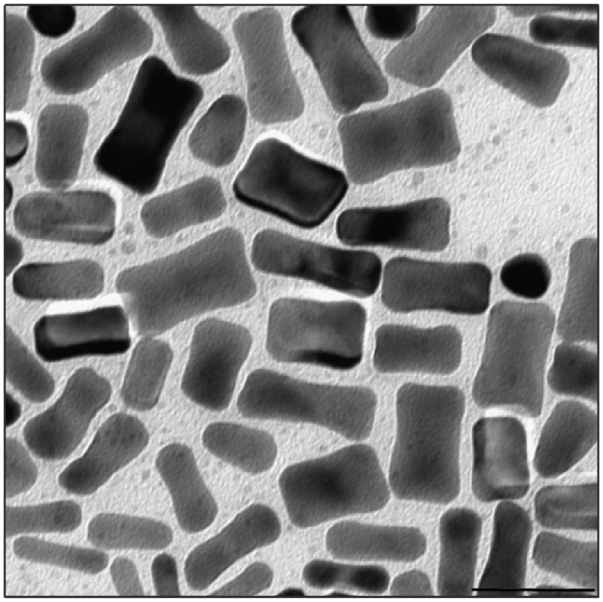

Figure 5.18: TEM image of rectangular plate like gold nanoparticles

5.4.4.2. Mechanism of formation of gold nanoplates

(i) Formation of Au^{I}

In the presence of an adsorption surface or Au seeds, ascorbic acid can reduce Au^{III} to Au^{I} and finally to Au^{0}. But in absence of any seed the reduction process stops at Au^{I} and there is no formation of Au^{0}. Hence, the aqueous solution containing Au^{III} and other reagents as mentioned earlier in the text (section 5.4.1) when mixed with ascorbic acid Au^{I} species were formed in the solution.

(ii) Formation of seed

In chemical method, seeds have to be added externally to the growth medium, so that Au^{I} in the solution gets adsorbed on these seeds and gets reduced by ascorbic acid to form nanoparticles. But in radiolytic method due to presence of reactive transient radiolytic species, seeds are generated *in situ*. The primary radiolytic products of water such as, e_{aq}^{-}, $H^{\bullet}$ and $^{\bullet}OH$ in presence of isopropanol ($(CH_3)_2$ CH OH) brings about the reduction of Au^{I} to Au^{0}. The irradiation was carried out for small duration of time to ensure that very low concentration of Au^{0} are generated in the growth solution and Au^{0} being unstable coalesce with each other to form Au seeds.

(iii) Formation of nanoplates

The seeds are generated in the solution by gamma irradiation. Immediately after the irradiation is stopped the growth process starts, which is visually observed as the color is developed in the previously colorless solution. The growth step is similar as in the case of chemical method.

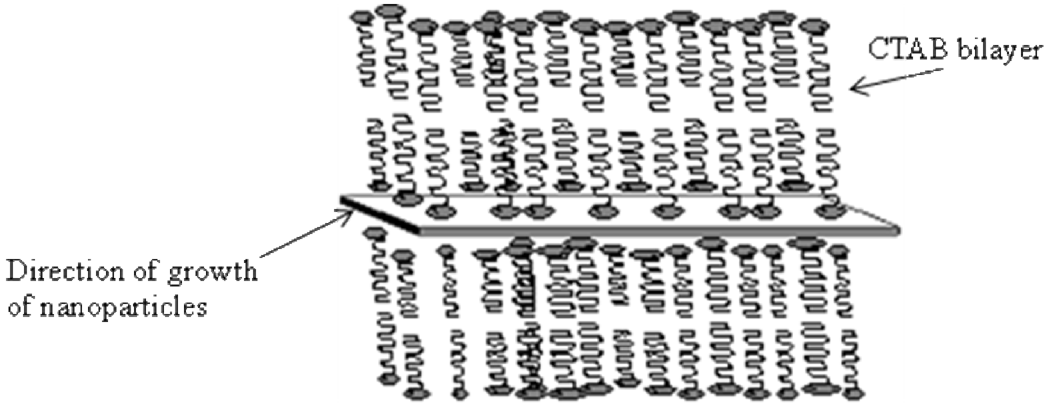

Figure 5.19: Proposed schematic of rectangular plate like gold nanoparticle formation

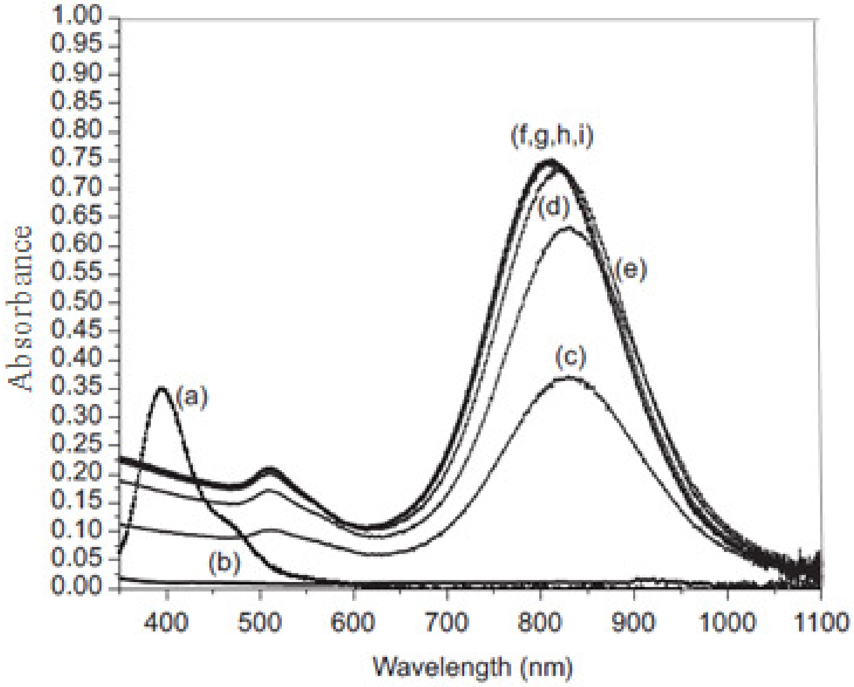

Figure 5.20: Absorption spectra of (a) growth solution containing Au^{III} before addition of ascorbic acid, (b) growth solution containing Au^{I} before irradiation. Absorption spectra of gold nanoparticle solutions, kinetics of growth of particles: time (in minutes) = (c) 15, (d) 20, (e) 25, (f) 30, (g) 35, (h) 45, (i) 65, for 4 x 10^{-4} mol dm^{-3} Au^{III}, 7.2 x 10^{-4} mol dm^{-3} ascorbic acid, 0.1 mol dm^{-3} CTAB, 6 x 10^{-5} mol dm^{-3} Ag^{+}, 0.2 mol dm^{-3} isopropanol and absorption dose of 56.6 Gy

The Au^{I} get adsorbed on the seeds and the ascorbic acid present in the solution reduces these adsorbed Au^{I} to Au^{0}. Though the exact mechanism of growth of nanoplates has not been clearly understood, it is proposed that the cationic surfactant CTAB forms a bilayer template as in case of nanorods formation, so that the addition of new Au^{0} atoms progress in the open ends of this bilayer to form rectangular shaped gold nanoparticles as shown in the Figure 5.19. The final shape of nanoparticle depends on the nature of seed particles and the facets present in the seeds. The progress of nanoplates growth was monitored to find the time for completion of the reaction. In Figure 5.20, the spectrum at 394 nm (Figure 5.20a) disappeared after addition of ascorbic acid (Figure 5.20b) indicating the reduction of Au^{III} to Au^{I} by ascorbic acid. The growth of nanoparticles was monitored after gamma irradiation, which is shown in Figure 5.20. Within15 minutes after irradiation the rectangular nanoplates are formed, after that their concentration increases with time and the particle formation saturates in 35 min.

5.4.4.3. Effect absorption dose

As mentioned earlier the seeds are generated by irradiating the growth solution. The absorbed dose was varied by varying the irradiation time. The concentration of the seeds was controlled by controlling the absorbed dose. The effect of dose on nanoplate formation is shown in Figure 5.17. for dose of 56.6 Gy, the longitudinal spectrum is narrower suggesting there is a narrow distribution of the size of gold nanoparticles.

5.4.4.4. Effect of ascorbic acid concentration (AA/Au^{III})

This may be due to uniformity in the size of seeds formed at this dose. For dose less than this value, the concentration of seeds produced is very low, which affects the final concentration of nanoparticles, resulting in lower longitudinal absorbance value.

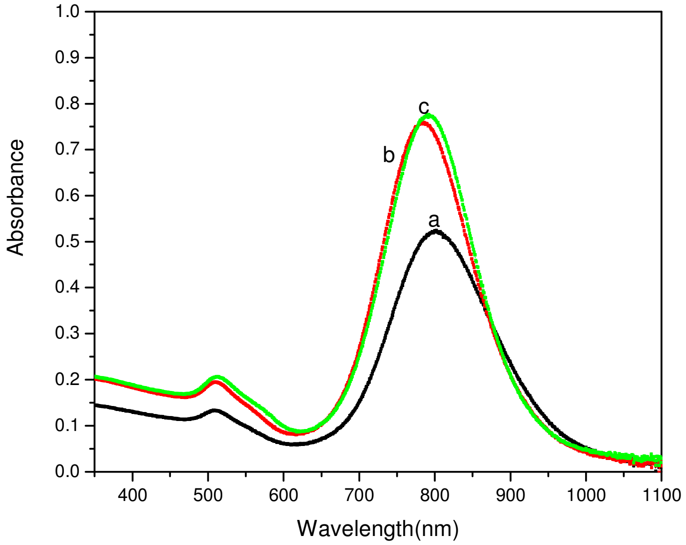

Figure 5.21: Absorption spectra of gold nanoparticle solutions for different ascorbic acid/Au^{III}: (a) AA/Au^{III} = 1.6, (b) AA/Au^{III} = 1.8 and (c) AA/Au^{III} = 2, for 4 x 10^{-4} mol dm^{-3} Au^{III}, 0.1 mol dm^{-3} CTAB and 0.2 mol dm^{-3} isopropanol and absorption dose of 56.6 Gy

As the dose increases from 56.6 Gy the longitudinal peak gets broadened due to wide size distribution of Au nanoparticles, because the sizes of seeds are not uniform. Hence in all other experiments the seed concentration corresponding to the absorption dose of 56.6 Gy is chosen. The effect of ascorbic acid concentration on Au nanoparticle formation is shown in Figure 5.21. It is more convenient to express this factor in terms of AA/ Au^{III} ratio. Ascorbic acid is a two hydrogen donor reducing agent. Hence for complete conversion of Au^{III} to Au^0, (AA/Au^{III}) should be more than1.5. Here it has been observed from Figure 5.21, at least AA/Au^{III} = 1.8 is required to get good uniformity in the particle size distribution, which is seen from narrower longitudinal peak in Figure 5.21b.

5.4.4.5. Effect of Au^{III} concentration

As the Au^{III} concentration increases from 1.06×10^{-4} to 1.0×10^{-3} mol dm^{-3} the longitudinal spectra in (Figure 5.22) blue-shift from 843 to 650 nm, which is an indication of shorter aspect ratio gold nanoplates formation for higher concentration of Au^{III} precursor ion.

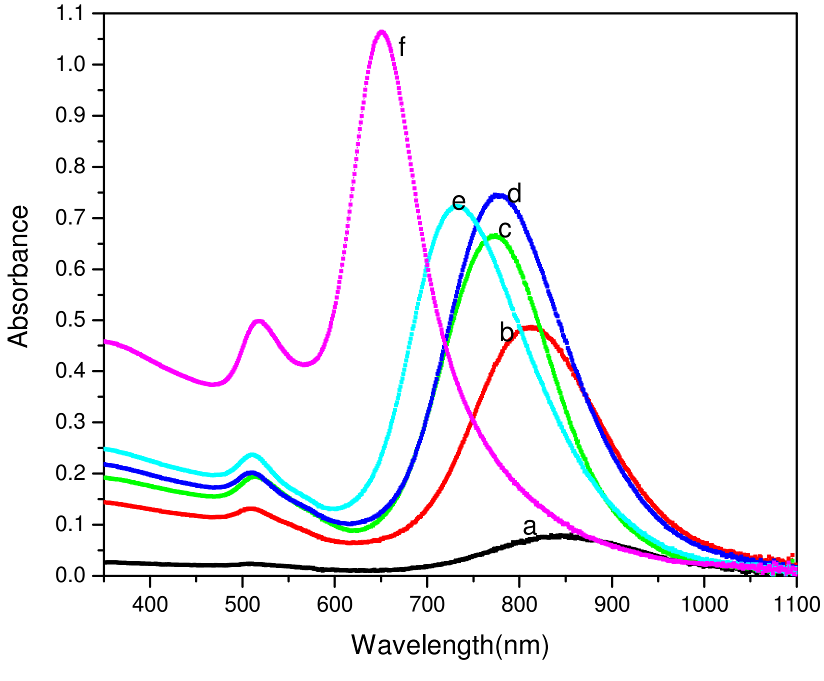

Figure 5.22: Absorption spectra of gold nanoparticle solutions, Au^{III} concentration variation: (a) [Au^{III}] = 1.06 x 10^{-4} mol dm^{-3}, (b) [Au^{III}] = 2.55 x 10^{-4} mol dm^{-3}, (c) [Au^{III}] = 4 x 10^{-4} mol dm^{-3}, (d) [Au^{III}] = 4.9 x 10^{-4} mol dm^{-3}, (e [Au^{III}] = 5.96 x 10^{-4} mol dm^{-3} and (f) [Au^{III}] = 1 x 10^{-3} mol dm^{-3}, for 7.2 x 10^{-4} mol dm^{-3} ascorbic acid, 0.1 mol dm^{-3} CTAB, 6 x 10^{-5} mol dm^{-3} Ag^+, 0.2 mol dm^{-3} isopropanol and absorption dose of 56.6 Gy

This result is in agreement with the results reported by Murphy et al. [88], wherein the authors suggested that the kinetics of addition of Au^{I} to the growing seeds governs the shape and size of the nanoparticles. In the present work as the Au^{III} concentration increases the kinetics of growth of nanoparticles also increases. It has been reported earlier (section 5.2, 5.3) that slower the kinetics, better the anisotropic growth. Hence at higher Au^{III} concentration shorter aspect ratio nanorods have been formed. The anisotropic gold nanoparticles have been synthesized by several researchers by taking low concentration of Au^{III} precursor ion [213,88,236], as at high concentration only nanospheres have been observed. But in this work even at 1.0×10^{-3} mol dm^{-3} of Au^{III} concentration anisotropic nanoparticles are formed.

5.4.4.6. Effect of $AgNO_3$ concentration

Silver nitrate plays a very important role in controlling the shape of naoparticles and also it affects the nanoparticle yield [92]. From Figure 5.23, in absence of $AgNO_3$, only the transverse band (Figure 5.23a) is present in the spectrum, hence only spheres are formed.

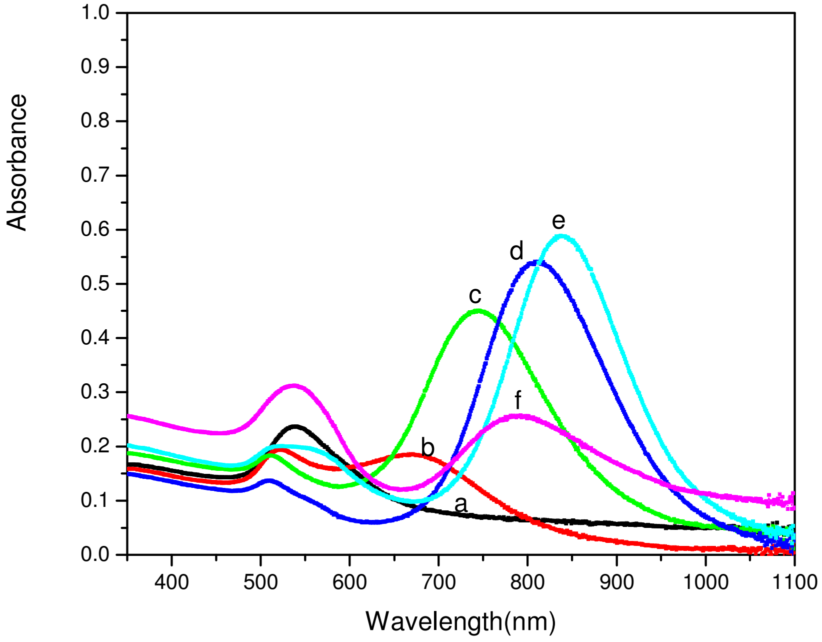

Figure 5.23: Absorption spectra of gold nanoparticle solutions, $AgNO_3$ concentration variation: (a) No $[Ag^+]$, (b) $[Ag^+] = 1 \times 10^{-5}$ mol dm^{-3}, (c) $[Ag^+] = 3 \times 10^{-5}$ mol dm^{-3}, (d) $[Ag^+] = 6 \times 10^{-5}$ mol dm^{-3}, (e) $[Ag^+] = 8 \times 10^{-5}$ mol dm^{-3}, (f) $[Ag^+] = 1 \times 10^{-4}$ mol dm^{-3} and (g) $[Ag^+] = 3 \times 10^{-4}$ mol dm^{-3}, for 4×10^{-5} mol $dm^{-3}Au^{III}$, 7.2×10^{-4} mol dm^{-3} ascorbic acid, 0.1 mol dm^{-3} CTAB, 0.2 mol dm^{-3} isopropanol and absorption dose of 56.6 Gy

When a small amount of $AgNO_3$ was added to the system the longitudinal band started to develop, and with increase in $AgNO_3$ concentration upto 8×10^{-5} mol dm^{-3} this band gradually red-shifts to 839 nm indicating increase in aspect ratio of gold nanoparticles. Above this concentration, the spectrum deforms (Figure 5.23f), so this is not a favorable condition for well defined nanoplate formation. The role played by Ag^+ in the synthesis of anisotropic Au nanoparticle is similar as explained in section 5.2.3.3. Also in chemical method Sau et al. reported that with further increase or decrease of Ag^+ concentration from a particular value affects the anisotropic growth due to change in kinetics of growth [212].

5.4.4.7. Effect of CTAB concentration

The variation of CTAB concentration is shown in Figure 5.24. For 0.1 mol dm^{-3} CTAB concentration the plasmon band is well defined and narrower. Below this concentration the spectrum deforms indicating wide distribution in shape of the nanoparticles at lower CTAB concentration [212]. Hence CTAB concentration below 0.1 mol dm^{-3} was unsuitable for formation of rectangular plate like gold nanoparticles.

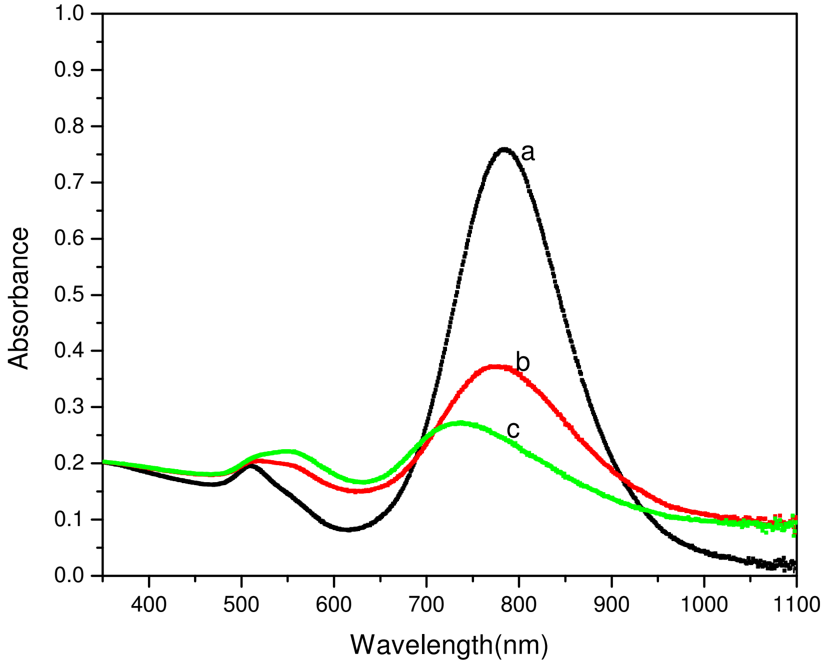

Figure 5.24: Absorption spectra of gold nanoparticle solutions, CTAB concentration variation: (a) [CTAB] = 0.1 mol dm^{-3}, (b) [CTAB] = 7 x 10^{-2} mol dm^{-3}, (c) [CTAB] = 5 x 10^{-2} mol dm^{-3}, for 4 x 10^{-4} mol dm^{-3} Au^{III}, 7.2 x 10^{-4} mol dm^{-3} ascorbic acid, 6 x 10^{-5} mol dm^{-3} Ag^+, 0.2 mol dm^{-3} 2-propanol and absorption dose of 56.6 Gy

5.4.4.8. PH effect

The pH was adjusted by using HCl and NaOH to growth solution before irradiation and the UV- visible spectra of nanoparticle solution at different pH has been shown in Figure 5.25. The natural pH of the growth solution is 3.24. For pH > 3.24, the solution instantly turns pink, which is an indication of sphere formation. The reason may be for pH more than 3.24 the reducing property of ascorbic acid changes [251]. At pH lower than 3.24 the system shows irregular spectral behaviour and for pH=1.56 the spectrum almost disappears probably due to presence of Cl^- from HCl. It is reported in the literature that Cl^- adversely affects the formation of anisotropic nanoparticle formation [252].

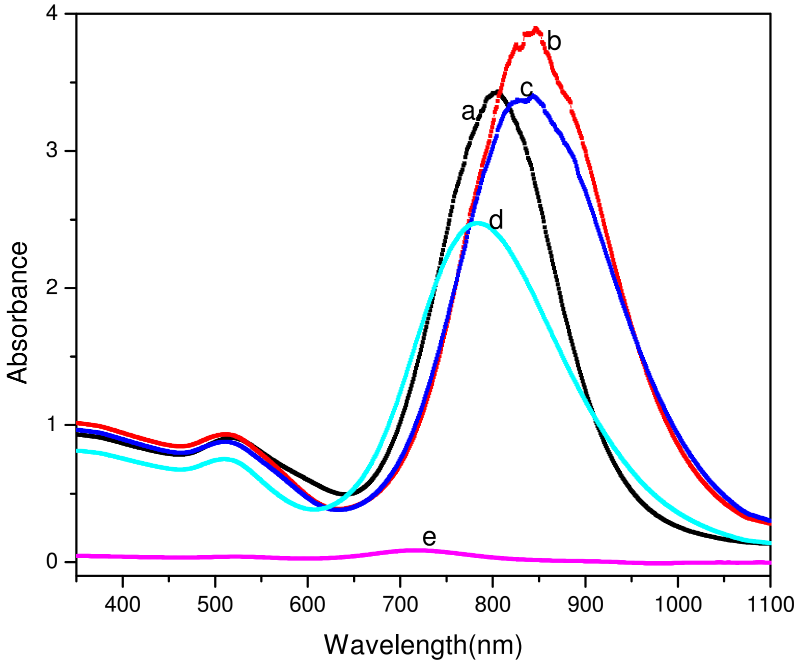

Figure 5.25: Absorption spectra of gold nanoparticle solutions. pH effect: pH = (a) 3.24 (natural pH of the solution), (b) 2.58, (c) 2.33, (c) 2.01 and (d) 1.56, for 4 x 10^{-4} mol dm^{-3} Au^{III}, 7.2 x 10^{-4} mol dm^{-3} ascorbic acid, 0.1 mol dm^{-3} CTAB, 6 x 10^{-5} mol dm^{-3} Ag^+, 0.2 mol dm^{-3} isopropanol and absorption dose of 56.6 Gy

5.5. Conclusions

In summary, the present study demonstrated that CTAB-capped anisotropic gold nanoparticles with novel and controllable sizes and shapes, such as rods (varying aspect ratio) and plates could be synthesized using radiolytic synthesis route. A simple, one-pot, seed-less method for synthesizing anisotropic gold nanoparticles, such as nanorods and nanoplates has been developed by using gamma irradiation technique. By proper choice of dose rate and precursor concentration and/or nature of reducing radical the gold nanorods can be synthesized in aqueous media. By combining both radiolytic and chemical method to synthesize rectangular gold nanoparticles in one-pot external addition of seed have been successfully avoided.

Chapter 6: Synthesis of gold nanoparticles in aqueous polyvinyl pyrrolidone by radiolytic method and their application for estimation of hydrogen peroxide

6.1. Introduction

Metal nanoparticles are currently being explored for their versatile applications as catalysts [253], chemical and bio sensors [254,255], antibacterial substances [256] and drug delivery systems [257]. Noble metal nanoparticles, such as Au, Ag possess bright color in aqueous solution [104] and are potentially useful as biosensor and for biological imaging. Radiolytic reduction route for generation of metal nanoparticles is being studied by many researchers in recent years [258–260]. The use of ionizing radiation for the synthesis of metal nanoparticles is promising as highly reactive species with high reduction potential are produced *in situ* by the radiation, which is hard to achieve by other chemical methods. These reactive species can easily reduce metal ions down to zero-valent state. Furthermore, because of its ability to fine-tune the radiation dose, dose rate and to selectively generate the required transient reactive radicals, it may offer better control over the size and the size distribution. Also it is a room temperature process and the reaction system is cleaner as it is devoid of any external chemical reducing agent. Irradiation of aqueous solution by high energy radiation generates transient radicals through water radiolysis. These transient radicals contain both reducing as well as oxidizing species. To create a total reducing condition specific solute is added, which can scavenge oxidizing species. The reducing radicals such as e_{aq}^{-} and $H^{\cdot}$ are utilized to reduce metal ion precussor to metal in zero valent state. These metal atoms coalesce to form metal nanoparticles in presence of a capping agent. Poly (N-vinyl-2-pyrrolidone) (PVP) has been reported as a suitable capping agent in preparation of metal nanoparticles [261–263], because it has functional group namely $>C=O$ and $>N-$ and long polymer chain. The functional groups containing lone pair of electrons help in stabilization of metal nanoparticles at their surface by covalent interaction, where as the polymer chain restricts aggregation of metal nanoparticles by steric hinderance. Apart from this, PVP is a biocompatible polymer. Hence nanoparticles synthesized in PVP can have potential biological applications. In this communication we report a facile method for synthesis of gold nanoparticles in PVP in presence of small amount of silver ion, isopropanol and acetone by using high energy gamma radiation. Different experimental parameters such as Au^{III} concentration, PVP concentration, Ag^+ concentration and molecular weight of PVP have been optimized to get Au nps of desirable size and size distribution. Hydrogen peroxide is widely used as an oxidant, a disinfectant and a bleaching agent in various industries, such as textile, paper and pulp, pharmaceutical industries [264]. It causes irritation to eye, skin and mucous membrane when present in the environment. Hydrogen peroxide is produced in stoichiometric amounts during the oxidation of biological analytes (e.g. glucose) by dissolved oxygen in the presence of corresponding oxidase. Hence micro and trace level determination of hydrogen peroxide is considerably important in clinical chemistry, analytical biochemistry and environmental science. Existing methods for the determination of hydrogen peroxide include titrimetry [265], spectrophotometry [266], kinetic flow-injection method [267], fluorescence [268], enzymatic method [269], chromatographic techniques [270] and electrochemical methods [271]. Recently a new method for determination of hydrogen peroxide based on a peroxidase-catalyzed reaction and using Au nanoparticles has been reported [272]. In this work the H_2O_2 concentration in aqueous solution was determined by monitoring the oxidation of o-phenylene diamine (o-PDA) by H_2O_2 in presence of enzyme, horse radish peroxidase (HRP). Au nanoparticle solution when added to the reaction system containing o-PDA, H_2O_2 and HRP the interaction of oxidation product with Au nanoparticles results in an enhanced absorption peak at 427 nm. The absorbance value of this peak at λ_{max} increases linearly with increase in H_2O_2 concentration in two ranges, i.e., 2.5×10^{-6} mol dm^{-3} to 2×10^{-4} mol dm^{-3} and 1×10^{-7} mol dm^{-3} to 3×10^{-6} mol dm^{-3} H_2O_2 in two separate set of experimental parameters. The detection limit is 1×10^{-7} mol dm^{-3}. Hence using this system H_2O_2 concentration can be estimated from 1×10^{-7} mol dm^{-3} to 2×10^{-4} mol dm^{-3} by choosing appropriate experimental parameters.

6.2. Results and discussions

6.2.1. Formation of Au nanoparticles and characterization

Irradiations were carried out in ^{60}Co gamma chamber having a dose rate of 2.2 kGy h^{-1} determined using Fricke dosimetry [148]. An aqueous solution containing 5×10^{-4} mol dm^{-3} Au^{III}, 0.5% PVP (M_w = 3,60,000 Da), 6×10^{-5} mol dm^{-3} $AgNO_3$, 0.2 mol dm^{-3} isopropanol and 5.8×10^{-2} mol dm^{-3} acetone was purged with N_2 and irradiated for an absorbed dose of 1.7 kGy. The formation of Au nanoparticles and the saturation dose was measured by spectroscopic monitoring.

When an aqueous solution containing Au^{III}, PVP, isopropyl alcohol, $AgNO_3$ and acetone is purged with N_2 and subjected to gamma irradiation, radiolysis of water takes place. As a result reactive transient species, viz. e_{aq}^-, $H^\bullet$, $^\bullet OH$ are generated (Equation 6.1). isopropyl alcohol present in the reaction medium reacts with $H^\bullet$ and $^\bullet OH$ to give isopropyl radical and acetone reacts with e_{aq}^- to give isopropyl radical (Equations 6.2 and 6.3). This isopropyl radical is capable of reducing Au^{III}. Hence the only reducing species present in the system is isopropyl radical, which reduces the metal ion to metal in zero valent state, i.e., Au^{III} to Au^0 as shown in the mechanism (Equations 6.4-6.7) [273].

$$H_2O \xrightarrow{\gamma} e_{aq}^- + H^\bullet + {}^\bullet OH \tag{6.1}$$

$$^\bullet OH/H^\bullet + (CH_3)_2CH\text{-}OH \longrightarrow (CH_3)_2{}^\bullet C\text{-}OH + H_2O/H_2 \tag{6.2}$$

$$e_{aq}^- + (CH_3)_2C{=}O \longrightarrow (CH_3)_2{}^\bullet C\text{-}OH + OH \tag{6.3}$$

$$Au^{III} + (CH_3)_2{}^\bullet C\text{-}OH \longrightarrow Au^{II} + (CH_3)_2C{=}O + H^+ \tag{6.4}$$

$$Au^{II} + Au^{II} \longrightarrow (Au^{II})_2 \tag{6.5}$$

$$(Au^{II})_2 \longrightarrow Au^{III} + Au^{I} \tag{6.6}$$

$$Au^{I} + (CH_3)_2{}^\bullet C\text{-}OH \longrightarrow Au^0 + (CH_3)_2C{=}O + H^+ \tag{6.7}$$

After generation of Au^0 coalescence step leads to formation of Au nanoparticles in presence of PVP as a capping agent. PVP contains functional groups like >C=O and >N− [274], which helps in anchoring metal nanoparticles on their surface. These Au nanoparticles show characteristic surface plasmon band at around 522 nm (Figure 6.1). Figure 6.1 shows the yield of Au nanoparticles increases with increase in absorbed dose till all precursor Au^{III} ions are exhausted.

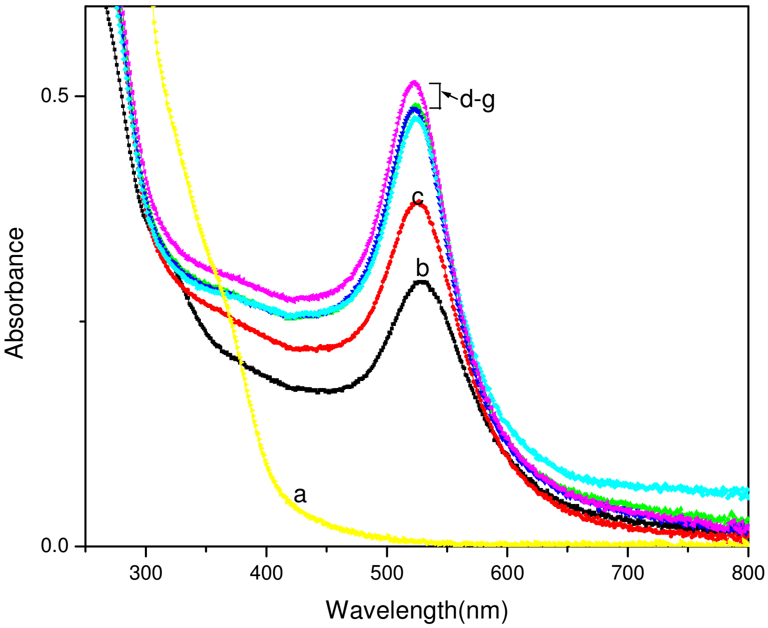

Figure 6.1: Absorption spectra of aqueous Au nanoparticle solution obtained at dose (a) unirradiated reaction mixture, (b) 0.5 kGy, (c) 0.9 kGy, (d) 1.3 kGy, (e) 1.5 kGy, (f) 1.6 kGy, (g) 1.8 kGy at a dose rate 2.2 kGy h^{-1}

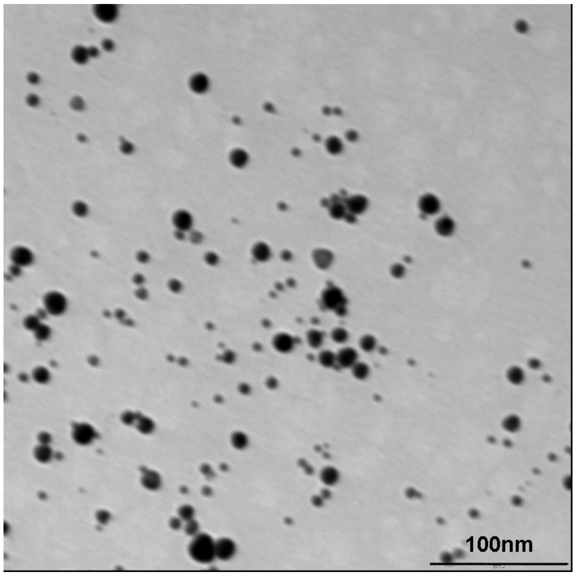

Figure 6.2: TEM image of Au nanoparticles prepared using PVP of molecular weight 3,60,000 Da

The TEM image (Figure 6.2) shows that Au nanoparticles formed in PVP of molecular weight 3,60,000 Da is spherical in nature with two types of size distribution having average particle size 13 nm and 6 nm.

6.2.2. Reduction under milder condition

It was observed that the presence of acetone affects the spectral behaviour of Au nanoparticles (Figure 6.3). In absence of acetone the reducing species are e_{aq}^{-} and isopropyl radical. e_{aq}^{-} (E^0 = -2.9 V_{NHE}) is a stronger reducing agent than isopropyl radical. Acetone is known to scavenge aqueous electron produced by water radiolysis to give isopropyl radical (E^0 = -1.8 V_{NHE}) (Equation 6.3). In presence of acetone and isopropyl alcohol the only reducing agent in the system is isopropyl radical (Section 5.3.3.1 in Chapter 5).

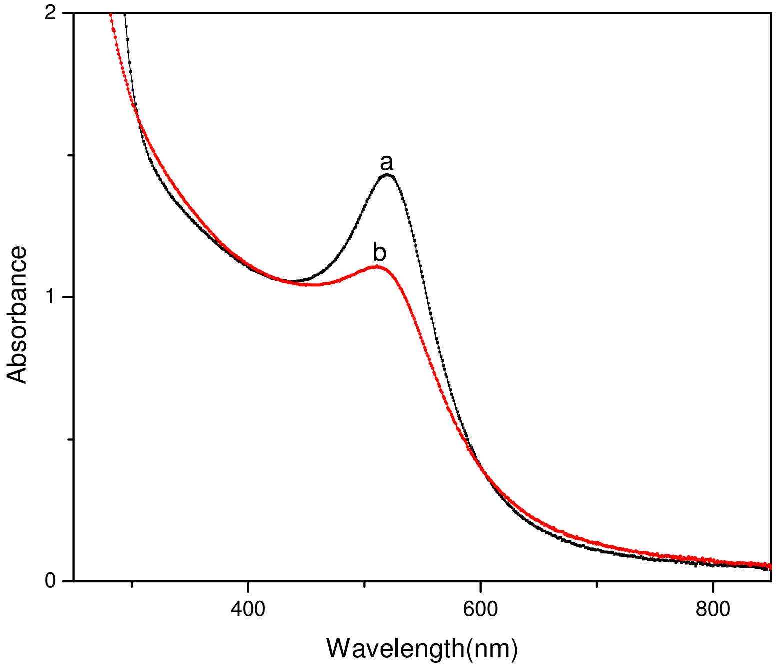

Figure 6.3: Absorption spectra of aqueous Au nanoparticle solution obtained (a) with acetone and (b) without acetone for 1.7 kGy of absorbed dose

The isopropyl radical is a milder reducing agent, so that reduction by this radical is slower than that by e_{aq}^{-}. Slower reduction rate is suitable for achieving narrower size distribution of Au nanoparticles as shown in Figure 6.3, also indicated by decrease in FWHM. Full width at half maximum (FWHM) can be useful to find size distribution of particles in a solution. The broader is the peak, the broader is the size distribution of the particles [275]. In case of smaller particles absorption is the prominent process. With increase in particle size the scattering of light becomes more pronounced. The scattering leads to broadening of plasmon band.

6.2.3. Role of $AgNO_3$ in nanoparticle formation

Comparing spectra of Au nanoparticles prepared in the presence and absence of a small amount of $AgNO_3$, the spectrum was found to be narrower in presence of $AgNO_3$ (Figure 6.4) indicating more uniform size distribution in this condition. Ag^+ at this concentration, i.e., 6×10^{-5} mol dm^{-3} is known to adsorb upon certain faces of Au crystal, leading to controlled growth. There is not much change in the spectral pattern in the $AgNO_3$ concentration range 6×10^{-5} mol dm^{-3} to 1.5×10^{-4} mol dm^{-3} (Figure 6.4).

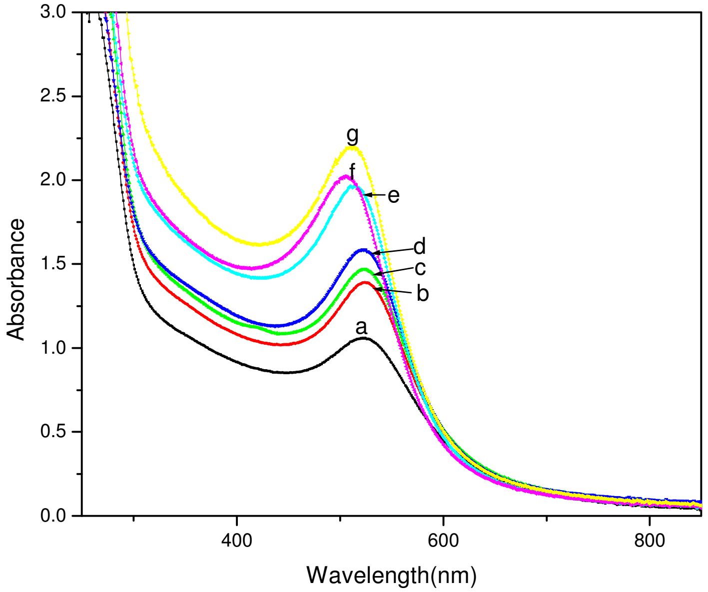

Figure 6.4: Absorption spectra of aqueous Au nanoparticle solution obtained for Ag^+ concentration (a) 0, (b) 6 x 10^{-5}, (c) 1 x 10^{-4}, (d) 1.5 x 10^{-4}, (e) 2 x 10^{-4}, (f) 3 x 10^{-4}, (g) 4 x 10^{-4} mol dm^{-3} for 1.7 kGy of absorbed dose

Beyond this concentration there is a blue shift in spectra, which may be due to AuAg alloy nanoparticle formation [276]. Hence in all the experiments 6×10^{-5} mol dm^{-3} $AgNO_3$ has been used.

6.2.4. Effect of variation of PVP concentration

The effect of variation of PVP concentration on Au nanoparticle formation was investigated. Figure 6.5 shows the absorption spectra for 4×10^{-4} mol dm^{-3} Au nanoparticle solution at various concentrations of PVP (M_w = 3,60,000Da). With increase in concentration of PVP from 0.1% to 2% (w/v) irregular spectral broadening was observed. This result is contrary to the earlier observed in case of Ag/guar gum system (Section 3.3.3, Chapter 3). As the PVP concentration is increased from 0.1% (w/v) to 0.5%, the intensity of the peak increases. But further increase in PVP concentration to 1% and 2% resulted in a decrease in intensity of the surface plasmon band. Hence an optimum concentration of PVP is essential to achieve maximum concentration of stable Au nanoparticles. In all other experiments 0.5% PVP concentration is maintained.

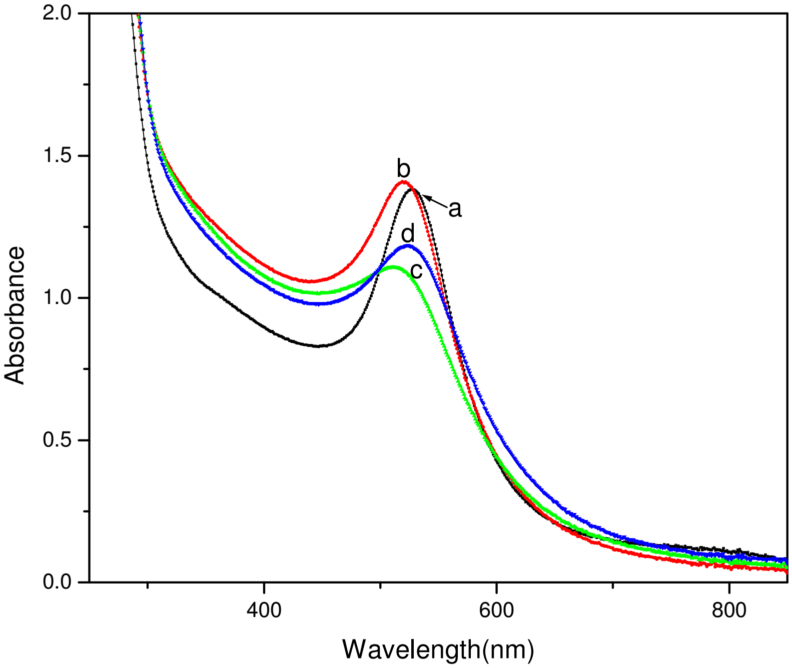

Figure 6.5: Absorption spectra of aqueous Au nanoparticle solution obtained for PVP concentration (a) 0.1%, (b) 0.5%, (c) 1%, (d) 2% for 1.7 kGy of absorbed dose

6.2.5. Effect of variation of Au^{III} concentration

From Figure 6.6 it can be observed that as Au^{III} concentration increases from 1×10^{-4} mol dm^{-3} to 1×10^{-3} mol dm^{-3} there is a steady increase in absorbance indicating increase in yield of Au nanoparticles. Initially there is a 27 nm redshift in the peak position as the concentration changes from 1×10^{-4} mol dm^{-3} to 4×10^{-4} mol dm^{-3}. At lower precursor concentration small nuclei are formed because of lower local concentration and beyond a certain size the growth is arrested because there is no further supply of Au^{III}, leading to formation of smaller particles. These smaller particles absorb at lower wavelength. Above 4×10^{-4} mol dm^{-3} of Au^{III} concentration there is not much shift in spectral peak as well as FWHM of the spectra. The narrow spectrum even at 1 × 10^{-3} mol dm^{-3} Au^{III} indicates good particle size distribution even at this concentration.

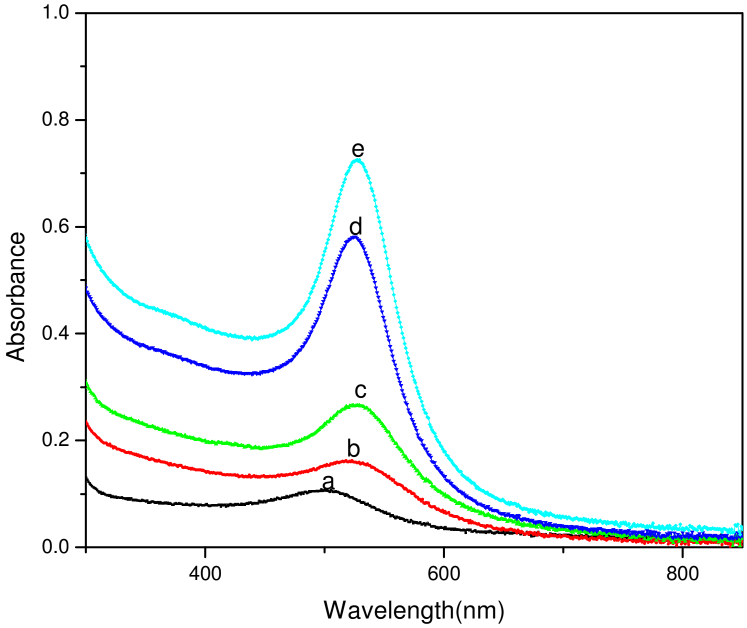

Figure 6.6: Absorption spectra of aqueous Au nanoparticle solution obtained for Au^{III} concentration (a) 1 x 10^{-4}, (b) 2.5 x 10^{-4}, (c) 4 x 10^{-4}, (d) 8 x 10^{-4}, (e) 1 x 10^{-3} mol dm^{-3} for absorbed dose of 0.4, 0.9, 1.5, 3.0 and 3.5 kGy respectively

It is reported in the literature that at higher precursor ion concentration the spectrum deforms and broadens due to large particle size distribution. But in this case, PVP appears to be an efficient stabilizer in which particle size with narrow distribution can be obtained even for 1 × 10^{-3} mol dm^{-3} precursor concentration.

6.2.6. Effect of PVP molecular weight on Au nanoparticle formation

In this study PVP of molecular weights 40,000; 1,60,000 and 3,60,000 Da have been used to find the effect of PVP molecular weight on Au nanoparticle formation. The molecular weight of PVP plays a very important role in controlling the shape and size of Au nanoparticles (Figure 6.7). Au nanoparticles stabilized by PVP having molecular weight 40,000 Da show a single intense peak at 533 nm and PVP having molecular weight 1,60,000 Da and 3,60,000 Da show similar broad peaks at 513 nm and 520 nm respectively. For higher molecular weight PVP only spherical Au nanoparticles with a little variation in size are generated as confirmed from the TEM image (Figure 6.2), whereas lower molecular weight PVP can stabilize different shaped Au nanoparticles other than spheres [277] by selectively blocking certain crystallographic faces of Au nanocrystal. Larger particle size is obtained in case of lower molecular weight PVP, because less steric effect is imparted by shorter carbon chain [278].

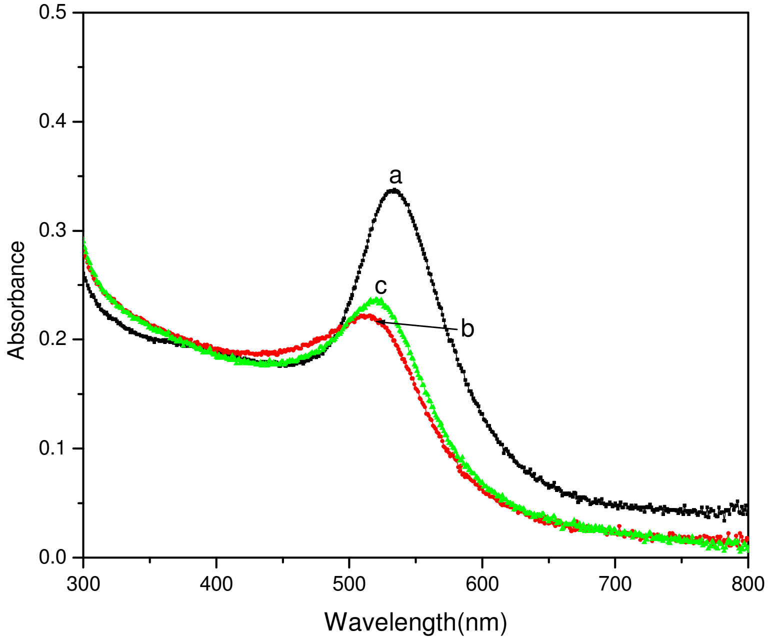

Figure 6.7: Absorption spectra of aqueous Au nanoparticle solution obtained for PVP of molecular weight (M_w) (a) 40,000 Da, (b) 1,60,000 Da, (c) 3,60,000 Da for 1.7 kGy of absorbed dose

6.2.7. Estimation of Hydrogen peroxide

6.2.7.1. Estimation of H_2O_2 in the range of 2.5×10^{-6} mol dm^{-3} to 2×10^{-4} mol dm^{-3}

An aqueous solution of horseradish peroxidase (HRP) was prepared by dissolving 0.125 mg HRP in 10ml nanopure water for further use. For estimation of H_2O_2 in the higher concentration range, 1×10^{-2} mol dm^{-3} citrate buffer (Citric acid/ Sodium citrate) solution, 1×10^{-4} mol dm^{-3} o-PDA, 125 μl of 0.125 mg/10ml of HRP and a certain quantity of H_2O_2 were successively added to a conical flask and the total volume was diluted to 20 ml with nanopure water. The reaction mixture was kept at room temperature for 30 minutes to allow the completion of the reaction between H_2O_2 and o-PDA. 5ml of a 5×10^{-4} mol dm^{-3} gold nanoparticle solution (in terms of Au^{III}) was added to this reaction mixture. The resulting solution was allowed to stand for another 30 minutes and subsequently the absorption spectra were recorded in the wavelength range of 250-800 nm.

6.2.7.2. Estimation of H_2O_2 in the range of 1×10^{-7} mol dm^{-3} to 3×10^{-6} mol dm^{-3}

For estimation of H_2O_2 at lower concentration range, 5×10^{-5} mol dm^{-3} o-PDA was taken. The concentrations of all the other reagents and the order of addition of these reagents remain same. Same procedure was followed as in section 6.3.1.

o-PDA under goes catalytic oxidation by H_2O_2 in presence of HRP [272]. The oxidation product of o-PDA has a weak absorption peak at 427 nm. As mentioned in section 6.3.1. Au nanoparticle solution was added to the reaction mixture after the product formation was over, i.e., after 30 minutes.

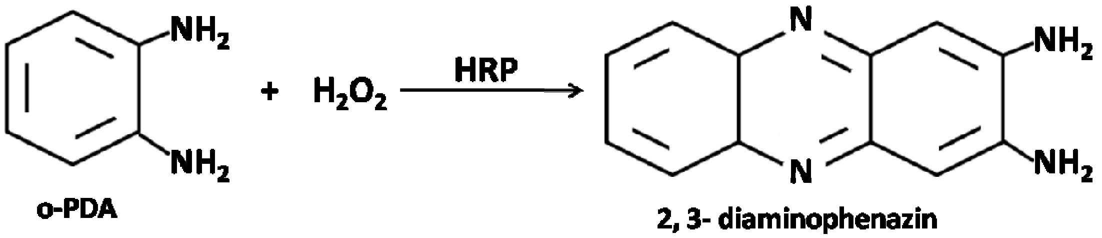

Figure 6.8: Enzymatic oxidation of o-PDA with H_2O_2

The Au nanoparticles generated through radiolytic method were found to enhance the absorption peak of the oxidation product of o-PDA. This may be due to the interaction of Au nanoparticles with 2, 3- diaminophenazine, which is the final oxidation product of o-PDA [279,280] (Figure 6.8). With varying concentration of H_2O_2 there is a systematic change in the absorption peak at 427 nm for 1×10^{-4} mol dm^{-3} Au nanoparticles (in terms of Au^{III}) stabilized by PVP of molecular weight 3,60,000 Da and for 1×10^{-4} mol dm^{-3} o-PDA as shown in Figure 6.9. When Au nanoparticles stabilized by PVP of different molecular weight, such as 40,000 Da and 1,60,000 Da were used for H_2O_2 estimation, similar results were observed for same range of H_2O_2 concentration. The absorbance value at λ_{max} (427 nm) for reaction mixture containing Au nanoparticles stabilized by different molecular weight PVP has been plotted against H_2O_2 concentration in Figure 6.9 (inset). The response is linear in the range of 2.5×10^{-6} mol dm^{-3} to 2×10^{-4} mol dm^{-3} H_2O_2 concentration with correlation factor $R > 0.998$ irrespective of PVP molecular weight. To estimate lower concentrations of H_2O_2, 5×10^{-5} mol dm^{-3} o-PDA was taken and all other reagents and experimental procedure kept same as above. The spectral change with change in concentration of H_2O_2 has been shown in Figure 6.10. The response is linear in the range of 1×10^{-7} mol dm^{-3} to 3×10^{-6} mol dm^{-3} H_2O_2 concentration with correlation factor $R = 0.995$ Figure 6.10 (inset).

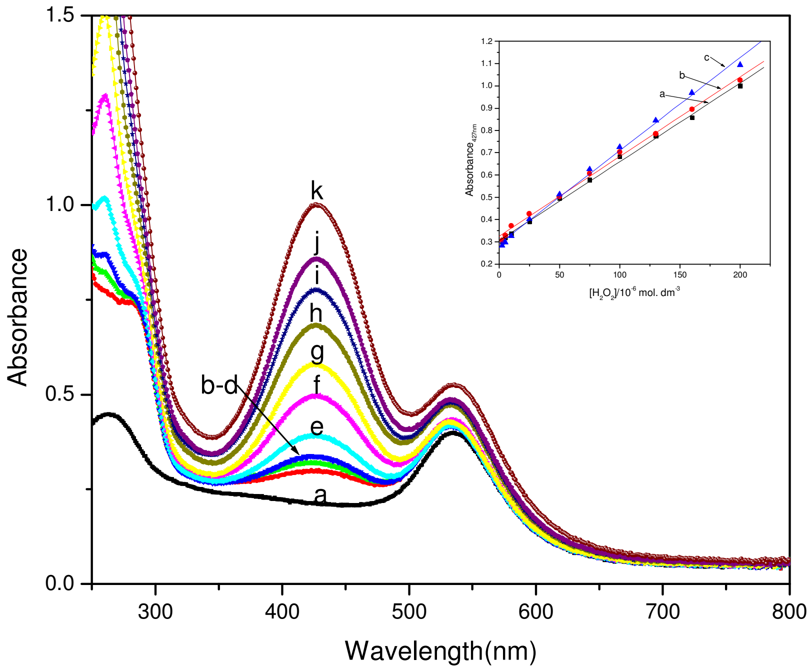

Figure 6.9: Absorption spectra of reaction medium containing OPD, HRP, H_2O_2 and Au nanoparticles (in PVP, M_w = 3,60,000 Da) in citrate buffer with varying H_2O_2 concentration (higher range of H_2O_2 concentration) (a) 0, (b) 2.5 x 10^{-6}, (c) 5 x 10^{-6}, (d) 1 x 10^{-5}, (e) 2.5 x 10^{-5}, (f) 5 x 10^{-5}, (g) 7.5 x 10^{-5}, (h) 1 x 10^{-4}, (i) 1.3 x 10^{-4}, (j) 1.6 x 10^{-4}, (k) 2 x 10^{-4} mol dm^{-3}
Inset: Linear plot of absorbance at 427 nm vs H_2O_2 concentration incase Au nanoparticle used was in PVP of molecular weight (a) 3,60,000Da (R=0.9986), (b) 1,60,000 Da (R=0.9981), (c) 40,000 Da (R=0.9981): H_2O_2 concentration range= 2.5 x 10^{-6} to 2 x 10^{-4} mol dm^{-3}

The detection limit in this system is 1×10^{-7} mol dm^{-3}. The colorimetric detection method reported by Wu et al. [272] is useful for detection of H_2O_2 in the range 1.3×10^{-6} mol dm^{-3} to 4.1×10^{-5} mol dm^{-3} with a detection limit 6×10^{-7} mol dm^{-3}. Also, they have reported a shift in the spectra of the chemically synthesized Au nanoparticles with change in H_2O_2 concentration, which was explained due to aggregation of Au nps. In our work, it was observed that there is no shift in the Au nanoparticle spectra with change in H_2O_2 concentration. The method reported in this communication is a better method for estimation of H_2O_2 because it can cover wider range and it has a lower detection limit, i.e., 1×10^{-7} mol dm^{-3} to 2×10^{-4} mol dm^{-3} and 1×10^{-7} mol dm^{-3} respectively.

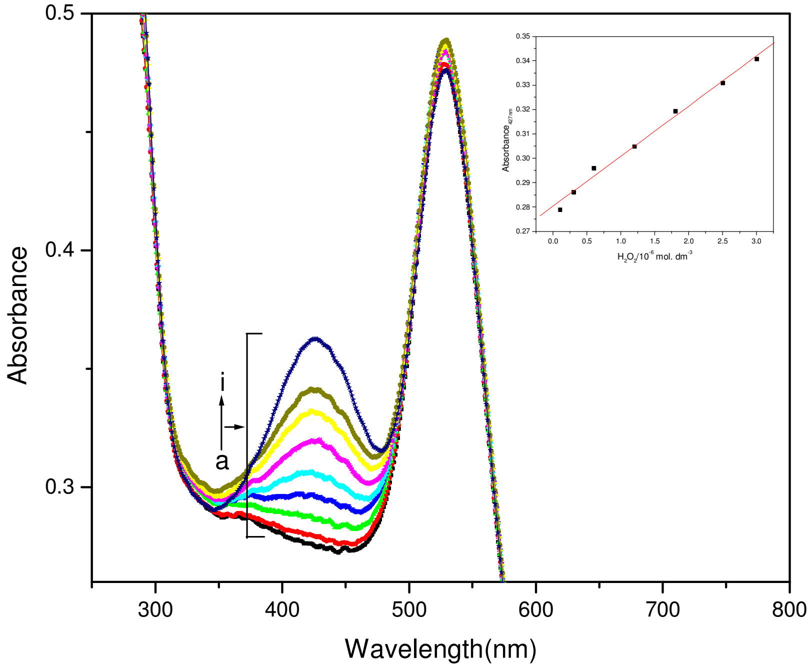

Figure 6.10: Absorption spectra of reaction medium containing OPD, HRP, H_2O_2 and Au nanoparticles (in PVP, M_w = 3,60,000) in citrate buffer with varying H_2O_2 concentration (lower range of H_2O_2 concentration) (a) 0, (b) 1 x 10^{-7}, (c) 3 x 10^{-7}, (d) 6 x 10^{-7}, (e) 1.2 x 10^{-6}, (f) 1.8 x 10^{-6}, (g) 2.5 x 10^{-6}, (h) 3 x 10^{-6}, (i) 5 x 10^{-6} mol dm^{-3}

Inset: Linear plot of absorbance at 427 nm vs H_2O_2 concentration incase Au nanoparticle used was in PVP of M_w = 3,60,000 Da(R=0.9954):H_2O_2 concentration range= 1 x 10^{-7} to 3 x 10^{-6} mol dm^{-3}

6.3. Conclusions

Au nanoparticles have been synthesized in PVP by radiolytic route and characterized by uv-visible spectroscopy and TEM. Different experimental parameters were standardized to generate uniform size distributed Au nanoparticles. No external reducing agent has been used in this method. A colorimetric method based on interaction of the oxidation product of o-PDA with radiolytically synthesized Au nanoparticles has been developed for estimation of H_2O_2. H_2O_2 in the concentration range of 1×10^{-7} mol dm^{-3} to 2×10^{-4} mol dm^{-3} can be estimated by this method by correctly choosing the reaction parameters as mentioned in the text. The detection limit for this method was found to be 1×10^{-7} mol dm^{-3}. The estimation of H_2O_2 using this particular system is independent of molecular weight of PVP in a wide range.

REFERENCES

1. Faraday, M., (1857) *Philos. Trans. R. Soc. Londo.,* 147, 145.
2. Zsigmondy, R., (December 11, 1926) "*Properties of colloids*", Nobel Foundation, Retrieved 2009-01-23.
3. Aiken, J. D. III, Finke, R. G., (1999) *J. Mol. Catal. A: Chem.* 145, 1.
4. Jain, P. K., Huang, X., El-Sayed, I. H., El-Sayed, M. A., (2008) *Acc. Chem. Res.* 41, 1578.
5. Murphy, C. J., Gole, A. M., Hunyadi, S. E., Stone, J. W., Sisco, P. N., Alkilany, A., Kinard, B. E., Hankins, P., (2008) *Chem. Commun.* 544.
6. Elghanian, R., Storhoff, J. J., Mucic, R. C., Letsinger, R. L., Mirkin, C. A., (1997) *Science* 277, 1078.
7. Schmid, G., Maihack, V., Lantermann, F., Peschel, S., (1996) *J. Chem. Soc., Dalton Trans.* 589.
8. Lin, Y., Finke, R. G., (1994) *J. Am. Chem. Soc.* 116, 8335.
9. Bonnemann, H., Braun, G. A., (1996) *Angew. Chem., Int. Ed. Engl.* 35, 1992.
10. Bonnemann, H., Richards, R. M., (2001) *Eur. J. Inorg. Chem.* 2001, 2455.
11. Remita, H., Lampre, I., Mostafavi, M., Balanzat, E., Bouffard, S., (2005) *Radiat. Phys. Chem.* 72, 575.
12. Cao, G., (2004) "*Nanostructures and nanomaterials: synthesis, properties and applications*", World scientific publishing Co. Pte. Ltd.
13. Wang, L., Zhao, W., Tan, W., (2008) *Nano. Res.* 1, 99.
14. Morrison, D. W. G., Docmeci, M. R., Demirci, U., Khademhosseini, A., (2008) Clinical Applications of Micro- and Nanoscale Biosensors, in "*Biomedical nanostructures*" (Eds. Gonsalves, K. E., Laurencin, C. L., Halberstadt, C. R., Nair, L. S.) JohnWiley & Sons, Inc. 433.
15. Vidotti, M., Carvalhal, R. F., Mendes, R. K., Ferreirab, D. C. M., Kubotab, L. T., (2011) *J. Braz. Chem. Soc.* 22, 3.
16. Wang, Z., Ma, L., (2009) *Coord. Chem. Rev.* 253, 1607.

17. Stuart, D.A., Haes, A.J., Yonzon, C.R., Hicks, E.M., Van Duyne, R.P., (2005) *IEE Proc.-Nanobiotechnol.*, 152, 13.
18. Knopp, D., Niessner, R., (2009) *Anal. Chim. Acta.* 647, 14.
19. Ghosh, S. K., Pal, T., (2007) *Chem. Rev.* 107, 4797.
20. Alonso, J. A., (2005) *"Structure and Properties of Atomic Nanoclusters"*, Imperial College Press, London.
21. Echt, O., Kandler, O., Leisner, T., Miehle, W., Recknagel, E., (1990) *J. Chem. Soc. Faraday Trans.* 86, 2411.
22. Poole, C. P., Owens, F. J., (2003) "*Introduction to nanotechnology*", Wiley Interscience Publication, New Jersey.
23. Kittel, C., (1996) "*Introduction to Solid State Physics*", 7th Ed., Wiley.
24. Defiano, S., Saccone, A., (2006) Chemistry of metals, in "*Inorganic and Bioinorganic chemistry – Vol. I*" (Eds. Bertini, I., Mori, M.), in *Encyclopedia of Life Support Systems* (EOLSS), Developed under the Auspices of the UNESCO, Eolss Publishers, Oxford, UK.
25. Schmid , G., (1994) "*Clusters and Colloids : From Theory to Application*", Weinheim, VCH.
26. Shan, J., Tenhu, H., (2007) *Chem. Commun. (Camb).* 44, 4580.
27. Khanna, P. K., Gokhale, R., Subbarao, V. V. V. S., (2004) J. Mater. Sci. 39, 3773.
28. Jana., N. R., (2005) *Small* 1, 875.
29. Yazid, H., Adnan, R., Hamid, S. A., Farrukh, M. A., (2010) *Turk. J. Chem.* 34, 639.
30. Yonezawa, T., Kunitake, T., (1999) *Colloid. Surface. A* 149, 193.
31. Derjaguin, B., Landau. L., (1941) *Acta Phys. Chem. (USSR)* 14, 633.
32. Huang, X., Neretina, S., El-Sayed, M. A., (2009) Adv. Mater. 21, 4880.
33. Scher, E. C., Manna, L., Alivisatos, A. P., (2003) *Phil. Trans. R. Soc. Lond. A* 361, 241.
34. Alivisatos, A. P., (1996) *Science* 271, 933.
35. Alivisatos, A.P., (1997) *Endeavour* 21, 56.
36. Chen, C., Herhold, A. B., Johnson, C. S., Alivisatos, A. P., (1997) *Science* 276, 398.
37. Riboh, J. C., Haes, A. J., McFarland, A. D., Yonzon, C. R., Van Duyne, R. P., (2003) *J Phys Chem B* 107, 1772.
38. Malinsky, M. D., Kelly, K. L., Schatz, G. C., Van Duyne, R. P., (2001) *J. Am. Chem. Soc.* 123, 1471.

39. Zynio, S. A., Samoylov, A. V., Surovtesva, E. R., Mirsky, V. M., Shirshov, Y. M., (2002) *Sensor.* 2, 62.
40. Hulteen, J. C., Treichel, D. A., Smith, M. T., Duval, M. L., Jensen, T. R., Van Duyne, R. P., (1999) *J. Phys Chem B* 103, 9846.
41. Henry, A. C., McCarley, R. L., (2001) *J Phys Chem B* 105, 8755.
42. Fuller, S. B., Wilhelm, E. J., Jacobson, J. M., (2002) *J. Microelctromech. Syst.* 11, 54.
43. Yin, Y., Lu, Y., Sun, Y., Xia, Y., (2002) *Nano. Lett.* 2, 427.
44. Haes, A. J., Stuart, D. A., Nie, S., Van Duyne, R. P., (2004) *J. Fluoresc.* 14, 355.
45. Hutter, E., Fendler, J. H., (2004) *Adv. Mater.* 16, 1685.
46. Kelly, K. L., Coronado, E., Zhao, L. L., Schatz, G. C., (2003*) J. Phys. Chem. B* 107, 668.
47. Link, S., El-Sayed, M. A., (1999a) *J. Phys. Chem. B.* 103, 4212.
48. Link, S., El-Sayed, M. A., (1999b) *J. Phys. Chem. B.* 103, 8410.
49. Dijken, A. v., Janssen, A. H., Smitsmans, M. H. P., Vanmaekelbergh, D., Meijerink, A., (1998) *Chem. Mater.* 10, 3513.
50. Andersen, K. E., Fong, C. Y., Pickett, W. E., (2002) *J. Non-Cryst. Solids*. 299-303, 1105.
51. Mie, G., (1908) *Ann. Phys.* 330, 377.
52. Link, S., El-Sayed, M. A., (2003) *Annu. Rev. Phys. Chem.* 54, 331.
53. Kreibig , U., Vollmer , M., (1996) “Optical Properties of Metal Clusters”, Springer, Berlin.
54. Kreibig, U., Vollmer, M., (1995) Optical Properties of Metal Clusters, in “Springer Series in Materials Science” (Ed. Paul, M.), Vol. 25, p 532, Springer-Verlag, Berlin.
55. Kreibig , U., and Genzel , U., (1985) *Surf. Sci.* 156, 678.
56. Alvarez, M. M., Khoury, J. T., Schaaff, T. G., Shaffigullin, M. N., Vezmar, I., Whetten, R. L., (1997) *J. Phys. Chem. B* 101, 3706.
57. Mulvaney, P., (1996) *Langmuir*, 12, 788.
58. Templeton, A. C., Wuelfing, W. P., Murray, R. W., (2000) *Acc. Chem. Res.* 33, 27.
59. van der Zande, B. M. I., Bohmer, M. R., Fokkink, L. G. J., Schonenberger, C., (2000) *Langmuir* 16, 451.
60. Gans, R., (1912) *Ann. Phys.* 342, 881.
61. Gans, R., (1915) *Ann. Phys*. 345, 270.
62. Eustis, S., El-Sayed, M.A., (2006a*) J. Appl. Phys.* 100, 044324/1.

63. Yu, Y. Y., Chang, S. S., Lee, C. L., Wang, C. R. C., (1997) *J. Phys. Chem. B* 101, 6661. *Sensors.* 2, 62.
64. Mohamed, M. B., Ismael, K. Z., Link, S., El-Sayed, M. A., (1998) *J. Phys. Chem. B* 102, 9370.
65. Farhataziz, Rodgers M. A. J. (1987) "*Radiation Chemistry",* VCH Pub. Inc., New York.
66. Mozumder, A., (1999) "*Fundamentals of radiation chemistry*", Academic press, San Diego.
67. Spinks, J. W.T., Woods, R. J., (1990) "*An introduction to radiation chemistry*", 3rd Ed., Wiley interscience publication.
68. Allen, A. O., (1961) *"The radiation chemistry of water and aqueous solutions"*, Van Nostrand, New York.
69. Hart, E. J., (1959) *J. Chem. Educ.* 36, 266.
70. Buxton, G. V., Greenstock, C. L., Helman, W. P., Ross, A. B., (1988) *J. Phys. Chem. Ref. Data*, 17, 513.
71. Buxton, G. V., (1968) *Radiat. Res. Rev.* 1, 209.
72. Hart, E. J., Anbar, M., (1970) "*The hydrated electron*"*,* Wiley Interscience, New York.
73. Wisenfield, J. M., Ippen, E. P., (1980) *Chem. Phys. Lett.* 73, 47.
74. Kassing, R., (2006) *Proceedings of the NATO Advanced Study Institute on "Functional properties of nanostructured materials"*, Springer Publication.
75. Hirsch, T., Zharnikov, M., Shaporenko, A., Stahl, J., Weiss, D., Wolfbeis, O. S., Mirsky, V. M., (2005) *Angew. Chem. Int. Ed.* 44, 6775.
76. Okitsu, K., Mizukoshi, Y., Yamamoto, T. A., Maeda, Y., Nagata, Y., (2007) *Mater. Lett.* 61, 3429.
77. Gutierrez, M., Henglein, A., (1993) *J. Phys. Chem.* 97, 11368.
78. Sato, T., Onaka, H., Yonezawa, Y., (1999) *J. Photochem. Photobiol. A* 127, 83.
79. Sau, T. K., Murphy, C. J., (2004b) *Langmuir* 20, 6414.
80. Turkevich, J., Stevenson, P. C., Hillier, J., (1951) *Discuss. Faraday. Soc*. 11, 55.
81. Kimling, J., Maier, M., Okenve, B., Kotaidis, V., Ballot, H., Plech, A., (2006) *J. Phys. Chem. B* 110, 1570085.
82. Male, K. B., Li, J., Bun, C. C., Ng, S., Luong, J. H. T., (2008) *J. Phys. Chem. C* 112, 443.
83. Guzman, M. G., Dille, J., Godet, S., (2008) *World Acad. Sci. Eng. Tech.* 43, 357.

84. Khanna, P. K., Singh, N., Charan, S., Subbarao, V. V. V. S., Gokhale, R., Mulik, U. P., (2005) *Mater. Chem. Phys.* 93, 117.

85. Chou, K. S., Ren, C. Y. (2000) Mater Chem Phys. 64, 241.

86. Norris, C. B., Joseph, P. R., Mackiewicz, M. R., Reed, S. M., (2010) *Chem. Mater.* 22, 3637.

87. Sun, K., Qiu, J., Liu, J., Miao, Y., (2009) *J. Mater. Sci.* 44, 754.

88. Murphy, C. J., Sau, T. K., Gole, A. M., Orendorff, C. J., Gao, J., Gou, L., Hunyadi, S. E., Li, T., (2005) *J. Phys. Chem. B* 109, 13857.

89. Sau, T. K., Rogach, A. L., (2010) *Adv. Mater.* 22, 1781.

90. Jana, N. R., Gearheart, L., Murphy, C. J., (2001b) *Chem. Commun.* 7, 617.

91. Treguer-Delapierre, M., Majimel, J., Mornet, S., Duguet, E., Ravaine, S., (2008) Gold Bull. 41, 195.

92. Perez-Juste, J., Pastoriza-Santos, I., Liz-Marzan, L. M., Mulvaney, P., (2005) *Coord. Chem. Rev.* 249, 1870.

93. Belloni, J., (1998) *Radiat. Res*, 150 Suppl., S9.

94. Braunstein, P., Oro, L. A., Raithby, P. R., (1999) Radiation induced metal clusters. Nucleation mechanisms and chemistry, in "*Metal Clusters in Chemistry*" (Eds. Belloni, J., Mostafavi, M.) Wiley, New York, 1213.

95. Belloni, J., Mostafavi, M., Remita, H., Marignier, J. L., Delcourt, M. O., (1998) *New J. Chem*. 22, 1239.

96. Ershov, B.G., Janata. E., Henglein, A., (1993a) *J. Phys. Chem*. 97, 339.

97. Ershov, B.G., Janata, E., Henglein, A., Fotjtik, A., (1993b) *J. Phys. Chem.* 97, 4589.

98. Gachard, E., Remita, H., Khatouri, J., Keita, B., Nadjo, L., Belloni, J., (1998) *New J. Chem.* 1257.

99. Henglein, A., (1977) *Ber. Bunsenges. Phys. Chem.* 81, 556.

100. Henglein, A., Meisel, D., (1998) *Langmuir* 14, 7392.

101. Belloni, J., (2006) *Catal. Today*.113, 141.

102. Belloni, J., Mostafavi, M., (2001) Radiation chemistry of nanocolloids and clusters, in "*Radiation Chemistry: Present Status and Future Trends*" (Eds. Jonah, C. D., Rao, B. S. M.) Elsevier, Amsterdam, p 411.

103. Wishart, J. F., Rao, B. S. M., (2010) "*Recent Trends in Radiation Chemistry*", World Scientific Publishing Co. pte. Ltd., Singapore.

104. Creighton, J. A., Eadon, D. G., (1991) *J. Chem. Soc., Faraday Trans.* 87, 3881.

105. Hovel, H., Fritz, S., Hilger, A., Kreibig, U., Vollmer, M., (1993) *Phys Rev B* 48, 18178.

106. Underwood, S., Mulvaney, P., (1994) *Langmuir* 10, 3427.

107. Kreibig, U., Vollmer, M., (1995) Optical Properties of Metal Clusters, in "Springer Series in Materials Science" (Ed. Paul, M.), Springer-Verlag, Berlin.

108. Wilcoxon, J. P., Williamson, R. L., Baughman, R., (1993) *J. Chem. Phys.* 98, 9933.

109. Kreibig, U., Fragstein, C. V., (1969) Z. Phys. A 224, 307.

110. Link, S., El-Sayed, M. A., (2000) *Int. Rev. Phys. Chem.* 19, 409.

111. Williams, D. B., Carter, C. B., (1996) "Transmission Electron Microscopy: A Text Book for Materials Science", Plenum, New York.Willner, I., Baron, R., Willner, B., (2006) *Adv. Mater.* 18, 1109.

112. Goldstein,J. I., Newbury, D. E., Joy, D. C., Lyman, C. E., Echlin, P., Lifshin, E., Sawyer, L., J., Michael, J. R., (2003) "Scanning Electron Microscopy and X-ray Microanalysis", 3rd Ed., Kluwer Academic Publishers, New York.

113. Blanchard, C. R., Campbell, J. B., (1995) Adv. Mater. Processes. 148, 62.

114. Hall, B. D., Zanchet, D., Ugarte, D., (2000*) J. Appl. Cryst.* 33, 1335.

115. Wu, D., Ge, X., Huang, Y., Zhang, Z., Ye, Q., (2003) *Mater. Lett.* 57, 3549.

116. Stokes, A. R., Wilson, A. J. C., (1944*) Proc. Phys. Soc.* 56, 174.

117. Patterson, A., (1939) *Phys. Rev.* 56, 978.

118. Skoog, D. A., Holler, F. J., Nieman, T .A., (1998) "*Principles of intstrumental analysis*", 5th Ed. Thomson Brooks/Cole: Belmont, CA, USA.

119. Bell, R. J., (1972) "*Introductory Fourier Transform Spectroscopy*", Academic Press, New York.

120. Griffiths, P. R., de Haseth, J. A., (1986) "*Fourier Transform Infrared Spectrometry*", Wiley, New York.

121. Hostetler, M. J., Stokes, J. J., Murray, R. W., (1996) *Langmuir* 12, 3604-12.

122. Woods, R. J., Pikaev, A.K., (1994) "*Applied Radiation Chemistry, Radiation Processing*", New York: John Wiley and Sons, Inc.

123. Laughlin, J. S., Gennes, S., (1966) in "*Radiation Dosimetry*", 2nd Ed., (Eds. Attix, F. H., Roesch, W. C., Tochilin, T.), Academic Press, New York, Vol.2, Chapter 16.
124. Domen, S. R., (1987) in "The dosimetry of Ionizing Radiation" (Eds. Kase, K. R., Bjarngard, B. E., Attix, F. H.), Academic Press, New York, Vol 2, Chapter 4.
125. Holm, N. W., Berry, R. J., (1970) "*Manual on Radiatio Dosimetry*", Marcel Dekker, New York.
126. Fricke, H., Morse, S., (1927) *Am. J. Roentgenol.* 18, 430.
127. Fricke, H., Morse, S., (1929) *Philos. Mag*. 7, 129.
128. Fricke, H., Hart, E. J., (1935) *J. Chem. Phys*. 3, 60.
129. McLaughlin, W.L., Miller, A., Fidan, S., Pejtersen, K. (1977) *Radiat. Phys. Chem.* 29, 119.
130. Reddy, T. T., Tammishetti, S., (2004) *Polym. Degrad. Stab.* 86, 455.
131. Malinsky, M. D., Kelly, K. L., Schatz, G. C., Van Duyne, R. P., (2001) *J. Am. Chem. Soc.* 123, 1471.
132. Zynio, S. A., Samoylov, A. V., Surovtesva, E. R., Mirsky, V. M., Shirshov, Y. M., (2002) *Sensor.* 2, 62.
133. Hulteen, J. C., Treichel, D. A., Smith, M. T., Duval, M. L., Jensen, T. R., Van Duyne, R. P., (1999) *J. Phys Chem B* 103, 9846.
134. Henry, A. C., McCarley, R. L., (2001) *J Phys Chem B* 105, 8755.
135. Fuller, S. B., Wilhelm, E. J., Jacobson, J. M., (2002) *J. Microelctromech. Syst.* 11, 54.
136. Yin, Y., Lu, Y., Sun, Y., Xia, Y., (2002) *Nano. Lett.* 2, 427.
137. Creighton, J. A., Blatchford, C. G., Albrecht, M. G., (1979) *J. Chem. Soc. Faraday. Trans. 2*75, 790.
138. Laserna, J. J., Cabalin, L. M., Montes, R., (1992) *Anal. Chem.* 64, 2006.
139. Vlckova, B., Solecka-Cermakova, K., Matejka, P., Baumurk, V., (1997) *J. Mol. Struct.* 408/409, 149.
140. Felidj, N., Aubard, J., Levi, G., (1999) *Phys. Status. Solidi.* 175, 367.
141. Feng, Z. C., Liang, C. H., Li, M. J., Chen, J., Li, C. J., (2001) *Raman. Spectrosc.* 32, 1004.
142. Etchegoin, P., Liem, H., Mahar, R. C., Cohen, L. F., Brown, R. J. C., Milton, M. J. T., Galop, J. C., (2003) *Chem. Phys. Lett.* 367, 223.

143. Patel, K., Kapoor, S.,Dave, D. P., Mukherjee, T., (2005) *J. Chem. Sci.* 117, 53.

144. Mieisel, D., (2004) *IAEA Techdoc* 1438, 125.

145. Monti, O. L. A., Fourkas, J. T., Nesbitt, D. J., (2004) *J. Phys. Chem. B* 108, 1604.

146. Zhang, H. Y., Zhang, J., Wang, H. Y., Chen, H. Y., (2004) *Mater. Lett.* 58, 2590.

147. Whistler, R. L, (1969) *The Encyclopedia of Polymer Science and Technology*, Wiley: New York, Vol. 11.

148. McLaughlin, W. L., Boyd, A. W., Chadwick, K. N., McDonald, J. C., Miller, A., (1980) *Dosimetry for Radiation Processing*; Taylor & Francis: London.

149. Wang, Q., Ellis, P. R., Ross-Murphy, S. B., (2000) *Food Hydrocolloids*14, 129.

150. Robinson, G., Ross-Murphy, S. B., Morris, E. R., (1982) Carbohydrate Res. 107, 17.

151. Mundargi, R. C., Agnihotri, S. A., Patil, S. A., Aminabhavi, T. M., (2006) *J. Appl. Polym. Sci.* 101, 618.

152. Tian, D., Hu, W., Zheng, Z., Liu, H., Xie, H. Q., (2006) *J. Appl. Polym. Sci.* 100, 1323.

153. Hund, J. F., Bertini, M. F., Zhand, G., Levantis, C. S., Levantis, N., Tokuhiro, A. T., Farmer, J., (2003) *J. Phys. Chem. B* 107, 465.

154. Ramnani, S. P., Biswal, J., Sabharwal, S., (2007) *Radiat. Phys. Chem*. 76, 1290.

155. Joshi, S. S., Patil, S. F., Iyer, V., Mahumuni, S., (1998) *Nanostruct. Mater.* 10, 1135.

156. Naik, D. B., Mukherjee, T., (2006) *Res. Che. Intermed.* 32, 83.

157. MacDiarmid, A. G., Chiang, J. C., Helperm, M., Huang, W. S., Mu, S. L, Somasiri, N. L. D., (1985) *Mol. Cryst. Liq. Cryst.* 121, 173.

158. Jumel, K., Harding, S. E., Mitchell, J. R., (1996) *Carbohydr. Res*. 282, 223.

159. El-Sayed, M. A., (2001) *Acc. Chem. Res.* 34, 257.

160. Sun, Y., Xia, Y., (2003) *Analyst* 128, 686.

161. Jensen, T. R., Malinsky, M. D., Haynes, C. L., Van Duyne, R. P., (2000) *J. Phys. Chem. B* 104, 10549.

162. Wei, H., Li, B., Li, J., Wang, E., Dong, S., (2007) *Chem. Commun.* 36, 3735.

163. Liu, J., Lu, Y., (2004) *J. Fluorescence* 14, 343.

164. Thaxton, C. S., Mirkin, C. A., (2004) DNA-gold-nanoparticle conjugates, in: *"Nanobiotechnology"* (Eds. Niemeyer, C. M., Mirkin, C. A.) Wiley-VCH, Weinheim, 288.

165. Baron, R., Zayats, M., Willner, I., (2005) *Anal. Chem.* 77, 1566.

166. Shang, L., Dong, S., (2008) *Nanotechnology* 19, 095502.

167. Hormozi Nezhad, M. R., Alimohammadi, M., Tashkhourian, J., Mehdi Razavian, S., (2008) *Spectrochimica Acta: Part A* 71, 199.

168. Willner, I., Baron, R., Willner, B., (2006) *Adv. Mater.* 18, 1109.

169. Wang, C., Luconi, M., Masi A., Fernandez, L., (2010) Silver nanoparticles as optical sensors, in: "*Silvernanoparticles*" (Eds. Perez, D. P.), ISBN 978-953-307-028-5, InTech, 225.

170. Wu, T., Li, Y., Huang, C., (2009) *Chin. Chem. Lett.*, 20, 611.

171. Anker, J. N., Hall, W. P., Lyandres, O., Shah, N. C., Zhao, J., Duyne, P. V., (2008) *Nature. Mater.* 7, 442.

172. Nair, A. S., Tom, R. T., Kumar, V. R. R., Subramaniam, C., Pradeep, T., (2007) *COSMOS* 3, 103.

173. Rao, T. U. B., Nataraju, B., Pradeep, T., (2010) *J. Am. Chem. Soc.* 132, 16304.

174. Shao, C., Yuan, B., Wang, H., Zhou, Q., Li, Y., Guan, Y., Deng, Z., (2011) *J. Mater. Chem.* 21, 2863.

175. Huang, Z., Pu, F., Hu, D., Wang, C., Ren, J., Qu, X., (2011) *Chem. Eur. J.* 17, 3774.

176. Guo, W., Yuan, J., Dong, Q., Wang, E., (2010) *J. Am. Chem. Soc.* 132, 932.

177. Ledo-Suarez, A., Rivas, J., Rodriguez-Abreu, C., Rodriguez, M. J., Pastor, E., Hernandez-Creus, A., Oseroff, S. B., Lopez-Quintela, M. A., (2007) *Angew. Chem., Int. Ed.* 46, 8823.

178. Henglein, A., (1989) *Chem. Rev.* 89, 1861.

179. Belloni, J., Amblard, J., Marignier, J. L., Mostafavi, M., (1994) in: "Cluster Atoms and Molecules", (Ed. Haberland, H.), Vol. 2. Springer, Berlin.

180. Doudna, C. M., Bertino, M. F., Tokuhiro, A. T., (2002) *Langmuir* 18, 2434.

181. Marignier, J. L., Belloni, J., Delcourt, M., Chevalier, J. P., (1985) *Nature* 317, 344.

182. Zhang, Z., Han, M., (2003) *J. Mater. Chem. Commun.* 13, 641.

183. Mallick, K., Witcomb, M. J., Scurrell, M. S., (2004) *J. Mater. Sci.* 39, 4459.

184. Singh, N., Khanna, P. K., (2007) *Mater. Chem. Phys.* 104, 367.

185. Longenberger, L., Mills, G., (1995) *J. Phys. Chem.* 99, 475.

186. Wang, L., Chen, D., (2006) *Colloid Polym. Sci.* 284, 449.

187. Pratesi, P., *(*1963*) Pure Appl. Chem.* 6*,* 435.

188. Chen, R. S., Huang, W. H., Tong, H., Wang, Z. L., Cheng, J. K., (2003) *Anal. Chem.* 75, 6341.

189. Raj, C. R., Okajima, T., Ohsaka, T., (2002) *J. Electroanal. Chem.* 543, 127.

190. Tsunoda, M., Imai, K., (2005) *Anal. Chim. Acta.* 541, 13.

191. Zhu, X. L., Shaw, P. N., Barrett, D. A., (2003) *Anal. Chim. Acta.* 478, 259.

192. Wang, H. Y., Hui, Q. S., Xu, L. X., Jiang, J. G., Suan, Y., (2003) *Anal. Chim. Act.* 497, 93.

193. Vlckova, M., Schwarz, M. A., (2007) *J. Chromatogr. A* 1142, 214.

194. Tsunoda, M., (2006) *Anal. Bioanal. Chem.* 386, 506.

195. Moini, M., Schultz, C. L., Mahmood, H., (2003) *Anal. Chem* 75, 6282.

196. Atta, N. F., Galal, A., Ahmed, R. A., (2010) *Anal. Biochem.* 400, 78.

197. Ghita, M., Arrigan, D. W. M., (2004) *Electrochim. Acta*, 49, 4743.

198. Bardajee, G. R., Pourjavadib, A., Soleyman, R., Sheikh, N., (2010) *J. Iran. Chem. Soc.* 7, 652.

199. Acharya, A., Mohan, H., Sabharwal, S., (2002) *Radiat. Phys. Chem.* 65, 225.

200. Nishimura, S., Mott, D., Takagaki, A., Maenosono, S., Ebitani, K., (2011) *Phys. Chem. Chem. Phys.* 13, 9335.

201. Venton, B. J., Wightman, R. M., (2003) *Anal. Chem.* 75, 414.

202. Serrano, D. P., Aguado, J., Escola, J. M., (2011) *Catalysis, 23, 253.*

203. Gilbert, O., Swami, B. E. K., Chandra, U., Sherigara, B. S., (2009) *J. Electro. Anal. Chem.* 636, 80.

204. Feldheim, D. L., Foss Jr., C. A., (2002) *"Metal Nanoparticles: Synthesis, Characterization and Applications",* Marcel Dekker, New York.

205. Daniel, M.C., Astruc, D., (2004) *Chem. Rev.* 104, 293.

206. Eustis, S., El-Sayed, M. A., (2006b) *Chem. Soc. Rev.* 35, 209.

207. Jiang, X. C., Brioude, A., Pileni, M. P., (2006) *Colloids Surf. A.* 277, 201.

208. El-Brolossy, T. A., Abdallah, T., Mohamed, M. B., Abdallah, S., Easawi, K., Negm, S., Talaat, H., (2008) *Eur. Phys. J. Special Topics.* 153, 361.

209. Chen, S., Wang, Z., Bollato, J., Foulger, S., Carroll, D., (2003b) *J. Am. Chem. Soc.* 125, 16186.

210. Sau, T. K., Murphy, C. J., (2004a) *J. Am. Chem. Soc.* 126, 8648.

211. Sau, T. K., Murphy, C. J., (2004b) *Langmuir* 20, 6414.

212. Kelly, K. L., Coronado, E., Zhao, L. L., Schatz, G. C., (2003*) J. Phys. Chem. B* 107, 668.

213. Johnson, C. J., Dujardin, E., Davis, S. A., Murphy, C. J., Mann, S., (2002) *J. Mater. Chem.* 12, 1765.

214. Hu, J., Wang, Z., Li, J., (2007) *Sensors* 7, 3299.

215. Sanc, R., Volkan, M., (2009) *Sens. Actuators. B* 139, 150.

216. Cao, Y., Wang, Z., Jin, X., Hua, X., Liu, M., Zhao, Y., (2009) *Colloids. Surf. A* 334, 53.

217. Haes, A. J., Haynes, C. L., McFarland, A. D., Schatz, G. C., Van Duyne, R. R., Zou, S. L., (2005) *Mater. Res. Bull.* 30, 368.

218. Hao, E., Bailey, R., Schatz, G., Hupp, J., Li, S., (2004) *Nano. Lett.* 4, 327.

219. Tsuji, M., Hashimoto, M., Nishizawa, Y., Tsuji, T., (2004) *Mater. Lett.* 58, 2326.

220. Alekseeva, A. V., Bogatyrev, V. A., Khlebtsov, B. N., Melnikov, A. G., Dykman, L. A., Khlebtsov, N. G., (2006) *Colloid. J*. 68, 661.

221. Gole, A., Murphy, C. J., (2004) *Chem. Mater.* 16, 3633.

222. Murphy, C. J., (2002) *Science* 298, 2139.

223. Gutierrez, M., Henglein, A., (1993) *J. Phys. Chem.* 97, 11368.

224. Sun, Y., Mayers, B., Herricks, T., Xia, Y., (2003) *Nano. Lett.* 3, 955.

225. Yin, B., Ma, H., Wang, S., Chen, S., (2003) *J. Phys. Chem. B* 107, 8898.

226. Pileni, M. P., (2003) *Nat. Mater.* 2, 145.

227. Jana, N. R., Gearheart, L., Murphy, C. J., (2001a) *J. Phys. Chem. B* 105, 4065.

228. Kim, F., Song, J., Yang, P. J., (2002) *J. Am. Chem. Soc.* 124, 14316.

229. Gai, P. L., Harmer, M. A., (2002) *Nano. Lett.* 2, 771.

230. Zhao, M., Sun, L., Crroks, R. M., (1998) *J. Am. Chem. Soc.* 120, 4877.

231. Ottaviani, M. F., Montalti, F., Turro, N. J., Tomalia, D. A., (1997) *J. Phys. Chem. B* 101, 158.

232. Ahmadi, T. S., Wang, Z. L., Green, T. C., Henglein, A., El-Sayed, M. A., (1996) *Science* 272, 1924.

233. Won, J., Ihn, K. J., Kang, Y. S. (2002) *Langmuir*. 18, 8246.

234. Temgire, K., Joshi, S. S., (2004) *Radiat. Phys. Chem.* 71, 1039.

235. Selvakannan, P. R., Dumas, E., Dumur, F., Pechoux, C., Beaunier, P., Etcheberry, A., Secheresse, F., Remita, H., Mayer, C. R., (2010) *J. Colloid Interface Sci.* 349, 93.

236. Nikoobakht, B., El-Sayed, M. A., (2003) *Chem. Mater.* 15, 1957.

237. Jiang, X. C., Pileni, M. P., (2007) *Colloids Surf. A* 295, 228.

238. Jana, N. R., Gearheart, L., Murphy, C. J., (2001b) *Chem. Commun.* 7, 617.

239. Jiang, X. C., Brioude, A., Pileni, M. P., (2006) *Colloids Surf. A.* 277, 201.

240. Nishioka, K, Niidome, Y., Yamada, S., (2007) *Langmuir* 23, 10353.

241. Wang, Q., Ellis, P. R., Ross-Murphy, S. B., (2000) *Food Hydrocolloids*14, 129.

242. Wang, Z. L., Mohamed, M. B., Link, S., El-Sayed, M. A., (1999) Surf. Sci. 440 809.

243. Mortier, T., Persoons, A. and Verbiest, T. (2006) *Cent. Eur. J. Chem.*4, 160.

244. Roy, M. B., Mandal, P. C., Bhattacharyya, S. N. (1994) *J. Radioanal. Nucl. Chem.* 191, 337.

245. Ershov, B.G., Janata, E. and Henglein, A. (1995) *J. Phys. Chem.* 98, 7619.

246. Tang, T., Hamley, I. W., (2009) *Colloid. Surface. A.* 336, 1.

247. Ah, C. S., Yun, Y. J., Park, H. J., Kim, W. J., Ha, D. H., Yun, W. S., (2005) *Chem. Mater.* 17, 5558.

248. Tsuji, M., Hashimoto, M., Nishizawa, Y., Tsuji, T., (2003) *Chem. Lett.* 32, 1114.

249. Luo, X., Imae, T., (2007) *Curr. Nanosci.* 3, 195.

250. Nezhad, M. R. H., Aizawa, M., Porter Jr., L. A., Ribbe, A. E., Buriak, J. M., (2005) *Small.* 1, 1076.

251. Okitsu, K., Sharyo, K., Nishimura, R., (2009) *Langmui*r 25, 7786.

252. Ha, T. H., Koo, H., Chung, B. H., (2007) *J. Phys. Chem. C* 111, 1123.

253. Crooks, R. M., Zhao, M., Sun, L., Chechik, V., Yeung, L. K., (2001) *Acc. Chem. Res.* 34, 181.

254. Liu. J., Lu. Y., (2003) *J. Am. Chem. Soc.* 125, 6642.

255. Kerman, K., Saito, M., Yamamura, S., Takamura, Y., Tamiya, E., (2008) *Trends Anal. Chem.* 27, 585.

256. Zhao, Y., Tian, Y., Cui, Y., Liu, W., Ma, W., Jiang, X., (2010) *J. Am. Chem. Soc.* 132, 12349.

257. Brown, S. D., Nativo, P., Smith, J., Stirling, D., Edwards, P. R., Venugopal, B., Flint, D. J., Plumb, J. A., Graham, D., Wheate, N. J., (2010) *J. Am. Chem. Soc. 132*, 4678.

258. Choi, S., Lee, S., Hwang, Y., Lee, K., Kang, H. (2003*) Rad. Phys. Chem.* 67, 517.

259. Choi, S., Park, H. G., (2005*) Appl. Surf. Sci.* 243, 76.

260. Gasaymeh, S. S., Radiman, S., Heng, L. Y., Saion, E., Saeed, G. H. M., (2010) *Am. J. App. Sci.* 7, 892.
261. Pimpang, P., Choopun, S., (2011) *Chiang Mai J. Sci.* 38, 31.
262. Wang, H., Qiao, X., Chen, J., Wang, X., Ding, S., (2005) *Mater. Chem. Phys.* 94, 449.
263. Borodko, Y., Habas, S. E.,Koebel, M.,Yang, P., Frei, H., Somorjai, G. A., (2006) *J. Phys. Chem. B* 110, 23052.
264. Li, Y., (1996) *Food Chem. Toxicol.* 34, 887.
265. Hurdis, E. C.,Romeyn, H., (1954) *Anal. Chem.* 26, 320.
266. Amin, V. M.,Olson, N. F., (1967) *J. Dairy Sci.* 50, 461.
267. Maeuchihara, N., Nakano, S., Kawashima, T., (2001) *Anal. Sci.* 17, 255.
268. Onoda, M., Uchiyama, T., Mawatari, K., Kaneko, K., Nakagomi, K., (2006) *Anal. Sci.* 22815.
269. Meyer, J., Karst, U., (1999) *Anal. Chim. Acta.* 401, 191.
270. Takahashi, A., Hashimoto, K., Kumazawa, S., Nakayama, T., (1999) *Anal. Sci.* 15, 481.
271. Brestovisky, A., Kirowa Eisner, E., (1983) *Anal. Chem.* 55, 2063.
272. Wu, Z. S., Zhang, S. B., Guo, M. M., Chen, C. R., Shen, G. L., Yu, R. Q., (2007) *Anal. Chim. Acta.* 584, 122.
273. Dey, G. R., ElOmar, A. K., Jacob, J. A., Mostafavi, M., Belloni, J., (2011) *J. Phys. Chem. A* 115, 383.
274. Oster, G., Immergut, E. H., (1954) *J. Am. Chem. Soc.* 76, 1393.
275. Sileikite, A., Puiso, J., Prosycevas, I., Tamulevicius, T., (2009) *Mater. Sci.* 15, 21.
276. Pal, S., De, G., (2007) *J. Nanosci. Nanotechnol.* 7, 1994.
277. Kemal, L., Jiang, X. C., Wong, K., Yu, A. B., (2008) *J. Phys. Chem. C* 112, 15656.
278. Shin, H. S., Yang, H. J., Kim, S. B., Lee, M. S., (2004) *J. Colloid Interface Sci.* 274, 89.
279. Jiao, K., Zhang, S. S., Wei, L., (1996) *Sci. China Ser. B* 26, 57.
280. Peter, J. T., Victor, P. C., Dave, W., (1987) *Anal. Biochem.* 165, 230.

LIST OF PUBLICATIONS

Journals:

1. **Jayashree Biswal**, S. P. Ramnani, Seema Shirolikar, S. Sabharwal, (2009), Synthesis of guar-gum-stabilized nanosized silver clusters with gamma radiation, *J. Appl. Polym. Sci.*, 114, 2348–2355.
2. **Jayashree Biswal**, S.P. Ramnani, R. Tewari, G.K. Dey, S. Sabharwal, (2010) Short aspect ratio gold nanorods prepared using gamma radiation in the presence of Cetyltrimethyl ammonium bromide (CTAB) as a directing agent, *Radiat. Phys. Chem.* 79, 441–445.
3. **Jayashree Biswal**, S. P. Ramnani, Seema Shirolikar and S. Sabharwal, (2010) Seedless synthesis of gold nanorods employing isopropyl radical generated using gamma radiolysis technique*, Int. J. Nanotechnol.* 7, 907– 918.
4. **Jayashree Biswal**, S. P. Ramnani, seema Shirolikar and S. Sabharwal, (2011) Synthesis of rectangular plate like gold nanoparticles by insitu generation of seeds by combining both radiation and chemical methods, *Radiat. Phys. Chem.* 80, 44–49.
5. Nilanjal Misra, **Jayashree Biswal**, Alka Gupta, J. K. Sainis, S. Sabharwal, (2012) Gamma radiation induced synthesis of gold nanoparticles in aqueous polyvinyl pyrolidone solution and its application for hydrogen peroxide estimation, *Radiat. Phys. Chem.* 81, 195–200.
6. **Jayashree Biswal**, Nilanjal Misra, Lalit. C. Borde, S. Sabharwal, (2013) Synthesis of silver nanoparticles in methacrylic acid solution by gamma radiolysis and their application for estimation of dopamine at low concentarions, *Radiat. Phys. Chem.* 83, 67–73.

Symposia:

1. **Jayashree Biswal**, S. Sabharwal, Synthesis of silver nanoparticles in methacrylic acid and studying its application as biosensor, National Symposium on Radiation and Photochemistry (NSRP), 14-17 Sep, 2010, Lonavala, India.
2. **Jayashree Biswal**, S. Sabharwal, Synthesis and characterization of controlled shape metal nanoparticles by using gamma radiation, International symposium on materials chemistry (ISMC), 7-11 Dec, 2010, BARC, Mumbai, India

3. **Jayashree Biswal**, S. P. Ramnani, S. Sabharwal, Synthesis of Metal Nanoparticles by High Energy Radiation, NAARRI international Conference (NIC), 13-15 Dec, 2010, Mumbai, India.
4. Nilanjal Misra, **Jayashree Biswal**, S. Sabharwal, Synthesis of Poyvinyl pyrrolidone capped gold nanoparticles by gamma radiolysis, National symposium on radiation and photochemistry (NSRP), 10-12 Mar, **2011**, JNV Univ., Jodhpur, India.